Enhancing Voltage Profile Problems in High-Voltage Transmission Lines Using Battery Supported STATCOM

(A Case Study of the Adama 132 KV Substation Electric Supply System)

Kibrom Berhe Mituku

A Thesis Submitted to

The Department of Electrical Power and Control Engineering,

School of Electrical Engineering and Computing

Presented in Partial Fulfillment of the Requirement for the Degree of Master's Science in Electrical Power and Control Engineering

(Specialization In Power System Engineering)

Office of Graduate Studies

Adama Science and Technology University

June, 2024

Adama, Ethiopia

Enhancing Voltage Profile Problems in High-Voltage Transmission Lines Using Battery Supported STATCOM

(A Case Study of the Adama 132 KV Substation Electric Supply System)

Kibrom Berhe Mituku

Advisor Name: Dr. Tefera T.

A Thesis Submitted to

The Department of Electrical Power and Control Engineering,

School of Electrical Engineering and Computing

Presented in Partial Fulfillment of the Requirement for the Degree of Master's Science in Electrical Power and Control Engineering

(Specialization In Power System Engineering)

Office of Graduate Studies

Adama Science and Technology University

June, 2024

Adama, Ethiopia

Declaration

I hereby declare that this Master Thesis entitled "**Enhancing Voltage Profile Problems in High-Voltage Transmission Lines Using Battery Supported STATCOM *(A Case Study of the Adama 132 KV Substation Electric Supply System)***" is my original work. That is, it has not been submitted for the award of any academic degree, diploma or certificate in any other university. All sources of materials that are used for this thesis have been duly acknowledged through citations.

Kibrom Berhe Mituku	____________________	__________________
Name of the student	Signature	Date

Recommendation

I, the advisor of this thesis, hereby certify that I have read the revised version of the thesis entitled "**Enhancing Voltage Profile Problems in High-Voltage Transmission Lines Using Battery Supported STATCOM (A Case Study of the Adama 132 KV Substation Electric Supply System)**" prepared under my guidance by Mr. Kibrom Berhe submitted in partial fulfillment of the requirements for the degree of Master's of Science in Power system Engineering. Therefore, I recommend the submission of revised version of the thesis to the department following the applicable procedures.

______________________	______________________	______________________
Major Advisor	Signature	Date

Approval Sheet

I, the advisor of the thesis entitled "**Enhancing Voltage Profile Problems in High-Voltage Transmission Lines Using Battery Supported STATCOM (A case study of the Adama 132 KV Substation Electric Supply System**" developed by Mr. Kibrom Berhe, hereby certify that the recommendation and suggestions made by the board of examiners are appropriately incorporated into the final version of the thesis.

Major Advisor	Signature	Date

We, the undersigned, members of the Board of Examiners of the thesis by Mr. Kibrom Berhe have read and evaluated the thesis entitled "**Enhancing Voltage Profile Problems in High Voltage Transmission Lines Using Battery Supported STATCOM (A Case Study of the Adama 132 KV Substation Electric Supply System**" and examined the candidate during open defense. This is, therefore, to certify that the thesis is accepted for partial fulfillment of the requirement of the degree of Master of Science in Power System Engineering.

Chairperson	Signature	Date
Internal Examiner	Signature	Date
External Examiner	Signature	Date

Finally, approval and acceptance of the thesis are contingent upon submission of its final copy to the Office of Postgraduate Studies (OPGS) through the Department Graduate Council (DGC) and School Graduate Committee (SGC).

Department Head	Signature	Date
School Dean	Signature	Date
Office of Postgraduate Studies, Dean	Signature	Date

Acknowledgment

First and foremost, I would like to thank the Almighty God for providing me with the strength, health, and perseverance to accomplish my thesis work. It would have been impossible without him! I'd like to thank my advisor, Dr. Tefera Terefe, for his expert guidance, encouragement, recommendations, and comments; without him, this work would not have been accomplished.

Finally, my deep gratitude and appreciation are conveyed to my big brother, Mr. Yirga Berhe, my mother, Belaynesh Assefa, and friends, especially Kuma Megersa (Msc), and others who have contributed directly and indirectly to my academic undertaking through all the stages.

Table of Content

List of Tables

List of Figures

List of Acronyms and Abbreviations

ADSS	Adama Substation
ADNSS	Adama New Substation
ASTSS	Asebe Teferi Substation
ATSS	Awash Traction Substation
AWFG	Adama Wind Farm Generation
AVSI	Advanced voltage stability index
A7KSS	Awash 7 Kilo Substation
BESS	Battery energy storage system
CA	Contingency Analysis
CSA	Canadian Standards Association
CSI	Composite severity indices
DVR	Dynamic Voltage Restorer
EEP	Ethiopia Electric Power
Eth	Ethiopia
FACTS	Flexible alternating current transmission system
GA	Genetic Algorithm
GWO	Grey Wolf Optimization
HVDC	High voltage direct current transmission
IEC	International Electro-technical Commission

IEEE	Institute of Electrical and Electronics Engineers
IPFC	Interline power feed controller
KV	Kilo Volt
KVar	Kilo Volt ampere rating
KWh	Kilo Watt hour
LFA	Load Flow Analysis
MOTSS	Mojo Traction Substation
MTT	Metehara Tap
MTSS	Metehara Substation
MU	Milion unit
MVA	Mega volt ampere
MVAR	Mega volt ampere rating
Mw	Mega watt
MU	Million units of electricity
NLDC	National Load Dispatch Centre
PCC	Point of common coupling
PSO	Particle swarm optimization
Pu	Per unit
SOSS	Sirba Ounkur Substation
SSA	Static security assessment
SVC	Shunt Compensation with Static Var Compensator

STATCOM	Static Synchronous Compensator
TCSC	Series Compensation with Thyristor-Controlled Series
UPFC	Unified Power Flow Controller

ABSTRACT

This thesis focuses on enhancing the voltage profiles of Ethiopia's Adama substation electric supply system, a critical hub in the country's power infrastructure. The Adama substation receives power from multiple sources, including the Koka hydroelectric plant, Adama I wind generation, and the Awash 7-kilo substation via a 132 kV transmission line. However, outages on the primary Koka line lead to significant voltage drops and reliability issues. These drops put additional strain on the Awash 7-kilo line, causing further voltage decreases and forcing load shedding.Several substations impact the Adama substation's high-voltage transmission line electricity supply system, particularly the A7KSS. These substations include the Adama new substation (ADNSS), Metehra substation (MTSS), Awash 7 kilo substation (A7KSS), Awash Traction substation (ATSS), Asebe Tefri substation (ASTSS), and Sirba Ounkur substation (SOSS). The Adama I wind farm faces interruptions due to under-voltage protection, which requires the voltage to be 0.9 p.u. or above to maintain generation. During normal and peak conditions, the system voltage ranges between 132 kV (1 p.u.) and 122.2 kV (0.925 p.u.) but can drop to as low as 0.85 p.u. (113 kV) during emergencies or Koka line outages. From January 30, 2023, to December 29, 2023, the Adama I wind farm lost 206,266 kWh of energy due to these outages, and due to the Koka outage, the overall lost energy resulted in 1,049,436.5 kWh of unsold energy over the year 2023.The primary objective of this thesis is to use a battery-supported STATCOM to address these voltage issues. Using Particle Swarm Optimization (PSO), a 15 MVAR battery-supported STATCOM was optimally placed at the A7KSS bus. Power flow analysis under the Koka contingency scenario showed significant voltage improvements across the network. Initially, during a 0.4 to 0.7-second simulation, the system voltage at various buses dropped to 0.68 p.u., 0.86 p.u., 0.7 p.u., 0.7 p.u., 0.7 p.u., 0.68 p.u., 0.68 p.u., 0.7 p.u., and 0.68 p.u., respectively. After installing the 15 MVAR STATCOM, the voltage profiles improved to 1 p.u., 1.02 p.u., 0.978 p.u., 1 p.u., 1 p.u., 0.98 p.u., 0.976 p.u., 1.02 p.u., and 0.977 p.u., respectively. These enhancements prevent voltage-related interruptions at the Adama wind farm and reduce load shedding across the network. Matlab 2021a was used for system implementation, analysis, and simulation.

Keyword: *BESS,Particle swarm optimization (PSO) , MATLAB,STATCOM,Voltage Drop*

CHAPTER ONE
INTRODUCTION

1.1 Background of the study

Ethiopian Electric Power has made remarkable progress in modernizing and growing its electrical infrastructure. High-voltage transmission lines span more than 17,000 kilometers, varying from 132 kV to 500 kV. The 230kV lines currently in use include MetuGambela, Giligel-GibeII-Jimma-Agaro Bedele, Alaba-Hosana, and Koka-Hurso-DireDawa. Among the notable lines in this extensive network are the 400kV Wolayta Soddo II-Addis Ababa and the 500kV Hidase-Didesa-Holeta. To facilitate efficient power transfer and distribution, Ethiopia has a network of 163 substations with voltages ranging from 132 kV to 500 kV. Among these 163 substations, some noteworthy ones include the 400 kV Gibe III substation, the 500 kV Didesa and Holeta substations, and the Hurso, Gambela, and Mehoni substations at 230 kV, and all of them actively assist the national grid. (EEP, 2019)

The 132 KV transmission line inside Ethiopia's Adama 132 KV Substation Electric Supply System has been a major area of attention for this study. As a crucial center for electricity distribution, this region is significant to the nation's power infrastructure. This hub gets power from some sources, including Adama I wind power, Koka, and the Awash 7-Kilo substation, through a 132 kV transmission line. In this network, the Adama 132kV/15kV substation is essential to maintaining dependable electricity distribution over the area. This substation effectively distributed the voltage. It is equipped with two 2*25MVA power transformers, one 50MVA mobile substation power transformer, and a 1x132kV Mojo traction outbound transmission line. With its 15 kV medium voltage feeders, it powers 11 outgoing feeders, improving the accessibility and distribution of electricity in the area even more. All things considered, this infrastructure is crucial to maintaining Ethiopia's economic development and progress, as well as guaranteeing a steady supply of electricity for its people.

Furthermore, a number of substations have an effect on the Adama substation's high voltage transmission line electricity supply system on one of the incoming lines, which is the A7KSS. These substations include the Adama new substation (ADNSS), Metehra substation (MTSS), Awash 7 kilo substation (A7KSS), Awash Traction substation (ATSS), Asebe Tefri substation (ASTSS), and Sirba Ounkur substation (SQSS).

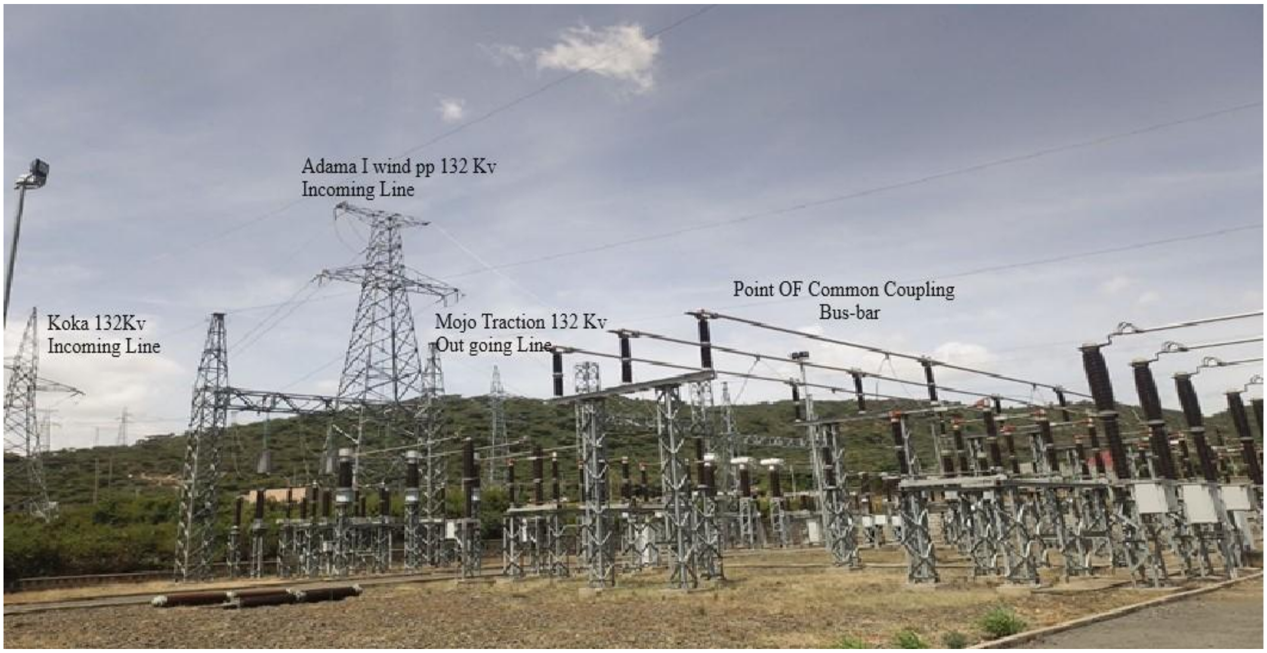

(a)

(b)

Figure 1.1 (a) and (b) Pictures of the Adama 132kV substation's initial case study region

The primary events that cause blackouts include (partial or entire) shortages of reactive power supplies, generation unit outages, and line problems, according to contingency data gathered from the EEP. Line failures and reactive power supply problems are the most significant events among them, making the power system as a whole more unreliable than other isolated occurrences. On EEP's 400 kV system, line faults and operational problems caused more than 256 outages between 2017 and 2020. Miscellaneous problems accounted for 9.77% of the disruptions, with lines accounting for 51.17% and operation and maintenance concerns for 39.06% of the total. Shunt capacitors and reactors continue to be responsible for loss reduction, reactive power compensation, and enhancement of the bus voltage profile. (Muluneh and Ashenaf 2022)

Adama Substation Network is currently facing critical challenges related to voltage stability and reliability. These issues primarily stem from interruptions in the main incoming line (Koka line), leading to voltage drops, overloading of the third incoming source line (Awash7 Kilo line), and necessitating load shedding. These challenges have far-reaching consequences, affecting the reliability of the wind farm power source and causing interruptions in wind-generated electricity. Where the wind farm disconnects generating due to the voltage drop.

Both the CSA C22.3 No. 9-08 and the IEEE STD 1547-2003 standards—which define the acceptable steady-state voltage variation in a medium voltage transmission line network—and the IEEE standard for connecting wind farm resources with electric power systems are extensively utilized to define acceptable steady-state voltage variation. A steady-state voltage restriction of ±6% of the nominal value at the PCC terminal was made possible by Hydro China's 2009 technical interconnection criteria, thanks to these standards. Adjusting reactive power appropriately is necessary to maintain the steady-state voltage within permissible limits. (Hagos and Milkias 2018)

Voltage instability, which can be brought on by issues with the circuit safety systems, transmission line tripping, or a loss of load in a particular area, can result in cascade system outages. Due to the customers' rapidly increasing power usage, the current scenario has placed a great deal of strain on the power system, reducing its stability margins. Voltage stability problems are classified into two groups: small and large, based on the magnitude of the disruption. It is further separated into long-term and short-term groups based on the duration of the disturbance. (Tebeje and Teshome 2022) The security and reliability of the electrical power system are seriously threatened by voltage instability these days. When a power system can maintain an equilibrium operating condition or maintain stability in the face of major disruptions or unforeseen events, it is said to have achieved voltage stability. (Ali et al , 2019) One way to characterize a contingency is the failure of a system component, such as issues with the transmission line that may arise from an overload or malfunction of the transmission network. Operators can use contingency analysis (CA) to assess the security of the system and decide whether control actions are required when a component fails. The amount of computation involved in contingency analysis might increase with the number of missing components and system size. (Muluneh and Ashenaf 2022)

The loss of the transmission lines may also affect the voltage instability of the overall networked system. The Flexible AC Transmission System (FACTS) has a Static Synchronous Compensation (STATCOM) device that is installed to address the issue. The voltage stability of the interconnected system might be preserved, although STATCOM installation might raise the voltage in other areas that are allowed. Installing a Static Synchronous Compensation (STATCOM) is necessary to guarantee that each substation's voltage profile on the subsystem falls within the parameters established under those conditions. (Ali et al, 2019)

A device where the voltage source is located behind a reactor is called a voltage source converter (VSC), also known as STATCOM. Due to the DC capacitor that makes up the voltage supply, a STATCOM can only provide very little active power. It is feasible to enhance the DC capacitor's active power capabilities by connecting a suitable energy storage device across it. The voltage source's amplitude controls the reactive power at the STATCOM terminals. When the VSC's terminal voltage is higher than the AC voltage at the connection point, for example, the STATCOM harvests reactive current. On the other hand, reactive power is absorbed when the amplitude of the voltage source is smaller than the AC voltage. (Harika and Madhavi, 2018)

Particle Swarm Optimization Algorithm is implemented in the test system, resulting in a considerable improvement in voltage stability and a reduction in both active and reactive power loss. To facilitate future research, STATCOM and intelligent control techniques should be used to increase the voltage stability of the transmission system. (Myat and Soe, 2022)

In this thesis, the particle swarm optimization technique in the MATLAB 2021a environment has been used to identify the optimal location and size of a STATCOM. Once the battery-supported STATCOM is positioned correctly, this thesis work improves the voltage profile of the system network buses ADSS, AWFG, MOTSS, ADNSS, MTT, MTSS, A7KSS, ATSS, ASTSS, and SOSS. The Newton-Raphson load flow method in MATLAB was used to analyze the system's power flow.

1.2 Statement of the Problem

The Adama Substation Network is grappling with severe voltage stability and reliability issues, and these problems originate from a series of events. It all starts with the frequent interruptions of the main incoming line, known as the Koka generation line. These interruptions trigger voltage instability and consequential drops in voltage levels, which in turn place a heavy burden on the third incoming source line, the Awash 7 kilo line. The Awash 7 kilo-line struggles to carry the entire substation load, leading to further voltage drops and eventually necessitating load shedding. It is significant to remember that the system voltage fluctuates between 132 kV(1 p.u) and 122.2 kV(0.925p.u) during typical operation and load conditions. However, the system voltage drops to as low as 113 KV(0.856p.u) during disruptions or emergencies, particularly during Koka line interruptions. These problems have ripple effects that extend beyond the substation itself. The recurrent interruptions of the Koka line, which occurred 11 times over the last year 2023, have resulted in a significant total unsold energy of 1,049,436.5kWh. Furthermore, these interruptions in the Koka line disrupt the supply of electricity from the Adama I wind farm, leading to an energy loss of 0.206266 MU (million units of electricity) over the last year 2023.To clarify, one unit of electricity is equivalent to one kilowatt-hour (KWh), and one kilowatt equals a thousand watts, making the loss equivalent to 206,266 KWh. To address these interconnected issues, measures will be taken, including load shedding within the subsystem network, specifically on the 15KV outgoing lines. This thesis work aims to comprehensively address these issues by implementing a Battery Supported STATCOM. The integrated solution seeks to mitigate voltage fluctuations, prevent interruptions, and ensure a reliable power supply. Additionally, this thesis focuses on Voltage profile improvement analysis during Koka Hydro plant contingency condition within the High-Voltage Transmission Lines of Adama Substation Electric Supply System.

1.3 Objectives

1.3.1 General Objectives

The general objective of this study is enhancing Voltage Profile Problems in High-Voltage Transmission Lines of Adama Substation Electric Supply System Using Battery-Supported STATCOM.

1.3.2 Specific Objectives

- Analyze existing system load flow to identify voltage drops and support needs for stable voltage levels under peak load and contingency conditions.
- Model and design the Adama I wind farm generation for stable voltage integration, minimized energy losses, and reliable operation within the grid.
- Determine optimal STATCOM device placement and size using particle swarm optimization to enhance voltage profiles, reduce energy losses, and ensure wind farm reliability.
- Develop a battery-supported STATCOM control strategy to precisely regulate voltage, minimize energy losses, and enhance wind farm stability.
- Simulate Adama Substation Electric Supply System high-voltage transmission lines with battery-supported STATCOM in MATLAB/Simulink to optimize voltage profiles, reduce energy losses, and ensure wind farm reliability.

1.4 Scope of the Study

The main focus of this work is the concerns about voltage stability and reliability in the high-voltage transmission lines of the electric supply system at Adama Substation. The main parts of this work are the assessment of load flow, the model and design of Adama I wind farm generation, the design and construction of a battery-supported STATCOM system, and operational simulations, where PSO handles the STATCOM placement and scaling.

MATLAB/Simulink will be used in the study to assess historical flow information and pertinent power system data in the context of the high-voltage transmission lines' electric supply of the Adama Substation Network.

1.5 Limitations of the Study

Limitations of the study included its narrow focus on voltage stability within the Adama Substation Electric Supply System, potentially limiting exploration of other critical aspects of power system operation and optimization. Assumptions made during modeling, such as constant wind farm speed and reliance on historical flow information, might have oversimplified system dynamics, potentially compromising analysis accuracy. Additionally, restricting analysis to voltage drop contingencies from the Koka Hydro Plant Generation Contingency Case might have overlooked other critical scenarios.

1.6 Significance of the study

This study holds substantial significance on multiple fronts.

- Firstly, it addresses the critical issue of voltage stability and reliability within the High-Voltage Transmission Lines of Adama Substation Electric Supply System.
- Secondly, the study contributes to energy efficiency by reducing energy losses resulting from interruptions and load shedding.
- Thirdly, the thesis promotes integrating renewable energy sources into the electrical system, focusing on the Adama I wind farm. Minimizing interruptions and energy losses enables more effective utilization of clean energy and contributes to environmental sustainability.
- Fourthly, the implementation of battery supported STATCOM represents a technological advancement with broader implications.

1.7 The Organization of the Thesis

The substance of this thesis is organized into five chapters, each of which is as follows: The first chapter of the work contains the general thesis introduction, which summarizes the main points of the thesis and offers direction for the thesis body. A summary of FACTS devices, contingency analysis, and voltage stability in the power system, the theoretical foundations of security and dependability, and a plan for improving transmission system performance are all covered in Chapter 2. It comprises a review of the literature based on the previous discoveries, which are related to the transmission system's power quality problem and specifically improve the voltage profile of the transmission line. The description of the case study area, the necessary data, the analysis of the data gathered, and the modeling of each power system device are covered in Chapter 3. In chapter four, the simulation results and discussion for battery-supported STATCOM in the high-voltage transmission line electric supply system of the Adama substation network with and without battery-supported STATCOM are given. In Chapter 5, the thesis's conclusion and recommendations were covered.

CHAPTER TWO

THEORETICAL BACKGROUND AND LITERATURE REVIEW

2.1 Power System Reliability and Security

Power systems must be operated in a way that respects the capabilities of their generation, transmission, and distribution components and does not compromise them over an extended period to meet system demands while maintaining system security. This is known as power system reliability. Regarding the capacity of the system to endure disturbances, including equipment failures or malfunctions, without suffering additional instability or cascading failures, system security is a component of system reliability (Chanan et al, 2019).

2.2 Voltage Stability in Power System

Voltage stability is defined as "a power system's ability to sustain stable voltages at all buses in the system following a disruption resulting from a specific starting operating condition" in electricity systems. The incapacity of a power system to maintain a consistent voltage across its buses in the wake of a disruption in the system is known as voltage instability. Voltage fluctuations are a significant issue with power systems. Lacking the reactive power essential to maintain the bus voltages steady within the required ranges. The problem of voltage stability is an important one. in the deployment of expanding or powerful systems. Failure events may also result in voltage instability in the power network at specific systemic locations or system levels. When voltage instability develops at the system level and prompt corrective control measures are not implemented, grid collapse, either partial or complete, may result (Bukola and Christopher , 2021).

2.3 Contingency Analysis

A contingency is described as an unexpected event that happens in the power system and lasts only a short while, signaling that one or more power system components have failed or are unavailable. (Ummidi et al ,2020) By monitoring the release of critical components including transformers, transmission lines, and generators, contingency analysis ascertains the post-contingency impact on the system's power flow and bus voltages. Contingency analysis will keep an eye on limitations including bus stress, channel loads, and spinning reserve availability(Sucita et al , 2018).

2.4 Flexible Alternating Current Transmission Systems (FACTS)

By using Flexible Alternating Current Transmission Systems (FACTS) devices, it is possible to enhance voltage profiles, reduce power losses, and improve system performance. Advanced power electronics are the foundation of FACTS devices. FACTS devices achieve these goals by controlling the flow of electrical power and improving the power system's efficiency. FACTS devices that reduce power loss and improve voltage profiles can be used for the following applications:

- Shunt Compensation with Static Var Compensator (SVC)
- Series Compensation with Thyristor-Controlled Series Capacitor (TCSC)
- Unified Power Flow Controller (UPFC)
- Static Synchronous Compensator (STATCOM)
- Dynamic Voltage Restorer (DVR)   (Bukola and Christopher , 2021)

The STATCOM shunt device, which is based on voltage-source inverters (VSIs), enhances power quality in transmission and distribution networks. The main advantage of STATCOM is that it can effectively manage the amount of current injected into the distribution bus due to its highly sophisticated power electronics-based control. Its second advantage is that it can be used for a lot of different things. For example, it can be used to manage distribution bus voltage to prevent sag or swelling, reduce the impact of low load power factors, mitigate the effect of harmonic content in load currents, and adjust for the reactive power needs of the load, among many other things (Suliman, 2023).

2.4.1 STATCOM (Static Synchronous Compensation.)

A shunt FACTS device, STATCOM, corrects reactive power by controlling power flow and enhancing the transient stability of the grid. When the system voltage is lowered, the PCC can generate reactive power, enabling it to operate as a capacitive device. That being said, the STATCOM can absorb reactive power at the PCC and operate as an inductive device if the system voltage remains high. Hence, this VAR-controlled device enhances the power factor and voltage profile of any distributed energy resource-integrated system in dynamic scenarios. Most of STATCOM is composed of the grid-side coupling transformer, DC capacitor, and voltage source converter (VSC)-based PWM converter. Via a coupling transformer, the VSC provides the grid system with three-phase power, and the DC capacitor guards against overvoltage on the system's constituent parts. On the DC side of the VSC, the capacitor serves as a supply of DC voltage. There are two modes of operation for it: voltage control mode, which keeps the node voltage constant, and reactive power control mode, which keeps the reactive power at a predetermined level(Fabliha et al 2021) .

2.5 Power system STATCOM components

To balance the reactive power in transmission lines, shunt FACTS devices such as STATCOM are employed. It can change power flows, take in, and produce reactive power. It improves the system's stability in all respects by offering dependable control over the transmission parameters, such as line impedance, phase angle, and voltage magnitude. Figure (a) depicts the fundamental parts of the STATCOM device(Rasool et al, 2022) .

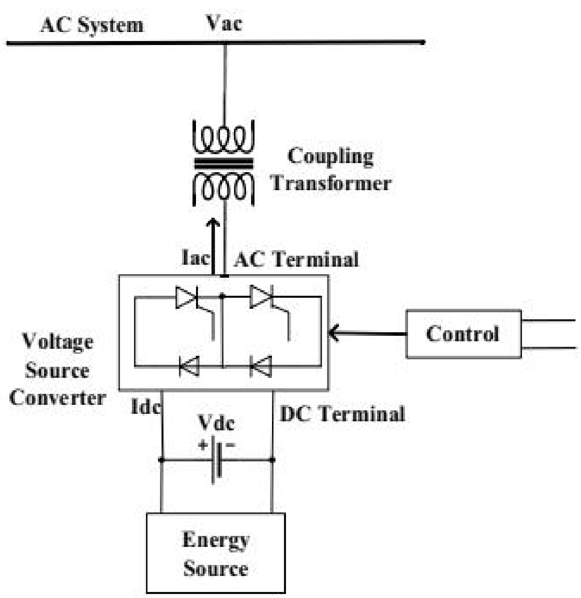

(a)

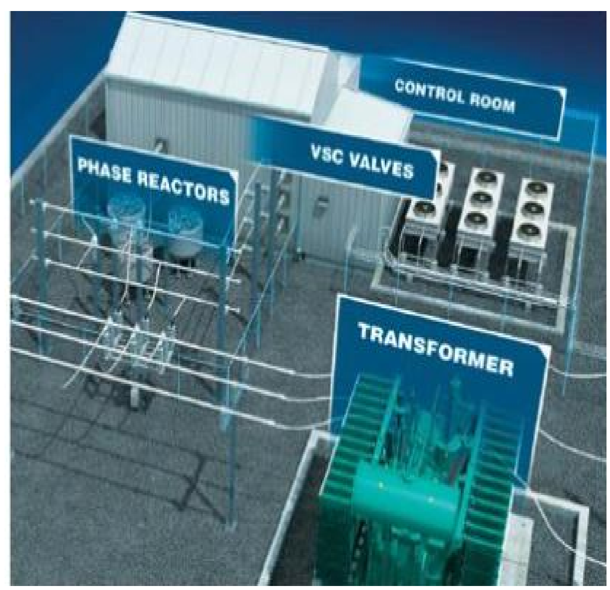

(b)

Figure 2.1 (a) Simple STATCOM Representation, (b) Basic STATCOM Configuration and Main Components (Hussein, 2021)

2.6 Battery Energy Storage System (BESS)

To improve the voltage level, frequency, system oscillation, transient stability, and dependability of the power supply in is-landed or weakly grid-connected mode, BESS is being used more and more in FACTS applications. The use of BESS in controlling the flow of both reactive and actual electricity has grown dramatically. To support the system voltage in the event of a severe fault, BESS can be installed at the distributed energy resource of the PCC or any other suitable point. By using a short ramping period, the proper location of BESS may guarantee both frequency regulation and voltage level. BESS can also lessen voltage sag and associated spikes, as well as ease issues with voltage management (Fabliha et al, 2021).

The excellent energy density, quick response time, and high efficiency of lithium-ion batteries make them ideal for integration with Flexible AC Transmission System (FACTS) devices. Their rapid charging and discharging capabilities make them perfect for dynamic uses like reactive power compensation and voltage management. In particular, during abrupt load shifts or disturbances, lithium-ion batteries can offer prompt assistance to regulate voltage levels and enhance power quality when linked with FACTS devices such as STATCOMs. They are also a sensible option for improving the performance and dependability of sophisticated power systems, guaranteeing a more robust and effective electrical grid, due to their extended cycle life and comparatively small size (Hongwen and Jinxin , 2011).

The integration of STATCOM and BESS aims to provide comprehensive voltage regulation capabilities, enhancing the reliability and performance of the electric supply system at the Adama substation. By combining STATCOM's rapid reactive power compensation with BESS's energy storage capabilities, the system can effectively stabilize voltage fluctuations and mitigate grid disturbances. This integrated approach optimizes grid performance, improves power quality, and reduces downtime, offering flexibility and adaptability to varying grid conditions.

2.7 Particle Swarm Optimization

(Harika and Madhavi, 2018) Particle swarm optimization (PSO), an inhabitants-based stochastic optimization technique developed in 1995 by Drs. Kennedy and Eberhard, took its cues from social behavior in fish schools and bird flocks. PSO allotments there are several parallels with the idea of evolutionary computing. Much like genetic algorithms (GA), the system starts with a population of arbitrary, practical responses and iteratively searches through updating generations in search of the best. Furthermore, PSO does not have evolution operators (i.e., GA) like transition and change do. The PSO algorithm has demonstrated excellent performance on the genetic algorithm test run. The goal function of this paper's optimal power flow (OPF) approach is a decrease in fuel costs. Here, we are utilizing STATCOM in addition to the other shunt FACTS devices to increase the line's capacity for power transfer. For the base case and optimal power generation with STATCOM included, the particle swarm optimization technique (PSO) is applied.

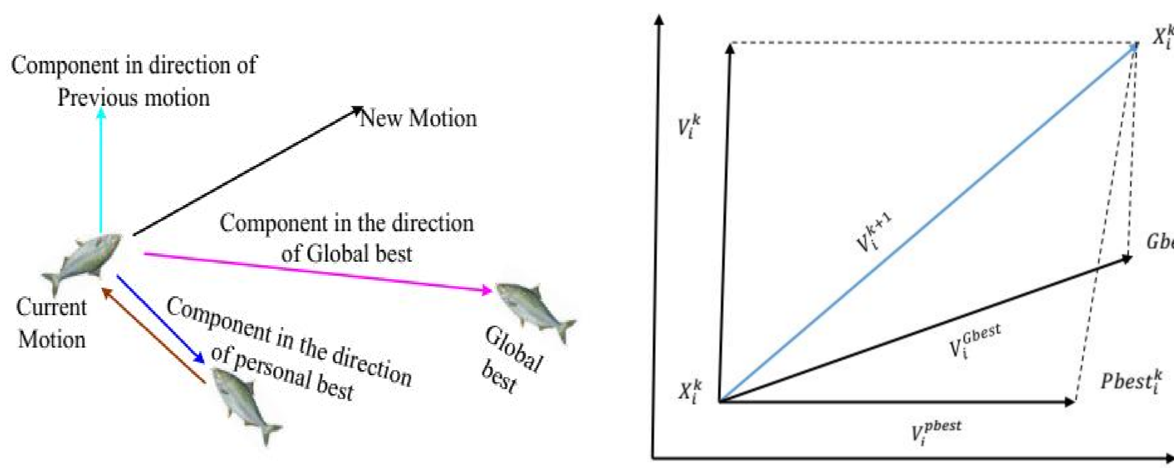

Figure 2.2 Concept of a searching point by PSO and multidimensional search space

2.8 Literature Review

(Myat and Soe, 2022) According to the study, STATCOM's application in the transmission system to control voltage with a fast and efficient reactive power supply is currently under discussion. For the Yangon Electricity Supply System, a voltage stability analysis is done. The voltage stability of the system is analyzed for a range of loading scenarios and contingency situations with the maximum loading. The result indicates that the bus voltage magnitude has increased as a result of reactive power assistance provided at the selected bus that is supported by the PSO method. It has been observed that the test system's voltage stability has significantly increased and that active and reactive power loss has decreased since implementing the particle swarm optimization technique.

However, a significant gap identified is the reliance on capacitors as the energy source for STATCOM. While capacitors provide effective short-term reactive power compensation, their limited energy storage capacity and slower response times constrain the system's performance under dynamic load conditions and disturbances. To address this limitation, integrating Battery Energy Storage Systems (BESS) with STATCOM offers a more versatile and robust solution. BESS can deliver both reactive and active power support, enabling quicker and more substantial responses to voltage fluctuations and transient events. This integration not only enhances the operational flexibility and responsiveness of the system but also improves overall voltage stability and reduces power losses more effectively than capacitors alone.

(Sucitam et al, 2018) This study aims to evaluate and improve the reliability of the 150 kV Subsystem Cirata electric power systems. This will be achieved by investigating how disturbance contingency (N-2) affects variations in current and voltage, identifying the bus voltage that exceeds operating limits, identifying the transmission line that was subjected to the imposition of critical/exceeds limit operation, and introducing load shedding to rectify the power system weaknesses brought about by disruption contingency. The investigation was conducted by collecting the necessary data for power flow simulation using ETAP 12.6.0's Newton-Raphson technique.The author explores contingency analysis and looks for ways to improve the system; in particular, load shedding is discussed as a way to guarantee voltage stability in the subsystem. All the same, it is crucial to understand that load shedding is not a complete solution. The rationale for this is that, despite its effectiveness in managing voltage stability, load shedding may result in power outages, which raises questions about the dependability of the system.

(Ali et al, 2019) The study offers recommendations for STATCOM installation to maintain the subsystem's voltage profile if the transmission lines are unavailable. Using a 150 kV interconnected subsystem, where the loss of two 150 kV transmission lines could result in voltage instability throughout the linked subsystem, the suggested approach is proven. The writers solely employ static synchronized compensation (STATCOM) to guarantee that the voltage profile is maintained in the event of transmission losses. Not accounted for are any other conditions, such as different load settings. The STATCOM is the only power source the system needs to function; no extra electricity is used.

(Tebeje and Teshome ,2022) The objective of this thesis was to enhance the voltage profile and reduce power loss for the transmission networks that make up Ethiopian Electric Power (EEP) systems, which include 400 kV, 230 kV, and 132 kV. The Newton-Raphson technique for power flow analysis was carried out using MATLAB code, and the system was simulated using PSAT (Power System Analysis Toolbox). The best position and size for the STACOM have also been determined using particle swarm optimization (PSO) techniques. Two objective functions and five restrictions are present in these methods. To identify unstable buses, a user-defined enhanced voltage stability index, or AVSI, has been put into place. This method makes greater sense for meshed and high-voltage transmissions. I only aim to bridge one single gap in this work: the performance of the Static Synchronous Compensator (STATCOM) through the application of hybridization. The voltage drop within the network is the sole thing being examined; a contingency analysis is not included.

(Marcin et al, 2021) This article introduces the idea of a battery energy storage system used as an emergency power source for a separate power network. One-side supply power substations could be able to function as islands. When power transmission is restricted due to damage or main power line disconnection, this system, which has an adequately sized energy storage capacity, increases the isolated network's stability and allows for greater power supply continuity for a certain length of time. In order to provide a backup power source for a different power network, this article suggests the idea of a battery energy storage system. It is anticipated that the use of this battery energy storage technology will cut the number of power outages that happen between three and one and a half hours in half. It is pointed out that a combination with a FACTS (Flexible AC Transmission System) device may enable even higher efficiency and a longer lifespan.

(Dung et al, 2019) This work introduced two Newton-Raphson method algorithms for load flow analysis in a power system with STATCOM. These techniques were used to create MATLAB programs that were implemented for the IEEE 5-bus, IEEE 14-bus, and IEEE 30-bus systems. Reactive power can be injected or absorbed by the STATCOM to control the voltage magnitude of the buses to which it is attached, according to the simulation results. The two algorithms' correctness was verified based on the findings received. In terms of computation speed, the direct algorithm is more dependable and efficient. For load flow analysis in a power system using STATCOM integration, two Newton-Raphson method algorithms were provided in this study. Notably, however, the positioning and balancing of the entire network system relies only on STATCOM's ability to supply or absorb reactive power to regulate the voltage magnitude at the buses that link to it. Integrating a battery energy system with STATCOM may enable the fulfillment of active power requirements and provide a more comprehensive power system solution.

(Okelola et al, 2021) For this reason, to increase system voltage magnitudes and minimize active power loss, particle swarm optimization, or PSO, is used in this research to distribute the STATCOM. An IEEE 14-bus network was used to test the proposed method using Matlab software, and the results were given. The statistics indicated a 6.90% reduction in the total active power loss. The system voltage profile improved for Buses 7 and 13 after their voltage magnitudes, which were over the maximum voltage limit, were lowered and brought within acceptable voltage limits. The efficiency and functionality of STATCOM through an appropriate allocation system swarm optimization (PSO) is shown to be beneficial for appropriate STATCOM allocation in this work, which focuses mainly on minimizing active power losses in the transmission line.

This study does, however, have a significant flaw in that it just looks at current system losses; contingencies are not taken into account, and there are no further sources of assistance, like battery energy storage.

(Muluneh and Ashenaf, 2022) In an N-1 contingency, the 400 kV Ethiopian Electric Power (EEP) system's static security assessment (SSA) with IPFC integration is examined in this study. The interline power feed controller's (IPFC) optimal location was identified by utilizing bus and line loading-based composite severity indices (CSI) to evaluate the system's state. In this study, the IPFC optimum was sized using the Grey Wolf Optimization (GWO) algorithm since it is a more straightforward method that requires less programming labor and has a higher computing efficiency than other complex programming and optimization techniques. This study assessed the viability of reducing power system safety hazards by utilizing IPFC in conjunction with MATLAB software.

One important problem I observed is the requirement for a backup BES option for the FACTS device. Having reviewed the body of literature in detail, a number of glaring gaps have emerged. I started the current project, which uses the battery-supported STATCOM to improve and optimize the voltage profile of the High voltage transmission line of Adama electric supply system, in response to these gaps. The STATCOM's positioning and sizing will be addressed using a particle swarm optimization (PSO) approach. The scenarios, including contingency scenarios and peak load situations that take transmission line losses into consideration, will be included in the project. The particular backup plan in this work concerns the possibility of the primary incoming power supply from the Koka 132kV line being interrupted. With the MATLAB/Simulink platform, the complete system will be painstakingly modeled in order to guarantee a thorough analysis.

CHAPTER THREE
MATERIALS AND METHODS

3.1 Materials

The project includes the integration of multiple essential materials and components in order to implement the battery-supported STATCOM solution for improving voltage profile issues in the electric supply system of the Adama substation's high-voltage transmission lines. The components include necessary parts like the battery-supported STATCOM, which consists of certain component units that can control transient fluctuations and inject reactive power to increase voltage stability. The project also includes the Battery Energy Storage System (BESS), which consists of batteries that have been designed to enable fast response times and energy storage for STATCOM operations. Advanced systems of monitoring and control, which include control mechanisms and monitoring devices, are an excellent complement to these components.

These systems are essential for managing the STATCOM and facilitating efficient cooperation with the BESS. Additionally, the PSO technique is used in order to specify the placement and size of the STATCOM. MATLAB/Simulink 2021 is the main software package used in this project for system modeling, simulation, and analysis. MATLAB code is used for load flow analysis, and Power World Simulator 2011 is used to construct the single diagram. This includes integrated STATCOM-BESS system simulation, control algorithm creation, and load flow studies. Furthermore, the project makes use of pertinent power system data unique to Adama's 132kV subsystem network, including exact characteristics that facilitate system modeling and simulation. Historical flow data is also utilized to evaluate simulation results and offer insights into energy losses and unsold energy during disruptions brought on by Koka line breakdowns.

3.2 Methodology

This methodology uses modern optimization and simulation tools to ensure a methodical approach to solving voltage stability issues in the electric supply system of the Adama substation.

- **System Analysis and Problem Identification:**Conducted a detailed analysis of the Adama substation's current voltage profile, focusing on the impact of outages from the Koka hydroelectric plant. And identified the critical substations (ADNSS, MTSS, A7KSS, ATSS, ASTSS, and SOSS) affecting the Adama substation’s voltage stability.
- **Data Collection:**Gathered voltage data and power flow statistics from January 30, 2023, to December 29, 2023, for the Adama substation and its connected sources. Documented instances of voltage drops, load shedding, and energy losses at the Adama I wind farm due to these drops.
- **Simulation Setup:** Modeled the Adama substation electric supply system in Matlab 2021a, including all relevant substations and power sources.Simulated the power flow and voltage profiles under normal and contingency (Koka outage) conditions.
- **STATCOM Design:** Utilized particle swarm optimization (PSO) to determine the optimal placement of the STATCOM, specifically targeting the A7KSS bus for maximum impact on voltage stability and designed a 15 MVAR battery-supported STATCOM tailored for the system’s requirements.
- **Implementation and Simulation:** Implemented the PSO algorithm in Matlab to find the best configuration for STATCOM. Integrated the STATCOM into the system model and performed power flow analysis under both normal and contingency conditions.
- **Performance Evaluation:**Compared voltage profiles at key buses (ADSS, AWFG, A7KSS, MTSS, ADNSS, ATSS, ASTSS, SOSS) before and after the STATCOM installation.Evaluated the system’s performance during simulation, focusing on voltage improvements and reductions in load shedding.
- **Validation:**Validated the simulation results by ensuring that the voltage profiles met the required thresholds (0.942 p.u. for Adama I wind farm).Assessed the overall impact on energy losses and unsold energy.

- ➢**Conclusion:**Summarized the improvements in voltage profiles and system reliability due to the STATCOM installation.Highlighted the reduction in energy losses and load shedding, validating the effectiveness of the battery-supported STATCOM solution.

3.2.1 Collecting and Assessing data

To perform an extensive investigation, data collection will take place in 2023. Primary and secondary data were gathered from EEP for this thesis project. The data gathered includes interruption data for Koka and Adama I wind farm generation. Incoming lines require several parameters, such as line impedance, line reactance, line length, bus description, bus nominal voltage, reactive and active power flow, transformer data, the actual voltage level of the line, and peak load data of the case study transmission network. The bus data and transmission line for the chosen system are stated below.

3.2.1.1 Koka 132 kV Incoming Line Interruption Data

This data indicates the date of the interruption, the case of the interruption, and the total unsold energy during the interruption. For this thesis work, this data is the main input because the status of the problem was triggered by this interruption issue, which caused the interruption at the Adama I wind farm. Load shedding and voltage drop will happen on the system network because the awash line cannot handle the whole system network load.where the source of the data is available in Appendix B.

Table 3.1 Koka 132 kV Incoming Line Interruption Data

SNo.	Koka 132kV Line Interruption Date	Cause of Interruption	Interr-uption time	Recon-nection time	Differ e-nce (hr)	Moment Load		Unsold Energy (KWh)
						MW	A	
1.	30/1/2023	Due To Over Current	12:27	12:50	0:23	65	294	24916.66
2.	29/3/2023	No signal	6:24	6:30	0:06	45.5	206	4550.00
3.	10/4/2023	CT Failure at Koka	15:17	17:42	2:25	47	212	113583.3
4.	18/4/2023	For Maintenance	23:12	00:58	01:46	34	155	60066.66
5.	23/6/2023	Due To Over Current	11:07	11:22	0:15	44	194	11000
6.	6/7/2023	Due To Over current	9:05	9:21	0:16	44	194	11733.33
7.	21/7/2023	For Maintenance	22:08	0:38	2:30	44	194	110000
8.	24/7/2023	Due To SC	4:37	7:03	02:26	30	135	73000
9.	31/8/2023	Due To Conductor Burst @B-Phase	06:43	12:27	05:44	39.8	185	218186.6
10.	18/9/2023	Defective relay to read the fault	16:02	18:30	02:28	34	158	83866.66
11.	24/9/2023	Due to over current	12:44	13:49	01:05	67	303	72583.33
12.	3/12/2023	For Maintenance	06:39	08:29	01:50	27	129	49500.00
13.	26/12/2023	Due to Earh Fault	09:58	10:08	00:10	56	280	9333.33
14.	29/12/2023	For Maintenance	6:48	8:37	1:49	47	212	85,383.3

3.2.1.2 Adama I Wind Power Plant Outage Report

The data below details interruptions at the Adama I Wind Farm, including unsold energy and the causes of these interruptions. The primary issue leading to these interruptions is a drop in system voltage, which is the main focus of this thesis work.

Table 3.2 Adama I Wind Power Plant Outage Report

No.	Interruption Date	Cause of Interruption	Interruption time	Re-connection time	Difference (hr)	Energy Loss(MU)
1.	30/01/2023	System Voltage drop 128kv-113kv	12:23	12:57	00:34	0 MU
2.	29/03/2023	External voltage block	06:25	06:57	00:32	0 MU
3.	10/4/2023	System Voltage drop _119kv	15:18	18:02	02:44	0.058MU
4.	10/5/2023	System Voltage drop_119kv	8:15	9:13	0:58	0.00197MU
5.	23/6/2023	System Voltage drop_ 114kv	11:08	11:39	0:31	0.0033MU
6.	6/7/2023	External Voltage Drop	9:05	9:52	0:47	0.0083MU
7.	24/7/2023	External Voltage Drop	04:35	06:25	01:50	0.041MU
8.	29/8/2023	External Voltage Drop	12:45	13:52	01:07	0.01716MU
9.	31/8/2023	External Voltage Drop	06:44	13:44	07:00	0.0557MU
10.	18/9/2023	External Voltage Drop	16:03	16:24	0:21	0.005022909 MU
11.	24/09/2023	External Voltage Drop	12:55	13:56	1:01	0.0003104 MU
12.	3/12/2023	External Voltage Drop	20:31	20:36	0:05	0.001156MU
13.	18/12/2023	External Voltage Drop	17:03	17:31	0:28	0.001107MU
14	26/12/2023	External Voltage Drop	9:53	10:17	0:24	0.01324 MU

3.2.1.3 The current one-line diagram for the EEP grid network

Over the last 20 years, Ethiopia has experienced steady and fast growth. This social and economic progress has been greatly aided by the advancement of electricity. The institution has been tasked with developing power plants, power transmission and substations, wholesale electricity, compliance research, design, and survey work, by the amended Regulation of the Council of Ministers of Ethiopia No. 381/2016, which was issued to establish the Ethiopian Electric Power.

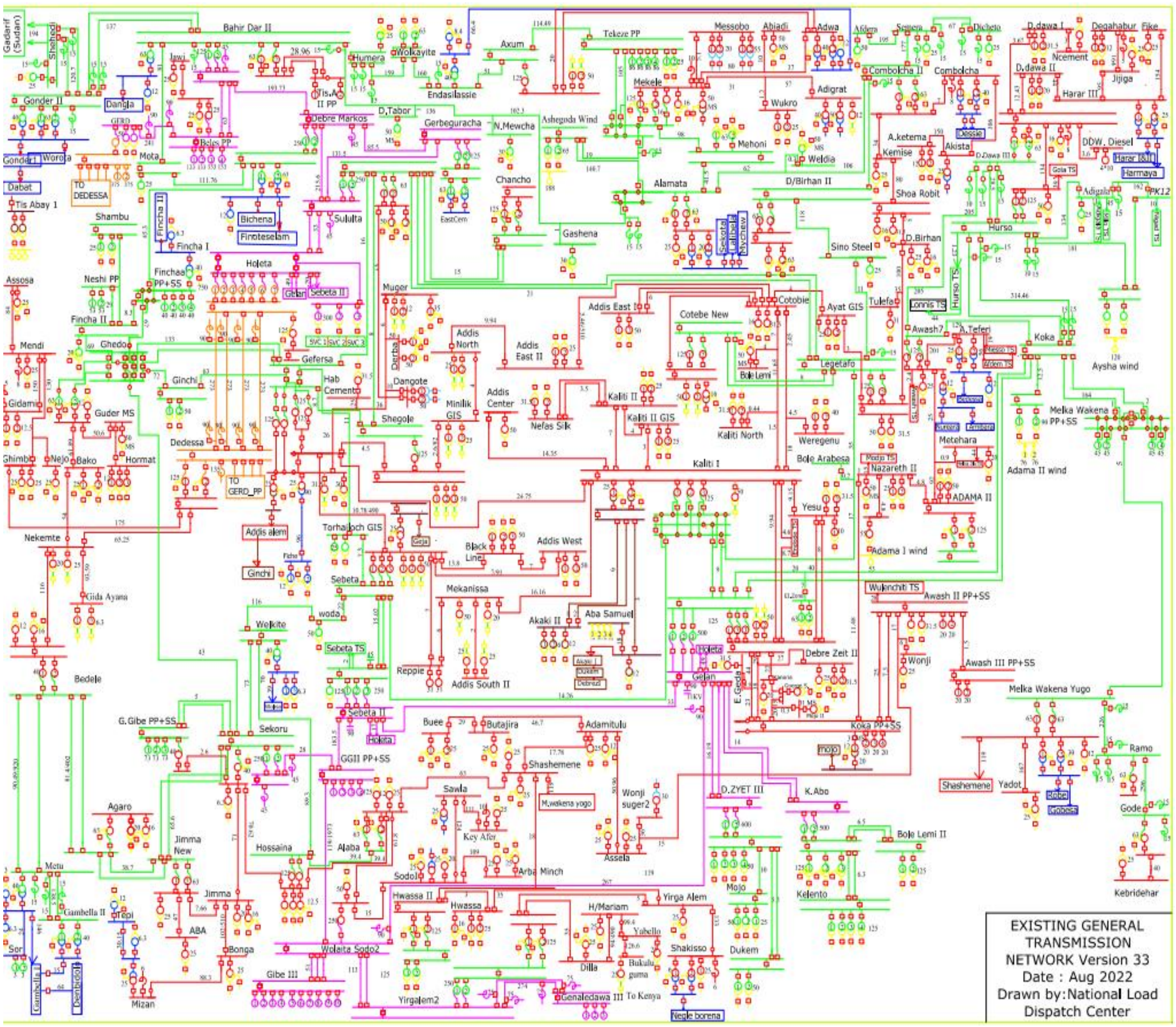

Figure 3.1 The National Load Dispatch Center's drawing of the current general transmission network

EEP is now in charge of twenty-two power plants. 16 of the 4818.2 MW produced by hydropower are hydro: Gibe III (1870 MW), Beles (460 MW), Gilgel Gibe II (420 MW), Tekeze (300 MW), Gilgel Gibe I (184 MW), Melka Wakena (153 MW), Fincha (134 MW), Amarti Neshe (95 MW), Tis Abay II (73 MW), Koka (43.2 MW), Awash II (32 MW), Awash III (32 MW), Tis Abay I (11.4 MW), Aba Samuel (6.6 MW); Genale Dawa III (254 MW) and the Grand Ethiopian Renaissance Dam (the two early generation units of 750 MW) are among.

Ayisha II (80 MW), Adama II (153 MW), Ashgoda (120 MW), and Adama I (51 MW) are the wind power projects that have started to function. The remainder should come from diesel and steam power reserves. High-voltage transmission lines and substations are necessary in addition to power plants to transfer generated power from the plant to the national power grid and to provide high-quality electricity throughout the nation. With voltages ranging from 132 kv to 500 kv, the nation's stretched high-voltage transmission lines are currently over 17,000 km long. These include the 500kv Hidase-Didesa-Holeta, 400kv Wolayta Soddo II-Addis Ababa, 230kv Koka-Hurso-Dire Dawa, 230kv Alaba-Hosana-Giligel GibeII-Gima-Agaro-Bedele, and 230kv Metu- Gambela transmission lines, which are currently in use. (EEP, 2019)

This study looks at the 132 KV transmission line, which is an essential component of Ethiopia's electrical infrastructure, as part of the high-voltage transmission line of the Adama substation electric supply system. A 132 kV transmission line supplies the Adama region with electricity from a number of sources, including the Adama I wind farm, the Koka hydroelectric plant, and the Awash 7-kilo substation. The delivery of power is made possible in large part by this region. This network contains a large number of strategically placed substations, such as Adama Substation (ADSS), Adama New Substation (ADNSS), Mojo Traction Substation (MTSS), Metehara Substation (MSS), Awash 7 Kilo Substation (A7KSS), Awash Traction Substation (ATSS), Asebe Tferi Substation (ASTSS), and Sirba Ounkur Substation (SOSS).

3.2.1.4 Transmission Line Data

There are approximately 11 transmission lines in the study area's current EEP high-voltage transmission network of the Adama substation electric supply system. Ten lines make up the 132 kV network, and one line makes up the 33 kV network. APPENDIX A shows data from the EEP transmission line. Wherein the entire bus system is 132 kV, absent the Adama I wind farm generation 33 kV and 620 V bus system.

Table 3.3 Transmission Line Data

No.	Name	Line length (km)	Transmission line Resistance (per unit)	Transmission line Reactance (per unit)	Transmission line Susceptance (per unit)
1.	KOKA Bus – ADSS Bus	11.49	0.017176	0.02797	0.005169
2.	ADSS Bus - AWFG Bus	4.8	0.007182	0.011695	0.002158
3.	ADSS Bus – MOTSS Bus	14.9	0.022283	0.036287	0.006702
4.	ADSS Bus – ADNSS Bus	12	0. 01088	0.017716	0.008904
5.	ADSS Bus – MTP Bus	92	0.137647	0.22415	0.041365
6.	MTP Bus – MTSS Bus	0.01	0.000015	0.000024	0.0000045647
7.	MTP Bus – A7KSS Bus	25	0.037404	0.06091	0.01124108
8.	A7KSS Bus – ATSS Bus	2.4	0.003589	0.005845	0.00107957
9.	A7KSS Bus – ASTSS Bus	201	0.300596	0.489504	0.09041175
10.	A7KSS Bus – SOSS Bus	30.02	0.044895	0.073109	0.013504
11.	AWFG Bus – AWFG33Kv Bus	7.3	0.017176	0.02797	0.005169

The following factors are calculated by Hoodapprprte: base MVA of 100 MVA (Sb) and base kV of 132 kV (Vb: transmission line length, positive sequence and zero sequence resistance, inductance, capacitance, and fundamental principles of impedance calculation per unit. (Anjali Atul Bhandakkar and Lini Mathew Dr, 2018)

$$Length\ of\ transmission\ line\ = (\frac{\sqrt{X}\sqrt{B}}{2\pi f}) * (Velocity\ of\ LIGHT\ in\ km/\text{sec}) \dots\dots. (3.1)$$

The transmission line length (km), line resistance (ohm/km), and line reactance (ohm/km) make up the EEP data that was gathered. For MATLAB/Simulink, the line length (km), line resistance (ohm/km), line capacitance (F/km), and line reactance (ohm/km) are utilized. However, while working with MATLAB/Simulink software, the reactance of the line must be converted to the inductance of the line.

Table 3.4 Actual values of positive sequence and zero sequence parameters of the transmission line

No	Name of Bus	R_1 $(\mho/km)$	R_0 $(\mho/km)$	L_1 (H/km)	L_0 (H/km)	C_1 (f/km)	C_0 (F/km)
1.	KOKA to ADSS Bus	0.26046	0.78138	0.00135	0.00405	$8.2489 * 10^{-7}$	$2.47467 * 10^{-6}$
2.	ADSS to AWFG Bus	0.2607	0.7821	0.00135	0.004055	$8.212 * 10^{-9}$	$2.4636 * 10^{-8}$
3.	ADSS to MOTSS Bus	0.2606	0.7818	0.001351	0.004053	$8.22 * 10^{-9}$	$2.466 * 10^{-8}$
4.	ADSS to ADNSS Bus	0.158	0.474	0.0008192	0.0024578	$1.3561 * 10^{-8}$	$4.068 * 10^{-8}$
5.	ADSS to MTP Bus	0.26067	0.782	0.001352	0.004056	$8.2179 * 10^{-9}$	$2.4653 * 10^{-8}$
6.	MTP to MTSS Bus	0.26136	0.78408	0.0013315	0.003994	$8.3429 * 10^{-9}$	$2.5028 * 10^{-8}$
7.	MTP to A7KSS Bus	0.26069	0.78207	0.0013519	0.0040559	$8.218 * 10^{-9}$	$2.4654 * 10^{-8}$
8.	A7KSS to ATSS Bus	0.26056	0.78168	0.0013514	0.004052	$8.2214 * 10^{-9}$	$2.4664 * 10^{-8}$

9.	A7KSS to ASTSS Bus	0.26057	0.78171	0.00135	0.00405	$8.2213 * 10^{-9}$	$2.4664 * 10^{-8}$
10.	A7KSS to SOSS Bus	0.260576	0.781729	0.0013513	0.004054	$8.2215 * 10^{-9}$	$2.4664 * 10^{-8}$
11.	AWFG to AWFG33Kv Bus	0.26046	0.78138	0.00135	0.00405	$8.2489 * 10^{-7}$	$2.47467 * 10^{-6}$

3.2.1.5 Bus Data with Power Generations/Demands

The maximum power capacity of all sources and the peak load statistics of each substation bus have been gathered and presented in the table below, which you may view in APPENDIX B.

Table 3.5 Bus Data with Power Generations/Demands

No.	Bus Name	Bus Type	Maximum Power Demand/Generation	
			P(MW)	Q(MVAR)
1.	KOKA Bus	Generation	82	10
2.	ADSS Bus	Load	80	20
3.	AWFG Bus	Generation	35	1
4.	MOTSS Bus	Load	20	5
5.	ADNSS Bus	Load	5	1
6.	MTSS Bus	Load	6	1.5
7.	A7KSS Bus	Generation	188	30.17
8.	A7KSS Bus	Load	22	5
9.	ATSS Bus	Load	40	10
10.	ASTSS Bus	Load	20	5
11.	SOSS Bus	Load	76	19

3.2.3 A single-line diagram of the interconnected power system's

Any power system issue should begin with the creation of an interconnected power system single-line diagram, which can be used to find computer solutions. Using the Power World Simulator 2011, a one-line diagram of the case study network, the high-voltage transmission lines of the Adama substation electric supply system, was created for this investigation. The one-line diagram was then fed with all of the organized data.

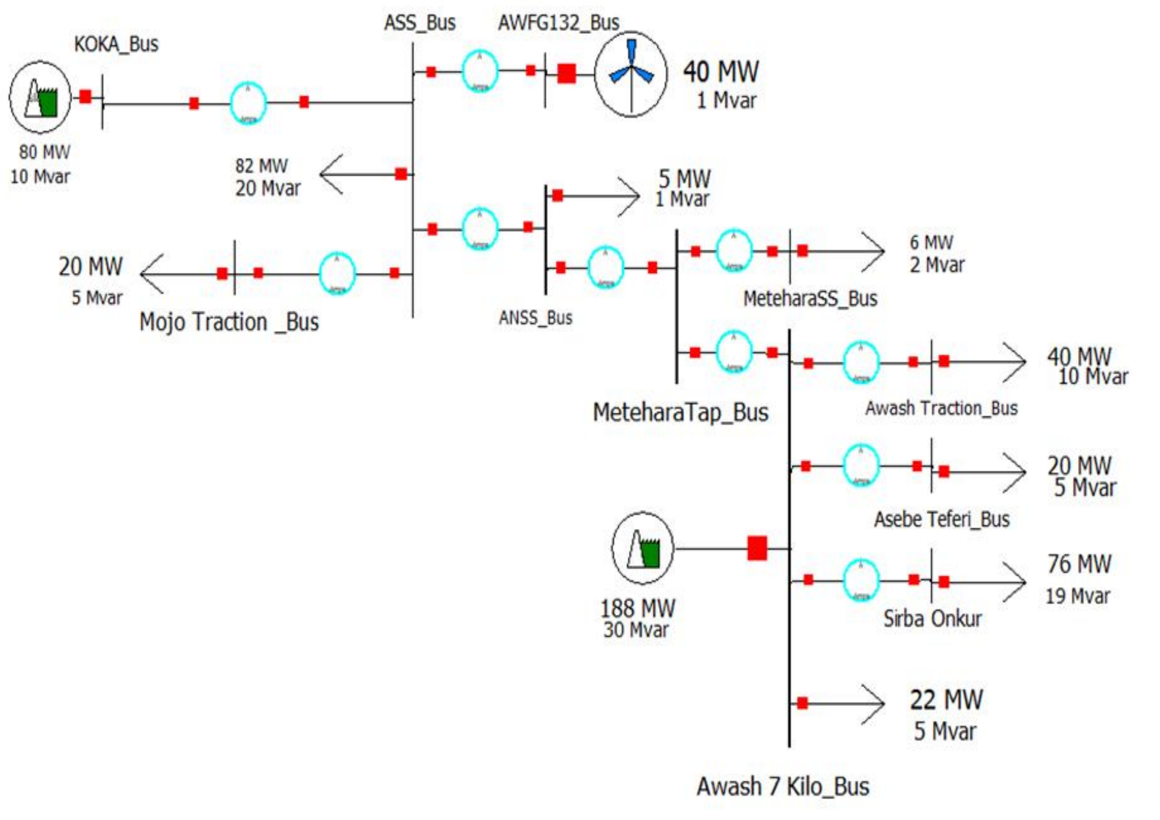

Figure 3.2 A single-line diagram of case study area

3.3 PMSG based grid connected wind turbine system modeling

Depending on how closely they are linked to the grid, wind farms are often classified as standalone or grid-connected. The grid-connected Adama-I wind farm, which is shown in Fig., has been selected for this work's case study. The wind turbine substation, the main grid, the WTG collecting and connecting transmission line, and transformers for step-up units are frequently included in this WF. By using wind turbine blades attached to a blade rotor, wind energy is transformed into mechanical energy that is fed into the generator shaft. Following WTG's conversion of the wind energy from mechanical to AC electric power, a generator-side filter filters the resulting AC electric power before a rectifier converts it to DC power.

The DC-DC boost converter raises the DC power, which is then converted into AC power using an inverter. Once again, the inverter voltage output is filtered using a grid-side filter. The voltage is then stepped up to medium (33 kV) using a WTG unit transformer. Once collected, the wind turbine unit transformer's AC power and voltage output are sent to the wind turbine main substation. As seen in Fig. 1, the wind farm substation raises the 33 kV line voltage to the 132 kV main grid line voltage via a substation transformer. After that, the main grid transmission line delivers the electricity to the national grid. (Hagos and Milkias, 2018)

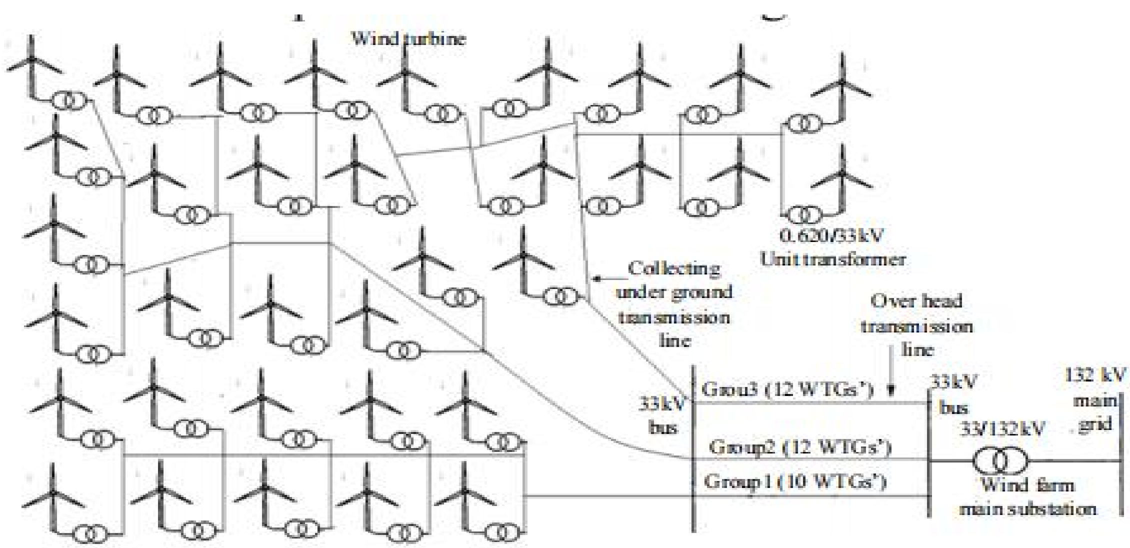

Figure 3.3 Simple layout design of the grid-connected Adama-I wind farm

3.3.1 Aerodynamic Modeling of Wind Turbines

To assess the efficiency of energy conversion in wind energy conversion systems, it is first necessary to calculate the quantity of energy that can be stored in the wind. The kinetic energy of a sizable number of air particles with a total mass of m and a wind velocity of V can actually be understood as the energy in the wind. Assuming that all air particles are moving in the same direction and at the same speed prior to colliding with the rotor blades of the wind turbine, equations (3.2) can be utilized to determine the potential accessible kinetic energy stored in the wind.

$$K_E = \frac{1}{2}\mathrm{mV}^2 \tag{3.2}$$

The total mass (m) of the particles for a given time interval, t, can be computed as follows, assu ming a constant wind velocity:

$$\mathrm{m} = \rho\mathrm{AVt} \tag{3.3}$$

Where, ρ is the air density.

$$K_E = \frac{1}{2}\rho\mathrm{AV}^3\mathrm{t} \tag{3.4}$$

The air power that travels across area A, like the space swept by the rotor blades, can be calculated as follows:

$$P_{\mathrm{W}} = \frac{\mathrm{d}\,K_E}{\mathrm{dt}} = \frac{1}{2}\rho\mathrm{AV}^3 = \frac{1}{2}\rho\pi\mathrm{r}^2\mathrm{V}^3 \tag{3.5}$$

The potential power in the wind can be found where the wind speed is increase. A modest increase in wind speed will result in a big increase in wind power, as we can see from expression (3.5), which states that wind power is proportional to the cube of wind speed. In addition, since power is related to the square of a rotor radius, it is also possible to boost power by increasing the wind turbine rotor radius.

As a result, the wind turbine's ex-tractable power for simulation purposes is provided by:

$$P_m = \frac{1}{2}\rho\mathrm{AV}^3\mathrm{Cp}(\lambda, \beta) \tag{3.6}$$

In this equation, λ is the tip speed ratio, β is the blade pitch angle, Pm is the mechanical power collected from the wind, and Cp is the power coefficient. The power coefficient Cp, also known as Betz's limit, limits the maximum power output of the wind turbine to 59.3%, the greatest theoretical efficiency achievable by a wind energy converter. (Mehedi and Abu, 2021)

A wind turbine's maximum power coefficient will never exceed the Betz factor. The simulation-used constant Cp can be characterized as follows as a function of the pitch angle of the blade and the tip-speed ratio:Where the valuse of power coffients

$$C_p\,(\lambda,\beta) = \mathrm{C1}\left(\frac{\mathrm{C2}}{\lambda i} - \mathrm{C3}\beta - \mathrm{C4}\right) e^{\frac{-\mathrm{C5}}{\lambda i}+\mathrm{C6}\lambda} \quad (3.7)$$

$$\frac{1}{\lambda i} = \frac{1}{\lambda - 0.08\beta} - \frac{0.035}{\beta^3 + 1} \quad (3.8)$$

The values listed in Appendix B for C1, C2, C3, C4, C5, and C6.

The rotor blade tip speed divided by the unaffected wind velocity is known as the tip speed ratio, and it is shown as follows:

$$\lambda = \frac{\text{blade tip speed}}{\text{wind speed}} = \frac{r\omega_r}{V} \quad (3.9)$$

Where is the wind turbine's tip speed ratio, V is its wind speed, r is its rotor radius, and ω_r is its angular speed generator.

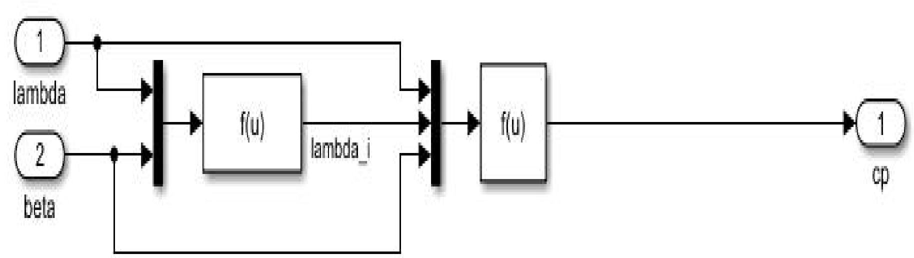

Figure 3.4 Matlab Simulink model for power Coefficients of the Rotor

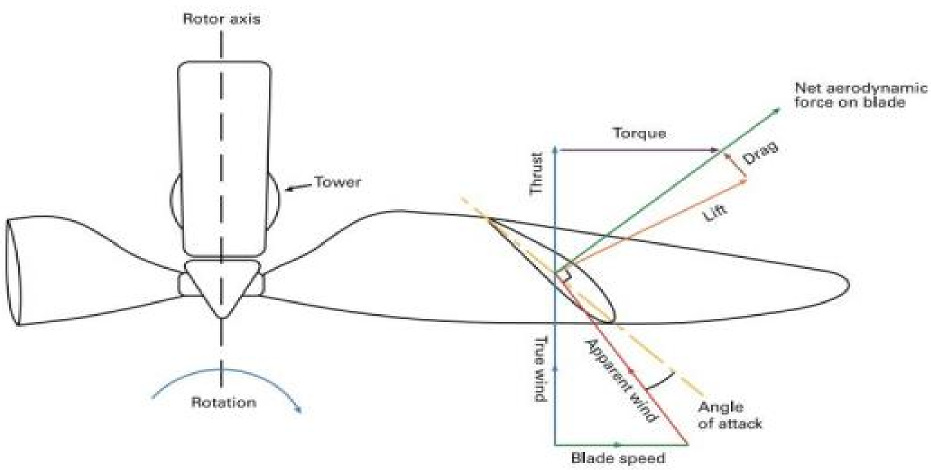

a. *Blade angle diagram*

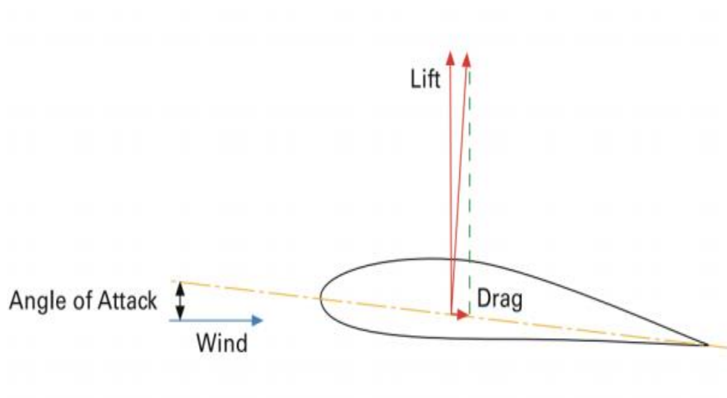

b. Lift and drag force on the blade

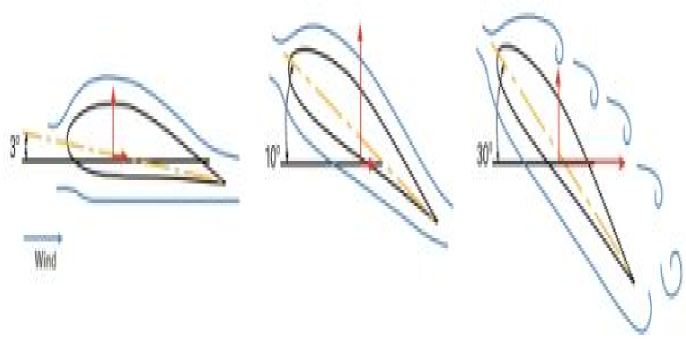

c. *Blade at low medium and high angles of attack*

Figure 3.5 Wind turbine blade angle diagram

Blade angle measurements are used in Figure 3.5 to show how wind velocity affects wind turbine blades. The blade angle is the angle that results from a blade's orientation and the wind velocity vector. When the blade encounters the entire wind velocity effect at β, the wind turbine will generate its maximum power from the wind. When the wind speed is lower than the system's specified wind speed, the blade angle is typically set to zero degrees to ensure optimal energy collection efficiency.If the blade angle stays at zero, when the wind speed exceeds the rated value, the system's power collection will be greater than the rated power. If this is done repeatedly, the generator and power equipment will be forced to run at a higher than rated output, which will be harmful to the system. This concern gives rise to the need for a wind turbine control system that can modify the blade angle in reaction to changing wind conditions. The mechanical torque of the wind turbine can be expressed as follows:

$$T_m = \frac{P_m}{\omega r} = \frac{1}{2}\rho\pi r^2 V^2 \frac{Cp}{\lambda} \quad (3.10)$$

Where r is the wind turbine's rotor speed and T_m is the mechanical torque it produces and the system parameters are shown in Appendix A.

3.3.2 Modeling of Drive Train

A hub with blades, a rotor shaft (which is relatively long in wind energy conversion systems with asynchronous generators), a gearbox with generator, and a blade pitching mechanism make up the drive train, or mechanical components, of a wind turbine system. The WTGS drive train system can be modeled as a single lumped mass, two lumped masses, three lumped masses, or even six lumped masses. An accurate transient study of WTGSs requires a six-mass drive train model. However, the lengthy and intricate mathematical computation with small time steps associated with a six-mass drive train model lengthens the simulation time. In order to streamline the computation and maintain a respectable level of transient process accuracy, reduced-mass models are taken into consideration. For the multi pole system generator in this study, no gearbox has been taken into consideration. In this instance, it is considered that the wind turbine is coupled to a low-speed permanent magnet synchronous generator. The one-lumped mass model drive train for the system analysis can be selected using this approximation, and it is provided by the following equation (3.11). [34]:

$$\frac{\mathrm{dwm}}{\mathrm{dt}} = \frac{1}{J_{eq}}(T_m - T_e - \mathrm{B}w_m) \tag{3.11}$$

A wind energy system's equivalent inertia consists of the inertia of the generator and turbine. The generator's rotational inertia can be expressed in kilograms per square meter using the following formula: $J_{eq} = J_g + \frac{J_w}{{n_g}^2}$, the gear ratio; in the present work, there is one since no gearbox has been taken into account, and the system parameters are shown in the Appendix A.

The generator's electrical angular speed (rad/sec) can be expressed as:

$$\omega\mathrm{e} = \frac{\mathrm{zp}}{2}\omega\mathrm{m} \tag{3.12}$$

3.3.3 Modeling of PMSG

Generators with permanent magnets that operate in harmony In wind power-generating systems, PMSGs are essential for converting mechanical power into electrical power. Both the investigation of the steady state and dynamic properties of wind energy conversion systems, as well as the creation of machine control algorithms, require comprehensive mathematical modeling of the PMSG. Several crucial presumptions must be established before creating the PMSG's mathematical model:

- ✓ The rotor and magnet damping effects are negligible;
- ✓ The magnetic saturation effects are disregarded;
- ✓ The eddy current and hysteresis losses are disregarded; and
- ✓ The back electromotive force (EMF) induced in the stator winding is sinusoidal.

3.2.3.1 PMSM modeling in the natural three-phase ABC Stationary Reference frame

A three-phase, two-pole PMSG cross-section is shown in Figure 3.8. The direction of the MMFs of the a, b, and c phase winding, which are caused by the time-varying three-phase AC currents in these stator phase windings, is indicated by the fixed abc axes. The direction of the d-axis fixed at the rotor is where the permanent magnet's flux is directed. In this instance, the rotor and PMSG's angular speeds coincide with the dq-axes' rotation, which indicates the angle between the d-axis and the q-axis, which is fixed.

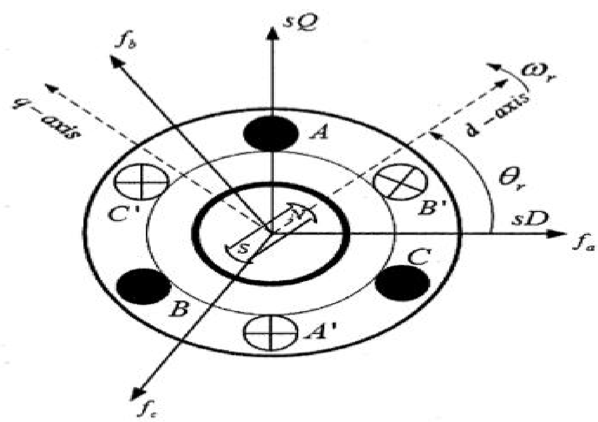

Figure 3.7 The PMSG in cross-section

The phase flux linkages resulting from the PMSG and stator currents, as well as the state space relationship between the PMSG terminal voltages and phase currents, may be calculated using the following equations (3.13).

$$\begin{cases} V_{as} = R_s\, i_{as} + \frac{d}{dt}\lambda_{as} \\ V_{bs} = R_s i_{bs} + \frac{d}{dt}\lambda_{bs} \\ V_{cs} = R_s\, i_{cs} + \frac{d}{dt}\lambda_{cs} \end{cases} \quad (3.13)$$

Where Vas, Vbs, Vcs and are the instantaneous a, b, and c three-phase stator voltages, and i_{as} ,i_{bs} , i_{cs} the instantaneous three-phase stator currents. Here, R_s is the stator winding resistance per phase, and again, λ_{as}, λ_{bs}, and λ_{cs} are the instantaneous flux linkages induced by the three-phase AC currents and the PMG ,which can be calculated in expanded form as the following equations (3.14).

$$\begin{bmatrix} \lambda_{as} \\ \lambda_{bs} \\ \lambda_{cs} \end{bmatrix} = \begin{bmatrix} L_{aa} & L_{ab} & L_{ac} \\ L_{ba} & L_{bb} & Lbc \\ L_{ca} & L_{cb} & Lcc \end{bmatrix} . \begin{bmatrix} i_{as} \\ i_{bs} \\ i_{cs} \end{bmatrix} + \begin{bmatrix} \lambda_r \cos(\theta) \\ \lambda_r \cos(\theta - \frac{2\pi}{3} \\ \lambda_r \cos(\theta + \frac{2\pi}{3} \end{bmatrix} \quad (3.14)$$

Where, L_{aa} , , L_{bb} and , L_{cc} are the self-inductances of the a, b, and c three-phases, and L_{ab}, L_{ac} ,L_{ba} , L_{bc}, L_{ca}, and L_c are the mutual inductances between these phases, while, λr , is the rotor flux linkage caused by the permanent magnet synchronous generator. The self-inductances and mutual inductances are all functions of θ. Thus, all of the inductances are time varying parameters. (Sibdas et al, 2014)

3.3.3.2 Modeling of the PMSG in the rotating reference frame using dq-axes

In order to streamline the examination of synchronous machinery models, the First presented by R. H. Park in 1929 (Sibdas et al, 2014) , Park's transformation is needed. The popular machine model in the dq-reference frame, where the d-axis is orthogonal to the d-axis and the d-axis is aligned with the magnet axis, is synchronously rotating with the rotor and is commonly used to analyze PM synchronous machines. Phase quantities, such as stator voltages, stator currents, and flux linkages, vary with time in three-phase systems, such as PMSMs. Park's transformation converts the AC numbers into DC quantities that are time-independent. Park's transformation is essentially the projection of the phase quantities onto a rotating two-axis reference frame.

An electrical system of any kind can be represented by the general technique known as the space phasor theory. It is capable of providing transformation equations for any kind of current, AC or DC-type machine, and number of phases. Complex space vectors are used to express machine quantities like voltage, currents, magnetic flux, etc. The space phasor theory is extremely significant since it accurately characterizes the machine's performance in both steady state and transient operation, and it holds true for any instantaneous variation in voltage and current. It gives a broad and comparatively simple model of poly-phase systems for both transient and steady-state processes, since it is not limited to studying simply the steady-state regime of a balanced three-phase system. (Sibdas et al, 2014)

By employing two orthogonal axes to describe the complex space vectors, this strategy allows the machine to be thought of as having two phases. Using the two-phase machine model reduces the number of equations in the design, making it simpler. The stator structure of a permanent magnet generator is comparable to that of a synchronous generator's wound rotor. The back electromagnetic field generated by an energized coil is the same as that generated by a permanent magnet. This means that a synchronous generator can be used to derive the mathematical model. The equation for the damper windings and the ability to eliminate the field current would be the only differences for a PMSG. (Zaid et al, 2023)

To simulate and comprehend the operation of the machine, analogous circuits are employed. System models are easier to understand and study with the help of this transformation technique. It is simple to extract and model the equivalent circuits of the PMSG from the d-q modeling of the AC machines with the stator voltage equations. It is assumed that the permanent magnet's rotor d axis flux is represented by a continuous current source, which may be explained by the formula $\boldsymbol{\Psi}$f = Lmif. Lastly,the figuree illustrates, using d-q modeling, the analogous circuit of a permanent magnet synchronous generator:(Zaid et al, 2023)

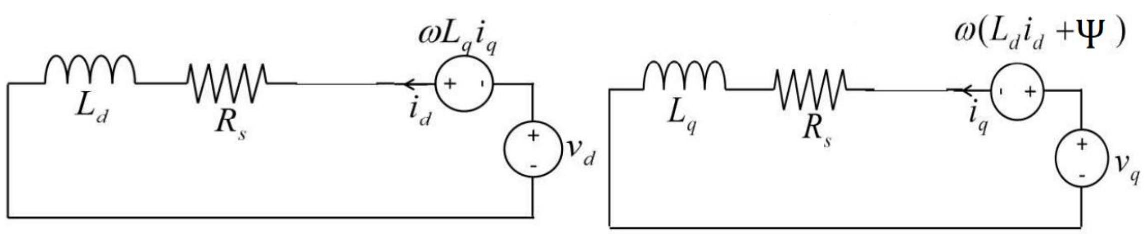

a. *d-axis Equivalent Circuit* *b. q-axis Equivalent Circuit*

Figure 3.8 Equivalent Permanent Magnet Synchronous Generator (PMSG) Circuits in DQ Axes

By applying Kirchhoff's voltage law to the equivalent circuits depicted in Figure 3.9 a and b, state voltage equations for the PMSG are provided in the following.(Zaid et al, 2023)

$$\begin{cases} V_q = \mathrm{Rs}\, i_q + L_q \dfrac{\mathrm{d}i_q}{\mathrm{dt}} - \omega\mathrm{e}\Psi_d \\ V_d = R_s\, i_d + \ L_d \dfrac{\mathrm{d}i_d}{\mathrm{dt}} - \omega\mathrm{e}\Psi_q \end{cases} \tag{3.15}$$

Flux Linkages are given by:

$$\begin{cases} \Psi_q = \mathrm{L}_q\mathrm{i}_q \\ \Psi_d = \mathrm{L}_d\mathrm{i}_d \ \ + \Psi_f \end{cases} \tag{3.16}$$

Substituting equations in (3.15) into (3.16) we can rewrite:

$$\begin{cases} V_q = \mathrm{R}_s\mathrm{i}_q + L_q \dfrac{\mathrm{d}i_q}{\mathrm{dt}} + \omega\mathrm{e}(\mathrm{L}_d\mathrm{i}_d \ \ + \mathit{\Psi}) \\ V_q = \mathrm{R}_s\mathrm{i}_q + L_q \dfrac{\mathrm{d}i_q}{\mathrm{dt}} + \omega\mathrm{e}(\mathrm{L}_d\mathrm{i}_d \ \ + \mathit{\Psi}) \end{cases} \tag{3.17}$$

The generated electromagnetic torque equation, which is provided below, must be completed the PMSG mathematical model and the system parameters are shown in Appendix A.

$$\text{Te} = 3\left(\frac{\text{Zp}}{2}\right)[\Psi iq + (Ld - Lq)idi_q] \quad (3.18)$$

The modeling equation has been constructed in a rotational reference frame (d-q) to help comprehend and study the behavior of a permanent magnet synchronous generator. Coordinates from the three-phase stationary coordinate system are transformed into the d-q rotating coordinate system using the d-q transformation. There are two steps in this transformation process:

- Clarke transformation (from the abc system to the αβ system)
- Park transformation (from the αβ system to the dq system)

Clarke transformation

Given that ia, ib, and ic represent the three-phase instantaneous currents, the complex current may be calculated as:

$$\overline{\text{is}} = \text{ia} + \alpha\text{ib} + \alpha^2\text{ic} \quad (3.19)$$

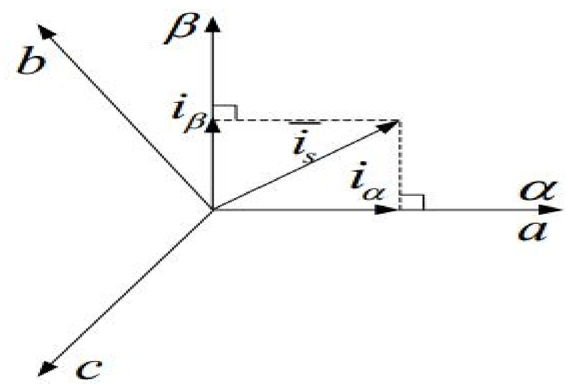

Figure 3.9 Clarke transformation

Where $\alpha = e^{\frac{2\pi}{3}}$ and $\alpha^2 = e^{\frac{-2\pi}{3}}$, represent the spatial operators. Figure 3.12 shows the Clarke transformation, where α and ɑ axis are in the same direction. The complex current $\overline{\text{is}}$ is projected on two orthogonal axes, which are α and β axes. These two axes are also static as the three-phase stationary coordinate system. The Clarke transformation is shown in Figure 3.12, with the α and α axes pointing in the same direction. The projection of the complex current (is) is made on the α and β orthogonal axes. The three-phase stationary coordinate system is also static with respect to these two axes.

Park transformation

The d axis in the Park transformation is in line with the position of the grid voltage. A projection called a "park transformation" projects Is onto dq's spinning orthogonal axes.

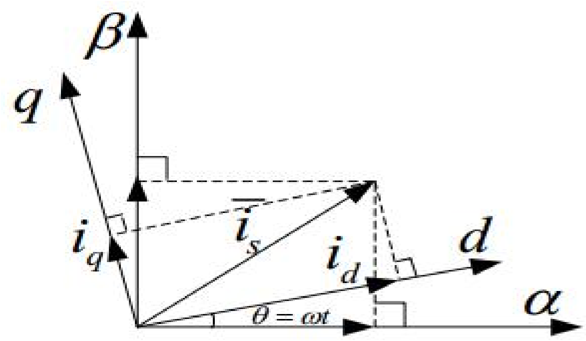

Figure 3.10 Park transformation

Figure 3.12 shows Park transformation, the dq coordinates system is a rotating system, where $\theta = \omega t$ is the grid voltage position. As a result, these two transformations can be combined and written as a matrix form,

$$\begin{cases} \begin{bmatrix} V_d \\ V_q \\ V_o \end{bmatrix} = \sqrt{\frac{2}{3}} \begin{bmatrix} \cos(\omega t) & \cos(\omega t - \frac{2\pi}{3}) & \cos(\omega t + \frac{2\pi}{3}) \\ -\sin(\omega t) & -\sin(\omega t - \frac{2\pi}{3}) & -\sin\left(\omega t + \frac{2\pi}{3}\right) \\ \frac{\sqrt{2}}{2} & \frac{\sqrt{2}}{2} & \frac{\sqrt{2}}{2} \end{bmatrix} \begin{bmatrix} V_a \\ V_b \\ V_0 \end{bmatrix} \\ \begin{bmatrix} i_d \\ i_q \\ i_o \end{bmatrix} = \sqrt{\frac{2}{3}} \begin{bmatrix} \cos(\omega t) & \cos(\omega t - \frac{2\pi}{3}) & \cos(\omega t + \frac{2\pi}{3}) \\ -\sin(\omega t) & -\sin(\omega t - \frac{2\pi}{3}) & -\sin\left(\omega t + \frac{2\pi}{3}\right) \\ \frac{\sqrt{2}}{2} & \frac{\sqrt{2}}{2} & \frac{\sqrt{2}}{2} \end{bmatrix} \begin{bmatrix} i_a \\ i_b \\ i_o \end{bmatrix} \end{cases} \quad (3.20)$$

The inverse transformation from d, q system to a, b, c system can be expressed as following.

$$\begin{cases} \begin{bmatrix} V_a \\ V_b \\ V_0 \end{bmatrix} = \sqrt{\frac{2}{3}} \begin{bmatrix} \cos(\omega t) & -\sin(\omega t) & \frac{\sqrt{2}}{2} \\ \cos(\omega t - \frac{2\pi}{3}) & -\sin(\omega t - \frac{2\pi}{3}) & \frac{\sqrt{2}}{2} \\ \cos(\omega t + \frac{2\pi}{3}) & -\sin\left(\omega t + \frac{2\pi}{3}\right) & \frac{\sqrt{2}}{2} \end{bmatrix} \begin{bmatrix} V_d \\ V_q \\ V_o \end{bmatrix} \\ \begin{bmatrix} i_a \\ i_b \\ i_o \end{bmatrix} = \sqrt{\frac{2}{3}} \begin{bmatrix} \cos(\omega t) & -\sin(\omega t) & \frac{\sqrt{2}}{2} \\ \cos(\omega t - \frac{2\pi}{3}) & -\sin(\omega t - \frac{2\pi}{3}) & \frac{\sqrt{2}}{2} \\ \cos(\omega t + \frac{2\pi}{3}) & -\sin\left(\omega t + \frac{2\pi}{3}\right) & \frac{\sqrt{2}}{2} \end{bmatrix} \begin{bmatrix} i_d \\ i_q \\ i_o \end{bmatrix} \end{cases} \quad (3.21)$$

Space Phasors of Generators Variables

If X_a ,X_b, and X_c are the 3-phase generators quantities the equations (3.14), where by: -

$$\begin{cases} X_a = \hat{x}\cos(\omega t) \\ X_b = \hat{x}\cos\left(\omega t - \frac{2\pi}{3}\right) \\ X_c = \hat{x}\cos\left(\omega t - \frac{4\pi}{3}\right) \end{cases} \quad (3.22)$$

The Space Phasor in the 3-phase system obtained from the vector sum of the 3-phase quantities, i.e.

$$\widehat{X} = \frac{2}{3}\left(Xa + Xb\, e^{\frac{j2\pi}{3}} + Xce^{\frac{j4\pi}{3}}\right) \quad (3.23)$$

Where; $$e^{\frac{j2\pi}{3}} = \cos\left(\frac{2\pi}{3}\right) + j\sin\left(\frac{2\pi}{3}\right) \quad (3.24)$$

$\widehat{X}$ is called the space phasor or complex space vector

In Stationary 2-Phase system, the space phasor is defined as: -

$$\widehat{X} = X_d + jX_q \quad (3.25)$$

The zero sequence component is zero in the case of three-phase balanced system variables. If not, the following formula can be used to determine the zero-sequence component:

$$\widehat{X} = \frac{1}{3}(X_a + X_b + X_c) \tag{3.26}$$

The Space phasor in the 2-phase system must equal that in the 3-phase system. Hence,

$$\begin{cases} X_d = \mathrm{Re}[\widehat{X}] = \mathrm{Re}\left[\frac{2}{3}(X_a + \alpha X_b + \alpha^2 X_c)\right] = \frac{2}{3}\left(X_a - \frac{1}{2}X_b - \frac{1}{2}X_c\right) \\ X_q = \mathrm{Im}[\widehat{X}] = \mathrm{Im}\left[\frac{2}{3}(X_a + \alpha X_b + \alpha^2 X_c)\right] = \frac{1}{\sqrt{3}}(X_b - X_c) \end{cases} \tag{3.27}$$

$\begin{bmatrix} X_d \\ X_q \\ X_o \end{bmatrix} = \begin{bmatrix} \frac{2}{3} & -\frac{1}{3} & -\frac{1}{3} \\ 0 & \frac{1}{\sqrt{3}} & -\frac{1}{\sqrt{3}} \\ \frac{1}{3} & \frac{1}{3} & \frac{1}{3} \end{bmatrix} \begin{bmatrix} X_a \\ X_b \\ X_0 \end{bmatrix}$, Under balanced Conditions, the Zero Sequence Component adds to Zero, i.e: $X_0 = (X_a + X_b + X_c) = 0$

Assuming the balanced Conditions, the abc-dq transformation:

$$X_{dq} = T_{abc} X_{abc} \tag{3.28}$$

Where;

$$T_{abc} = \begin{bmatrix} \frac{2}{3} & -\frac{1}{3} & -\frac{1}{3} \\ 0 & \frac{1}{\sqrt{3}} & -\frac{1}{\sqrt{3}} \\ \frac{1}{3} & \frac{1}{3} & \frac{1}{3} \end{bmatrix}$$

The Inverse Transform (dq-abc transformation) is given by:

$$X_{abc} = T_{abc}{}^{-1} X_{dq} \tag{3.29}$$

Where;

$$T_{abc}{}^{-1} = \begin{bmatrix} 1 & 0 & 1 \\ -\frac{1}{2} & \frac{\sqrt{3}}{2} & 1 \\ \frac{-1}{2} & -\frac{\sqrt{3}}{2} & 1 \end{bmatrix}$$

$$\begin{cases} X_a = X_d + X_0 \\ X_b = -\frac{1}{2}X_d + \frac{\sqrt{3}}{2}X_q + X_0 \\ X_c = -\frac{1}{2}X_d - \frac{\sqrt{3}}{2}X_q + X_0 \end{cases} \quad (3.30)$$

By using equation (3.29) the three phase currents, can be determined as follows. (Boldea, 2017)

$$\begin{cases} i_a = i_\alpha + i_0 \\ i_b = -\frac{1}{2}i_\alpha + \frac{\sqrt{3}}{2}i_\beta + i_0 \\ i_c = -\frac{1}{2}i_\alpha - \frac{\sqrt{3}}{2}i_\beta + i_0 \end{cases} \quad (3.31)$$

The elements on the fixed (α-β) reference frame can be converted to the rotating (d-q) reference frame of coordinates, so they become independent of time. For instance, the following equation can be used to find the current components i_d and i_q in a d-q reference frame (Hau, 2013):

$$\begin{cases} i_d = i_\alpha \cos\theta + i_\beta \sin\theta \\ i_q = -i_\alpha \sin\theta + i_\beta \cos\theta \end{cases} \quad (\ 3.32)$$

It is assumed that the d-axis in the rotor flux-oriented d-q system is aligned with the rotor flux space phasor, with θ representing the rotor flux position. In this instance, the components that produce flux and torque are denoted as i_d and i_d, respectively. Since the phasor components in this reference frame are independent of time, they can be readily manipulated. The components of the d-q coordinate system can be computed from the foregoing equations (3.20) using the direct computation for cos θ and sin θ, given the rotor position θ. Equation (3.32) can be used to compute cos θ and sin θ directly.

$$\begin{cases} \sin\theta = \frac{\Psi_{r\beta}}{\Psi_{r\alpha}} \\ \cos\theta = \frac{\Psi_{r\alpha}}{\Psi_{r\beta}} \end{cases} \quad (3.32)$$

Based on the components i_d and i_q from d-q reference frame, the α-β system Coordinates can be determined by using the following equation (3.33).

$$\begin{cases} i_\alpha = i_d \cos\theta - i_q \sin\theta \\ i_\beta = i_d \sin\theta + i_q \cos\theta \end{cases} \quad (3.33)$$

This model was designed using the above equations in order to perform the conversion from d-q to a-b-c (equation 3.30 and 3.33). By using equation (3.34) the three phase voltages, can be determined as follows.

$$\begin{cases} V_a = V_\alpha + V_0 \\ V_b = -\frac{1}{2}V_\alpha + \frac{\sqrt{3}}{2}V_\beta + V_0 \\ V_c = -\frac{1}{2}V_\alpha - \frac{\sqrt{3}}{2}V_\beta + V_0 \end{cases} \quad (3.34)$$

3.3.4 Uncontrolled Diode Rectifier

The diode rectifier is used in this work for converting the three-phase output AC voltage at the terminals of the PMSG into a DC voltage. The rectified Output dc voltage (V_{rec}) from a three-phase diode rectifier is given by : (Monika et al, 2020)

$$V_0 = V_{rec} = \frac{3\sqrt{2}}{\pi} V_{llrms} \quad (3.35)$$

Where, V_{llrms} is the rms value of the line-to-line voltage applied to the rectifier.

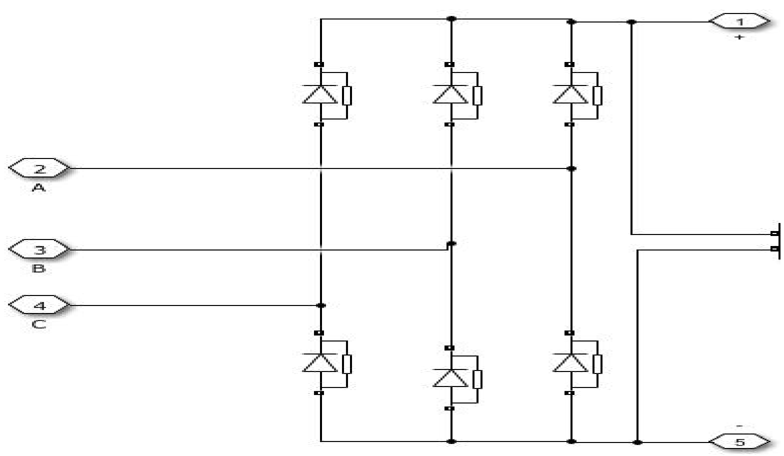

Figure 3.11 Three-phase diode Rectifier

3.3.4.1 DC/DC Converter

This electronic device modifies the DC voltage input level to provide an alternate DC voltage output. There are three main configurations for the dc-dc converter architecture. In this work, boost converters have been utilized.

3.3.4.2 Boost converter

The boost converter is made up of four components: an electrical switch, a capacitor, a diode, and an inductor. The boost converter's components are shown in the diagram below. Put another way, the average output voltage is determined by the length of time that switching is on and off. This is conceivable thanks to the PWM signal. A regular frequency adjustment is made to the ON and OFF periods of the switch. The ON time to switching time ratio is known as the switching duty cycle, or D. The energy absorption and injection in proportion to the duration of the switching period determine the two different modes of operation for the converter: continuous conduction mode (CCM) and discontinuous conduction mode (DCM).

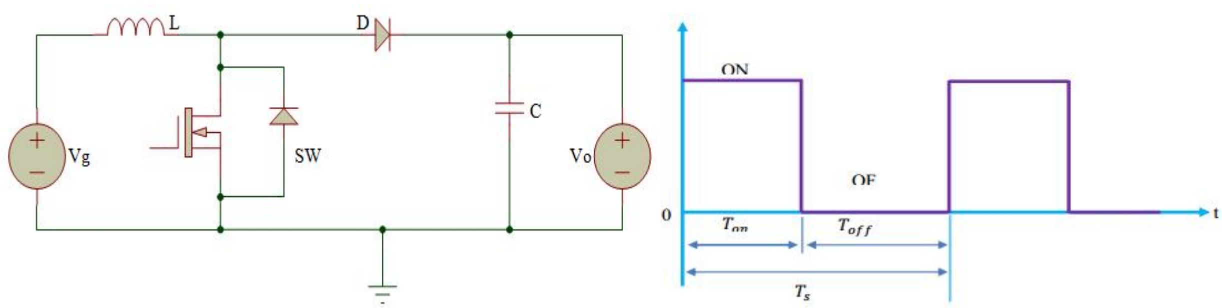

(a) *(b)*

Figure 3.12 a,b Circuit Diagram of Boost Converter and Waveform of PWM.

3.3.5 DC-link model

Figure 3.13 shows the equivalent circuit. The DC-link capacitor connects the grid side converter and the machine side converter (Mahdieh et al, 2021) (Karrar et al, 2021) (William et al, 2003).

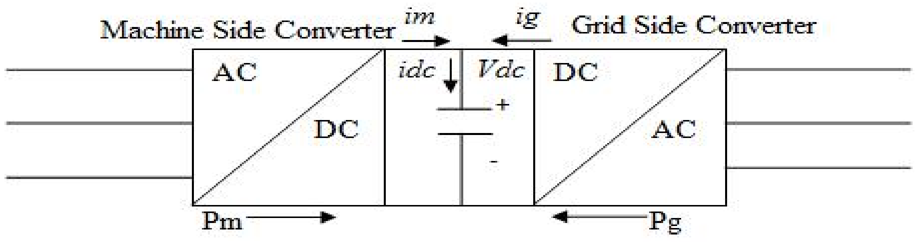

Figure 3.13 DC-link Model

Figure 3.13 shows the DC-link voltage as well as the capacitance and power flows from renewable sources to the machine-side converter (Pm) and grid-side converter (Gd). Equation (3.42) provides the amount of energy that is stored in the capacitor.

$$W_{dc} = \frac{1}{2}CV^2 \qquad (42)$$

The energy in the DC-link capacitor is dependent on both machine-side and grid-side power flows when the energy losses are negligible enough to be ignored. Equation (3.43) is one way to represent the relationship.

$$\frac{dW_{dc}}{dt} = P_g + P_m \qquad (43)$$

Extracting the derivative part, then (3.42) becomes (3.43).

$$CdV_{dc}\frac{dV_{dc}}{dt} = P_g + P_m \qquad (44)$$

Where;

$$P_m = V_d\, i_d + V_q\, i_q$$

$$P_g = V_{dg}\, i_{dg} + V_{qg}\, i_{qg}$$

Equation (3.44) makes it evident that a continuous DC-link voltage is needed, $-P_g = P_m$ necessitating the delivery of all machine power to the grid side.

3.3.6 Grid side converter

Typical DC/AC inverters, like the one shown in Figure 3.14, consist of six IGBTs that reverse a DC power input into a controlled three-phase AC power output in response to control signals provided to the IGBTs' gate circuits. An IGBT's gate circuits typically use control signals that are produced by a PWM signal generator. A comparator and a saw tooth or triangle waveform with repeating switching frequencies are needed to obtain a PWM signal in the simplest method. A sinusoidal control signal and a triangle waveform are compared in order to generate a sinusoidal output voltage waveform.

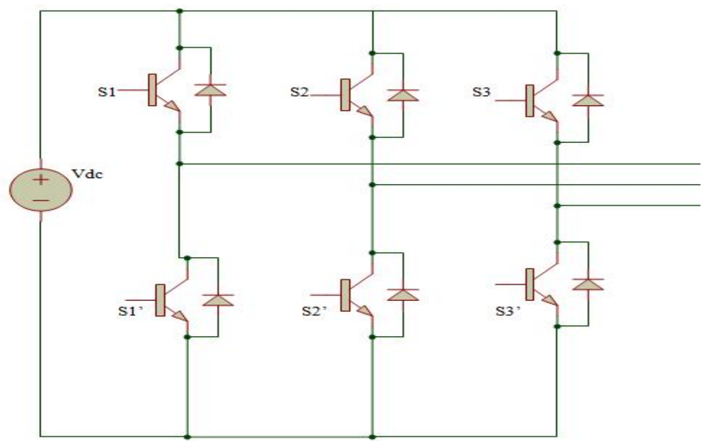

Figure 3.14 Three-Phase Voltage Source

A consistent value, such as 1 V, is always maintained for the triangular waveform's amplitude. The PWM generator output is either in the high or low state, depending on whether the value of the sinusoidal control signal is greater than the value of the triangle waveform. The primary output voltage waveform frequency and the sinusoidal control signal frequency are both determined by the frequency of the triangle waveform, which also generates the inverter switching frequency. Within the PWM algorithm, two terms are defined: frequency modulation ratio and amplitude modulation ratio. It is defined as the amplitude modulation ratio.

$$m_a = \frac{V_{control}}{V_{tri}} \qquad (3.45)$$

Where;

V_{tri} is the sinusoidal control signal amplitude, and $V_{control}$ is the amplitude of the triangle waveform. It is defined as follows: the frequency modulation ratio

$$m_f = \frac{f_{tri}}{f_{control}} \qquad (3.46)$$

Where; f_{tri} is the sinusoidal control signal's frequency, and $f_{control}$ is the frequency of the triangle waveform, commonly known as carrier frequency [47].

3.3.6.1 The grid-side converter system's mathematical model

PWM and vector control techniques are used by the converter. In a dq rotating reference frame, let us assume that are the DC-link voltage and that are the d and q components of the converter output voltages. The d and q component signals needed to generate gate signals are $V_{dnorm} = \frac{V_{d1,2}}{V_{dc}}$ and $V_{qnorm} = \frac{V_{Q1,2}\text{Vq1.2}}{V_{dc}}$, respectively, if the amplitude of the triangle waveform in the PWM generator is 1 V. The PWM generator's amplitude modulation ratio is hence $ma = \sqrt{{V_{dnorm}}^2 + + {V_{qnorm}}^2}$ and the converter output phase peak voltage can be extracted.

It is possible to think of the grid-side converter as a gain control voltage output. In the dq axis reference frame, figure 3.19 depicts the analogous circuit of the grid-side converter with grid filter. In an analogous circuit, where resistance and inductance are substituted, the grid filter is composed of a resistor and an inductor.

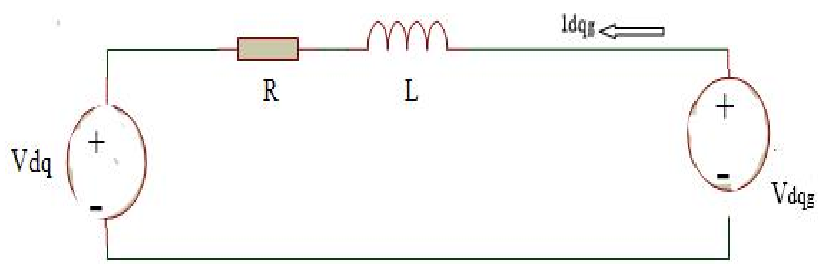

Figure 3.15 Grid Side Equivalent Circuit for Converter in the dq axes reference frame

Applying d, q reference frame, (3.47) becomes (3.48),

$$\begin{bmatrix} V_{dg} \\ V_{qg} \end{bmatrix} = R_f \begin{bmatrix} i_{dg} \\ i_{qg} \end{bmatrix} + \text{Lf}\frac{\text{d}}{\text{dt}}\begin{bmatrix} i_{dg} \\ i_{qg} \end{bmatrix} + \omega s L_f \left[\begin{bmatrix} -i_q \\ i_d \end{bmatrix}\right] + \begin{bmatrix} V_d \\ V_q \end{bmatrix} \quad (3.47)$$

$$\text{V}_{\text{dqg}} = R_f . i_{dqg} + \frac{\text{d}i_{dqg}}{\text{dt}} + \text{ j}\omega\text{s } L_f . i_{dqg} + V_{dq} \quad (3.48)$$

V_{dqg}, i_{dq} and V_{dq} , ωs represent, respectively, the angular frequency of the grid voltages, the instantaneous space vectors of the line current, the converter output voltage, and the grid voltage.The grid development illustrated in Figure employs MATLAB/SIMULINK. The 620V generated by the wind farm is stepped up to 33kV, and after 7.3km of transmission line, it steps up once more to 132kV within the wind farm. Following the stepped-up voltage, the 132 kV enters the Adama 132 kV substation as one of the three incoming source lines, where it goes through the 4.8 km of transmission line. The transformer parameters are displayed in Appendix A.

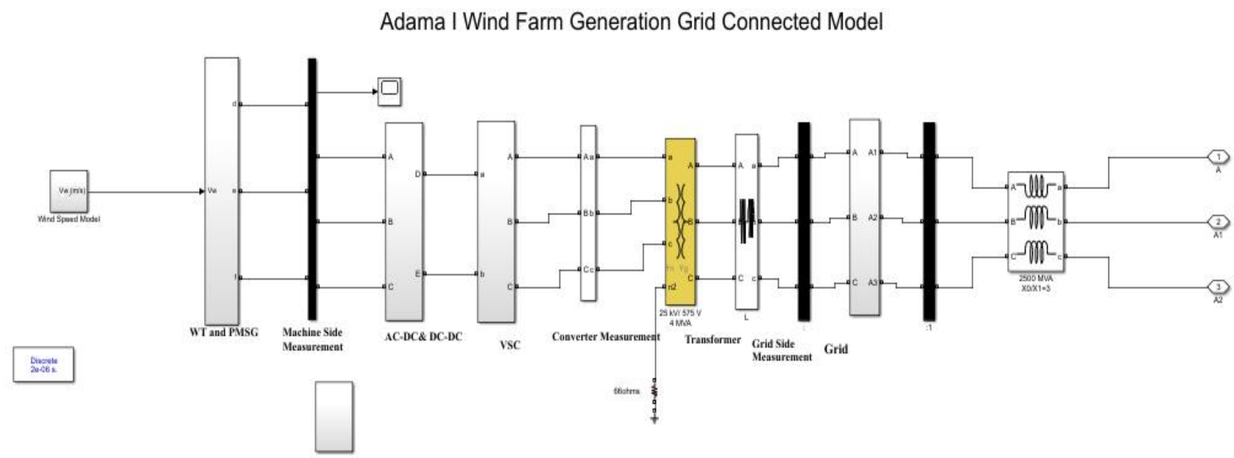

Figure 3.16 Matlab Simulink Model of overall AWFG grid connected

3.4 Model of STATCOM Controller

The STATCOM model is composed of a DC capacitor, three-phase IGBTs or GTOs, and a voltage source converter (VSC). The producing source has three phases at a supply voltage of Vs. The transmission line is represented by an equivalent impedance (Rs + jLs). The load is linked at the common coupling point. A coupling transformer and filter with impedance (Rsh + jLsh) are used to link VSC to the PCC bus, as shown in Figure 1. The inverter's reactive power is sent to the network more easily thanks to the coupling transformer. By dynamically absorbing or generating reactive power, the STATCOM controls the bus voltage. The secondary voltage of the transformer and the network voltage are in phase. (Mahdieh et al, 2021) (Karrar et al, 2021)

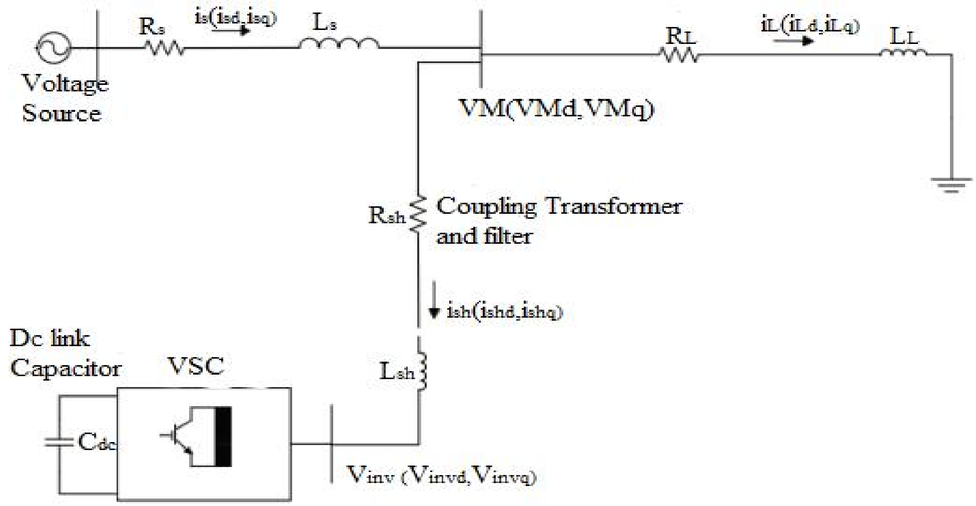

Figure 3.17 Single line circuit of a STATCOM.

3.4.1 Differential equations for the load, shunt, and source components

KVL equations are obtained from Figure (3.26) for the source side, load side, and shunt side of the system. The source-side KVL equations are as follows:

$$\frac{di_{sd}}{dt} = \omega i_{sq} - \frac{R_s i_{sd}}{L_s} + \left(\frac{V_{sd} - V_{Md}}{L_s}\right) \tag{3.49}$$

$$\frac{di_{sq}}{dt} = -\omega i_{sd} - \frac{R_s i_{sq}}{L_s} + \left(\frac{V_{sq} - V_{Mq}}{L_s}\right) \tag{3.50}$$

Equation at load side:

$$\begin{cases} \dfrac{di_{Ld}}{dt} = \omega i_{Lq} - \dfrac{R_L i_{Ld}}{L_L} + \dfrac{V_{Md}}{L_L} \\ \dfrac{di_{Lq}}{dt} = -\omega i_{Ld} - \dfrac{R_L i_{Lq}}{L_L} + \dfrac{V_{Mq}}{L_L} \end{cases} \tag{3.51}$$

Equation at shunt side:

$$\begin{cases} \dfrac{di_{shd}}{dt} = \omega i_{shq} - \dfrac{R_{sh} i_{shd}}{L_{sh}} + \left(\dfrac{V_{Md} - V_{invd}}{L_{sh}}\right) \\ \dfrac{di_{shq}}{dt} = -\omega i_{shd} - \dfrac{R_{sh} i_{shq}}{L_{sh}} + \left(\dfrac{V_{Mq} - V_{invq}}{L_{sh}}\right) \end{cases} \tag{3.52}$$

3.4.2 STATCOM's state space representation

Apply the power balance equation to the inverter's DC side as follows:

$$P_{dc} = P_{ac} \tag{3.53}$$

The dc side power in terms of (Vdc,idc) and the inverter side power in terms of matching current are swapped as follows:

$$V_{dc}i_{dc} = \frac{3}{2}(V_{invd}i_{shd} + V_{invq}i_{shq}) \tag{3.54}$$

Current expression across a capacitor can be written as:

$$i_{dc} = C_{dc}\frac{dV_{dc}}{d_t} \tag{3.57}$$

From equation (3.51) and (3.52).

$$\begin{cases} \dfrac{dV_{dc}}{dt} = \dfrac{3}{2C_{dc}V_{dc}}\left(V_{invd}i_{shd} + V_{invq}i_{shq}\right) \\ \dfrac{di_{ishd}}{dt} = \dfrac{1}{L_{sh}}\left(V_{Md} - V_{invd} - R_{sh}i_{shd} + \omega i_{shq}\right) \\ \dfrac{di_{ishq}}{dt} = \dfrac{1}{L_{sh}}(V_{Mq} - V_{invq} - R_{sh}i_{shq} + \omega i_{shd}) \end{cases} \tag{3.58}$$

The duty ratio d_{abc} , dc voltage of capacitor and inverter voltage of the STATCOM are given by:

$$\begin{bmatrix} d_a \\ d_b \\ d_c \end{bmatrix} = \begin{bmatrix} \frac{1}{2} \\ \frac{1}{2} \\ \frac{1}{2} \end{bmatrix} + \frac{1}{V_{dc}}\begin{bmatrix} V_{inva} \\ V_{invb} \\ V_{invc} \end{bmatrix} \tag{3.59}$$

Using park’s transformation where $[C]$matrix is given as :

$$\begin{bmatrix} \cos\theta & \cos\left(\theta - \frac{2\pi}{3}\right) & \cos\left(\theta + \frac{2\pi}{3}\right) \\ -\sin\theta & -\sin\left(\theta - \frac{2\pi}{3}\right) & -\sin\left(\theta - \frac{2\pi}{3}\right) \\ \frac{1}{2} & \frac{1}{2} & \frac{1}{2} \end{bmatrix} \tag{3.60}$$

Therefore,

$$\begin{cases} d_d = \dfrac{V_{invd}}{V_{dc}} \\ d_q = \dfrac{V_{invq}}{V_{dc}} \\ d_0 = \dfrac{1}{2} + \dfrac{V_{invd}}{V_{dc}} \end{cases} \tag{3.61}$$

Hence equation 3.10 can be written as:

$$\frac{dV_{dc}}{dt} = \frac{3}{2}(d_d i_{shd} + d_q i_{shq})$$

Thus, the state space model can be written as follows:

$$\begin{bmatrix} \dfrac{di_{shd}}{dt} \\ \dfrac{di_{shq}}{dt} \\ \dfrac{dV_{dc}}{dt} \end{bmatrix} = \begin{bmatrix} -\dfrac{R_{sh}}{L_{sh}} & \omega & -\dfrac{d_d}{L_{sh}} \\ -\omega & -\dfrac{R_{sh}}{L_{sh}} & -\dfrac{d_q}{L_{sh}} \\ \dfrac{3}{2C_{dc}}d_d & \dfrac{3}{2C_{dc}}d_q & 0 \end{bmatrix} \begin{bmatrix} i_{shd} \\ i_{shq} \\ V_{dc} \end{bmatrix} + \begin{bmatrix} \dfrac{1}{L_{sh}} & 0 \\ 0 & \dfrac{1}{L_{sh}} \\ 0 & 0 \end{bmatrix} \begin{bmatrix} V_{Md} \\ V_{Mq} \\ 0 \end{bmatrix} \tag{3.62}$$

Representing (3.62),in the general state space form:

$$\dot{X} = [A]X + [B]U \tag{3.63}$$

The 48-pulse converter does not require AC filters for usage in high-voltage and high-power applications due to its extremely low harmonic distortion content on the AC side. As illustrated in Figure below, this converter is made up of four identical three-level GTO converters, each of which needs twelve control pulses. The converters are connected by four phase-shifting transformers. Transformers fulfill two distinct functions in our application: they enhance the output voltage and adjust it to the network's, matching the very high voltage while also performing the phase shifts needed to provide multi-level voltage. We employ full-wave control, which results in the fewest switching losses, to prevent an excessively high number of switching operations. (Hassen et al, 2021) For this thesis work 48-pulse VSC is designed on Matlab, and its specifications can be seen in Appendix A.

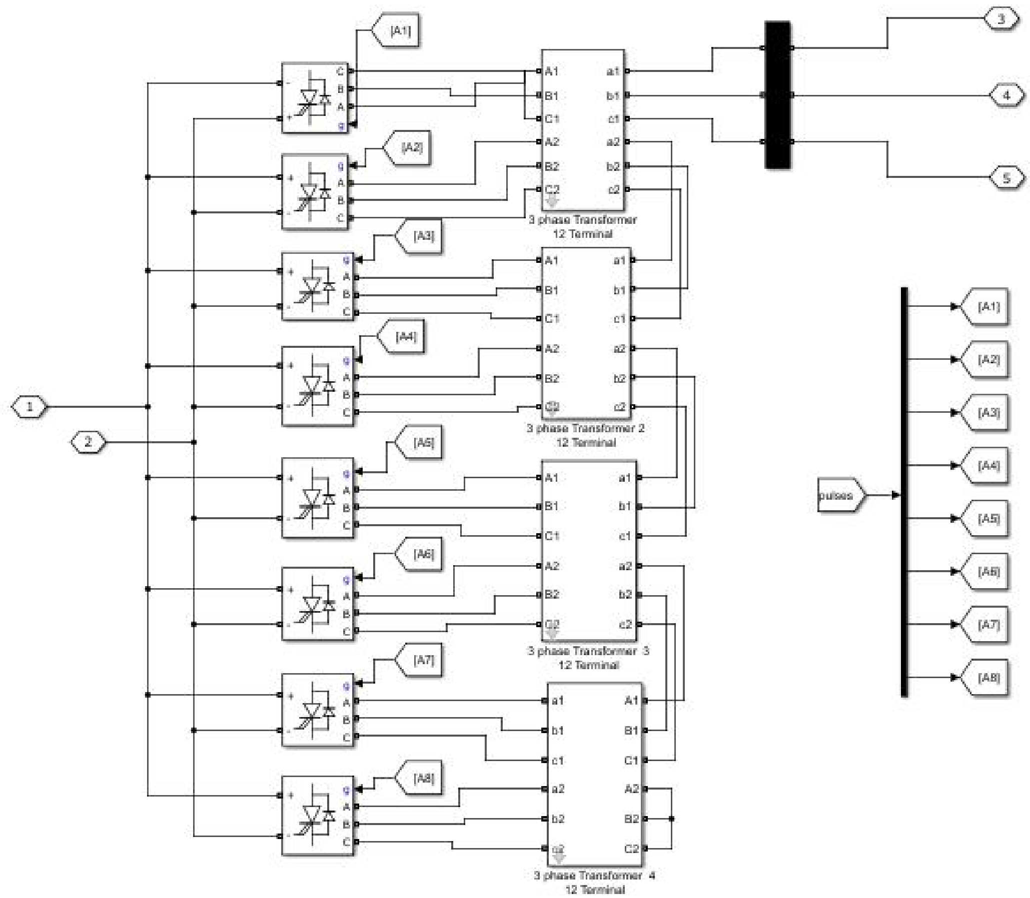

Figure 3.18 48-pulse GTO's voltage source converter.

3.4.3 STATCOM Control Algorithm

The primary function of the Dc-Link Voltage Controller (PI) is to keep the "equal to the". This is accomplished by altering and then moving actual power from the AC system to the DC link. The relationship between the direct current and voltage is provided by (3.64).

$$V_{dc} = \frac{1}{C} \int i_{dc}\, dt$$

$$\text{Transfer function} = \frac{V_{dc}}{I_{dc}} \tag{3.64}$$

In Laplace domain, the transfer function = $\frac{1}{C_S}$, $K_p = \frac{C}{T_s}$; $K_i = \frac{K_P}{T_s}$

The controller that regulates reactive power (Q_g) keeps the variable 'Q_{inv}' at its reference value 'Q_{inv_ref}'. As a result, the controller uses the tuned controller parameters to compute the reference quadrature axis current 'i_{shqref}' as illustrated in (3.65). after which 'i_{shqref}' is supplied to the current controller, where k is a specific time instant.

$$i_{shqref(\mathrm{k})} = i_{shqref}(\mathrm{k}-1) + K_P[Q_{inv(k)} - Q_{inv}(\mathrm{k}-1)] + K_i[Q_{inv(k)})] \quad (3.65)$$

Where $$Q_{inv(k)} = [Q_{inv(k)} - Q_{inv(k)}] \quad (3.66)$$

The reactive power Q_{inv} in the above equation (3.21) is given by (3.23)

$$Q_{inv} = \frac{3(V_{invq}i_{shd} - V_{invd}i_{shq})}{2} \quad (3.67)$$

The single input, single output system (SISO) can be easily analyzed using the current controller design. Consequently, the system must be changed from multiple input, multiple output (MIMO) to single-input, single-output (SISO). While the system's and STATCOM's instantaneous voltages are independent, the active and reactive currents are related by a coupling term. Therefore, the active and reactive shunt currents must be disconnected in order to construct the controller. (3.25) is the differential equation for.

$$\frac{\mathrm{di_{shd}}}{d_t} = \frac{1}{L_{sh}}(V_{Md} - V_{invd} - R_{sh}\, i_{shd}) + \frac{1}{\mathrm{Lsh}}(\omega L_{sh}\, i_{shq}) \quad (3.68)$$

The values that are not controlled are assumed to be constant.

$$K_1 = \frac{1}{\mathrm{Lsh}}(V_{Md} - V_{invd} - \omega L_{sh}\, i_{shq})$$

Similar analysis is done for q component:

$$\frac{\mathrm{di_{shq}}}{d_t} = \frac{1}{L_{sh}}\left(V_{Mq} - V_{invq} - VR_{sh}\, i_{shq} + \omega L_{sh}\, i_{shd}\right) \quad (3.69)$$

$$K_2 = \frac{1}{\mathrm{Lsh}}(V_{Mq} - V_{invq} - \omega L_{sh}\, i_{shd})$$

$$\begin{bmatrix} \frac{\mathrm{di_{shd}}}{d_t} \\ \frac{\mathrm{di_{shq}}}{d_t} \end{bmatrix} = \begin{bmatrix} \frac{-R_{sh}}{L_{sh}} & 0 \\ 0 & \frac{-R_{sh}}{L_{sh}} \end{bmatrix} \begin{bmatrix} i_{shd} \\ i_{shq} \end{bmatrix} + \frac{1}{L_{sh}} \begin{bmatrix} K_1 \\ K_2 \end{bmatrix} \quad (3.70)$$

Comparing (3.27) and (3.18),

Transfer Function = $\mathrm{C(sI\ - A)^{-1}\ B + D} = \frac{1}{R_{sh} + sL_{sh}}$, The transfer function of PI controller is given by: Transfer Function =$(1 + \frac{1}{s\tau_1})$ $\quad K_P = \frac{L_{sh}}{T_s}; K_1 = \frac{K_p}{\tau_1};\ \tau_1 = \frac{L_{sh}}{R_{sh}}$

From the closed loop transfer function obtained, it is seen that the values of K_P and $K_i$are decided by circuit parameters R_{sh} andL_{sh}.

3.4.4 Phase Locked Loop

Phase-locked loops (PLLs) are systems that synchronize their output signal in both frequency and phase with a reference or input signal. This non-linear closed-loop control automatically adjusts a controlled oscillator's frequency based on the frequency and phase of the input signal, synchronizing the output with the input signal or reference in both frequency and phase.

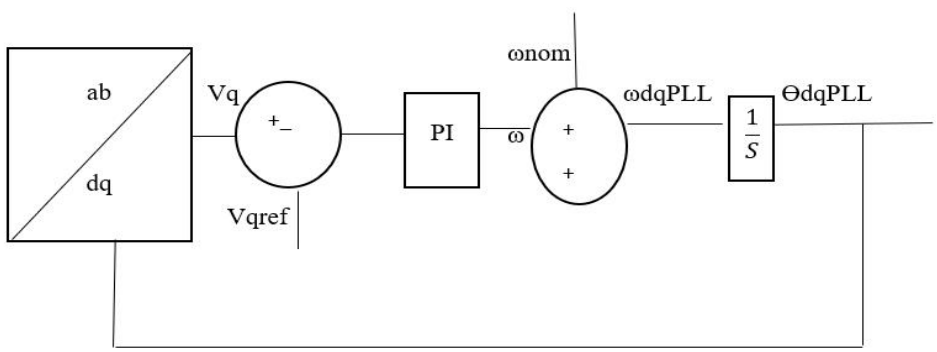

Figure 3.19 The structure of a dq PLL

- **Synchronous Reference Frame PLL (dq PLL)**

Equation 3.71 illustrates how the dq PLL translates the ABC natural rotating reference frame into the dq-Synchronous Reference Frame (SRF). The basic configuration is displayed in Figure 3.28.

$$\begin{bmatrix} V_d \\ V_q \end{bmatrix} = \frac{2}{3}\begin{bmatrix} \cos\theta & \cos(\theta - 120^0) & \cos(\theta + 120^0) \\ -\sin\theta & -\sin(\theta - 120^0) & -\sin(\theta + 120^0) \end{bmatrix}\begin{bmatrix} V_a \\ V_b \\ V_c \end{bmatrix} \quad (3.71)$$

For the purpose of estimating frequency and subsequently phase angle in this PLL, the direct or quadrature axis components of voltage may be taken into consideration. The requirement that the d-axis (V_d) voltage lie on phase A's voltage is a key component of the transformation. This is accomplished by tracking the zero voltage of the q-axis (V_q) using a proportional-integral (PI) controller, which enables the estimation of phase and frequency ω_{dqPLL} and phase, Θ_{dqPLL} The loop filter function of the basic PLL is carried out by the PI controller in this PLL. By using the error signal $V_q - V_{qref}$ in the dq frame to integrate the output, the angle Θ_{dqPLL} is obtained.

3.5 Control and modeling of the battery energy storage system

One tool for converting chemical energy into electrical energy is a battery. The battery is represented as a nonlinear voltage source with an output voltage that is dependent on both the battery's state of charge (SOC), which is a nonlinear function of both time and current (Beiming et al, 2018) . The following two parameters are crucial in representing the battery's SOC and terminal voltage:

$$V_0 + R_b i_b - K\frac{Q}{Q + \int ibdt} + A\exp\,(B\int ibdt) \quad (3.72)$$

$$SOC = 100\left(1 + \frac{\int i_{bdt}}{Q}\right)$$

The State of Charge (SOC) of a rechargeable battery is its percentage of its maximum possible charge. This includes the battery's internal resistance R_b , its open circuit voltage V_0 , its charging current I_b, its polarization voltage K, its battery capacity Q , its exponential voltage A , and its exponential capacity B.

3.5.1 Battery Voltage and Current Controller Design

The components of the energy storage system include a battery, a control system, and a bidirectional DC/DC converter. Figure 3.31 illustrates the bi-directional converter's control system, which can regulate power flow in both directions. When IGBT is activated and deactivated, the converter turns on and off as a boost circuit during battery discharge and on and off as a buck circuit during battery charging. The supply of a superior, dynamic DC bus voltage is the control's main objective. This scheme compares the DC bus voltage to its reference voltage, sends the difference to a PI controller to obtain the battery current reference, which serves as the inner loop's input signal, and then injects the battery current difference into another PI controller to obtain the signal for the PWM generator to drive and turn on or off. And,Please refer to Appendix A for the system parameters. (Beiming et al, 2018).

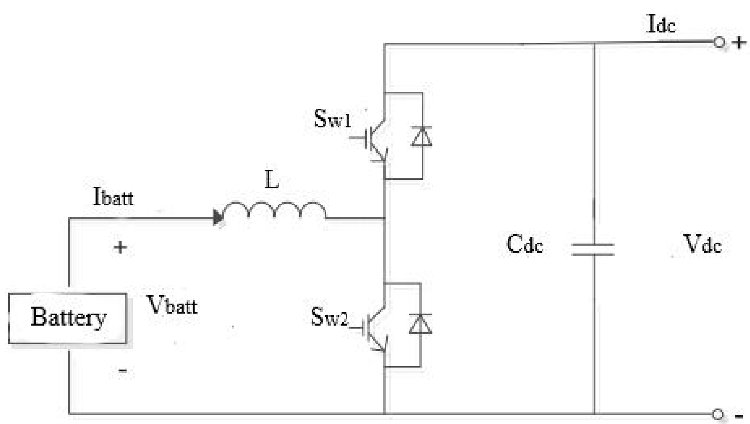

Figure 3.20 Control Strategy of battery charge and discharge

$$L = \frac{V_{batt} * (V_{dc} - V_{batt})}{I_{batt} * f_s * V_{dc}} \quad (3.73)$$

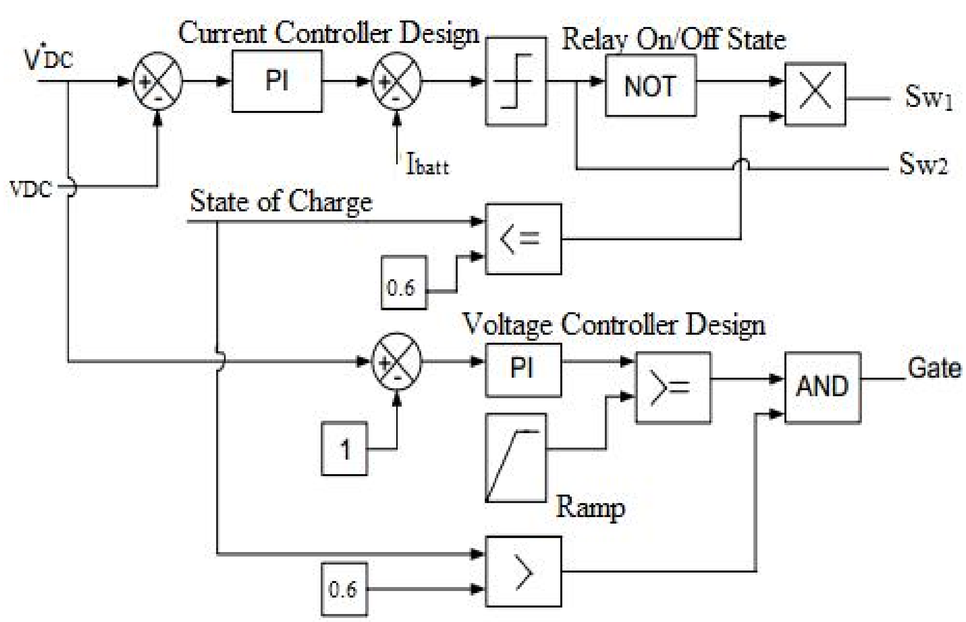

Figure 3.21 Control Strategy of battery charge and discharge

3.6 STATCOM Mathematical Model for Load Flow

To determine the ideal size and location of STATCOM, which will have a major impact on the sy stem, a single-objective function method was used in this work. This shunt connected controller may be positioned in the midst of the transmission lines.Power Injection Mode (PIM) based on STATCOM was modeled mathematically using voltage source representation. For the purpose of performing the load flow analysis on the transmission lines, the Newton - Raphson (NR) load flow approach was employed because of its quick quadratic convergence and reliable answer.The following reasons led to the selection of PSO as the optimization technique: low memory requirements, computational efficiency, robust control over a small number of para meters, ease of application to nonlinear noncontinuous optimization problems, high periodicity a nd diversity in the solution. The transmission network's ideal placement for the created STATCOM model had zero active power and the appropriate voltage magnitude. generation that calculates the active and reactive power losses, utilizing power injection as a mismatch calculation criterion. The shunt controller injects electricity to create a favorable power flow across the transmission line in order to install STATCOM. The following presumptions guide STATCOM's adoption of the power injecting mathematical equations mode (Ebenezer,et al2023):

Ignored are the harmonics produced by the STATCOM.

Three-phase balance is assumed for both the system and the STATCOM.

A controllable fundamental frequency positive sequence voltage source can be used as an equivalent representation of the STATCOM.The voltage source representation can be stated as follows:

$$E_{STC} = V_{STS}\,(Cos_{\delta STC} + jSin_{\delta STC}) \qquad (3.74)$$

For the STATCOM voltage source and bus k, the following simplified active and reactive power equations were found:

$$S_{STC} = V_{STS}\, I_{STC}^{*} \qquad (3.75)$$

$$S_{STC} = V_{STS}\, Y_{STC}^{*}(V^{*}_{STC} - V^{*}_{k}) \qquad (3.76)$$

$$P_{STC} = V^{2}_{STS}\, G_{STC} + V_{STC}V_{k}[G_{STC}\ Cos_{(\delta_{STC} - \theta_{k})} + B_{STC}\ Sin_{(\delta_{STC} - \theta_{k})}] \qquad (3.77)$$

$$Q_{STC} = -V^2{}_{STS}\,G_{STC} + V_{STC}V_k[G_{STC}\,Sin_{(\delta_{STC}-\theta_k)} + B_{STC}Cos_{(\delta_{STC}-\theta_k)}] \quad (3.78)$$

$$P_k = V^2{}_k\,G_{STC} + V_kV_{STC}[G_{STC}\,Cos_{(\theta_k-\delta_{STC})} + B_{STC}Sin_{(\theta_k-\delta_{STC})}] \quad (3.79)$$

$$Q_k = -V^2{}_kG_{STC} + V_k\,V_{STC}[G_{STC}\,Sin_{(\theta_k-\delta_{STC})} + B_{STC}Cos_{(\theta_k-\delta_{STC})}] \quad (3.80)$$

The NR load flow set of equations incorporated the STATCOM mathematical model.

$$\begin{bmatrix} \Delta P_k \\ \Delta Q_k \\ \Delta P_{STC} \\ \Delta Q_{STC} \end{bmatrix} = \begin{bmatrix} \frac{\partial P_k}{\partial \theta_k} & \frac{\partial P_k}{\partial V_k}V_k & \frac{\partial P_k}{\partial \delta_{STC}} & \frac{\partial P_k}{\partial V_{STC}}V_{STC} \\ \frac{\partial Q_k}{\partial \theta_k} & \frac{\partial Q_k}{\partial V_k}V_k & \frac{\partial Q_k}{\partial \delta_{STC}} & \frac{\partial Q_k}{\partial V_{STC}}V_{STC} \\ \frac{\partial P_{STC}}{\partial \theta_k} & \frac{\partial P_{STC}}{\partial V_k}V_k & \frac{\partial P_{STC}}{\partial \delta_{STC}} & \frac{\partial P_{STC}}{\partial V_{STC}}V_{STC} \\ \frac{\partial Q_{STC}}{\partial \theta_k} & \frac{\partial Q_{STC}}{\partial V_k}V_k & \frac{\partial Q_{STC}}{\partial \delta_{STC}} & \frac{\partial Q_{STC}}{\partial V_{STC}}V_{STC} \end{bmatrix} \begin{bmatrix} \Delta \theta_k \\ \frac{\Delta V_k}{V_k} \\ \Delta \partial_{STC} \\ \frac{\Delta V_{STC}}{V_{STC}} \end{bmatrix} \quad (3.81)$$

The voltage magnitude V_{STC} and phase angle δ_{STC} of STATCOM state variables are stated as follows $\left|V^{(i+1)}{}_{STC}\right| = \left|V^{(i)}{}_{STC}\right| + \Delta\left|V^{(i)}{}_{STC}\right|$ (3.82)

$$\delta^{(i)}{}_{STC} = \delta^{i}{}_{STC} + \Delta\delta^{i}{}_{STC} \quad (3.83)$$

The residual power is expressed as :$\Delta P^{(i)}{}_k = \Delta P^{sch}{}_k - P^i{}_k$ (3.84)

$$\Delta Q^{(i)}{}_k = \Delta Q^{sch}{}_k - Q^i{}_k \quad (3.85)$$

V_{STC} is the STATCOM voltage magnitude, δ_{STC} is the STATCOM phase angle , $I^*{}_{STC}$ is the STATCOM reference current , $Y^*{}_{STC}$ is the STATCOM reference admittance, $V^*{}_{STC}$ is the STATCOM reference voltage, $I^*{}_k$ is the reference bus current at bus k, G_{STC} is the STATCOM conductance , B_{STC} is the STATCOM susceptance, θ_k is the firing angle at bus k, V_k is the bus voltage at bus k.

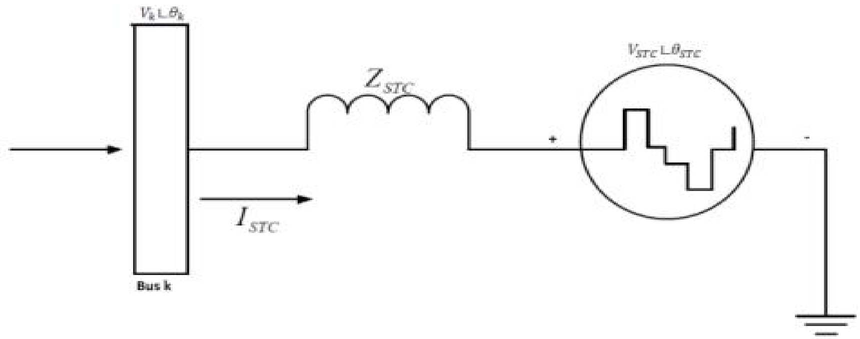

Figure 3.22 Equivalent circuit of STATCOM

3.6.1 Formulation of Problems

In Figure (3.23), the IEEE 11-bus network model is displayed. There are three generator buses, eight load buses, and ten lines in the system. The VAR output from the shunt compensating STATCOM controller, the transformer tap setting, and the generator bus voltage magnitude are the control variables that need to be optimized. The values of these control parameters are modified to reduce loss. In the table below, the control variables for PSO parameters are factually explained.

Table 3.6 Control Variable Limits

Control Variables	Limits
Generation Voltage(V_{Gi})	(0.95 - 1.05)p.u
Transformer Tap setting (T_{pi})	(0.90 - 1.10)p.u
Static Compensator (Q_{STC})	(0.0 - 100)Mvar

3.6.2 Define the Objective Function

The objective function evaluates the system's performance based on the placement and sizing of the STATCOM. In this case, it focuses on improving the voltage profile.

Objective: Minimize the deviation of bus voltages from the desired value (usually 1 p.u.)

Formula : Cost $=\sum (V_{desired} - V_{actual})^2$ (3.87)

Where $V_{desired}$ is the desired bus voltage (1 p.u) and V_{actual} is the actual bus voltage:under the following restriction,as stated.Below were the equality and inequality constraints applied:

3.6.3 Constraints

1) Bus Voltage Limits: Ensure that the bus voltages remain within acceptable limits (0.5 p.u. to 1.05 p.u.). Check and adjust voltages during the evaluation step.

2) STATCOM Sizing Limits: Limit the size of the STATCOM to feasible and practical values (10 MVAR to 100 MVAR).Clip particle positions to stay within the specified sizing bounds.

3) STATCOM Placement: Limit the possible buses where the STATCOM can be placed (buses 1 to 11).Clip particle positions to stay within the specified bus placement bounds.

4) Feasibility of Power Flow: Ensure that the power flow calculations remain feasible after placing the STATCOM.Include a feasibility check in the power flow calculation function.

3.7 Algorithm for particle swarm optimization

To decrease the system's Voltage deviation and active power loss, the STATCOM controller was positioned appropriately using the use of Particle Swarm Optimization (PSO). PSO is an optimization technique inspired by nature that has a low memory requirement, is computationally efficient, and converges quickly. (Okelola,et al 2021)explained PSO algorithms as follows:

1. Each of the individual particles i possesses these properties :a current velocity V_i a personal searh space position y_i and a current search space position x_i.

2. The personal best position y_i is the position in search space where particle i presents the smallest errors determined by the objective function f assum a minimization task.

3. The global best position y denotes the position that yields the lowest error among all the y_i.

The personal best position and global best position modification are expressed as :

$$y_i(t+1) = \begin{cases} y_i(t) & if\ f(y_i(t) \leq f(x_i(t+1))) \\ x_i(t+1) & if\ f(y_i(t) > f(x_i(t+1))) \end{cases} \tag{3.88}$$

$$\mathrm{y(t)} = \min\{\mathrm{f(y)/f(y(t))} \tag{3.89}$$

$$y \in \{ y_0(t),\ y_i(t) \ldots\ldots\ldots\ldots\ y_s(t)\}$$

The current velocity and next position are modified according to Equations 1 and 2.

$$V_{i,j}(t+1) = wV_{i,j} + c_1 r_1(t)[y_{i,j}(t) - x_{i,j}(t)] + c_2 r_2(t)[y_{i,j}(t) - x_{i,j}(t)] \quad (3.90)$$

$$x_i(t+1) = x_i(t) + V_i(t+1) \quad (3.91)$$

The inertial weight w that controls the PSO convergence behaviour in Equation (3.90) is given as :

$$W = W_{max} - \frac{W_{max} - W_{min}}{iter_{max}} * iter \quad (3.92)$$

Where iter is the current number ,$iter_{max}$ is the maximum iteration number,W_{max} *and* W_{min} are the maximum and minimum number of weighting factors.

3.7.1 An Application of PSO Algorithm to IEEE-BUS 11

The impact of the PSO method for the proper placement and scaling of STATCOM on the 11-Bus IEEE Standard Test Transmission Network was inferred using the subsequent stages.

Step1: Based on the IEEE 11-bus system's PSO parameters, population of the control variables,size, and number of iterations

Step 2: Assign a zero iteration value.

Step 3: Use their velocities to generate the populated particles at random

Step 4: To achieve voltage enhancement , run the NR load flow for each particle.

Step 5: Use Equation 23 to get the fitness function of each particle.

Step 6: Determine the particles' new Gbest (global best) and Pbest (position best) fitness values.

Step7: Make the iteration count one.

Step 8: Using Equation 26, calculate the velocities of each particle and look for any potential limit violations.

Step 9: Utilizing Equation 27, determine the new particle position.

Step10: Run the NR load flow and determine the voltage divation and losses using the STATCOM that is included for every particle.

Step 11: Set Pbest = P ,but only if each particle's current fitness P exceeds Gbest.

Step12: Designate Pbest as Gbest.

Step 13: Continue increasing the iteration count if the maximum number of iterations has not been achieved.

Stage 14: Continue steps 7 through 12 until convergence is attained.

Where the matlab code is shown in Appendix D.

3.8 Matlab simulink model for overall System Network

(a) System model without Battery supported STATCOM

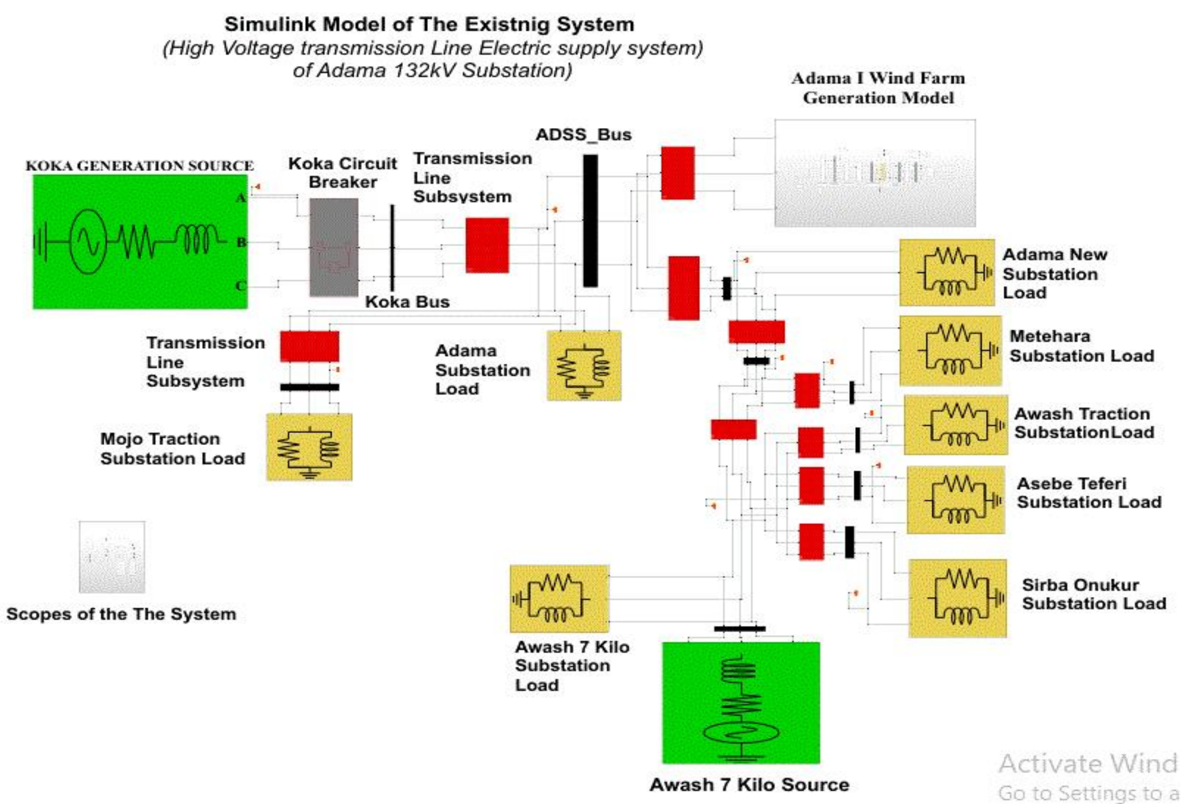

Figure 3.23 simulink Model of the overall High voltage transmission network of Adama substation electric supply system

(b) System model with Battery supported STATCOM

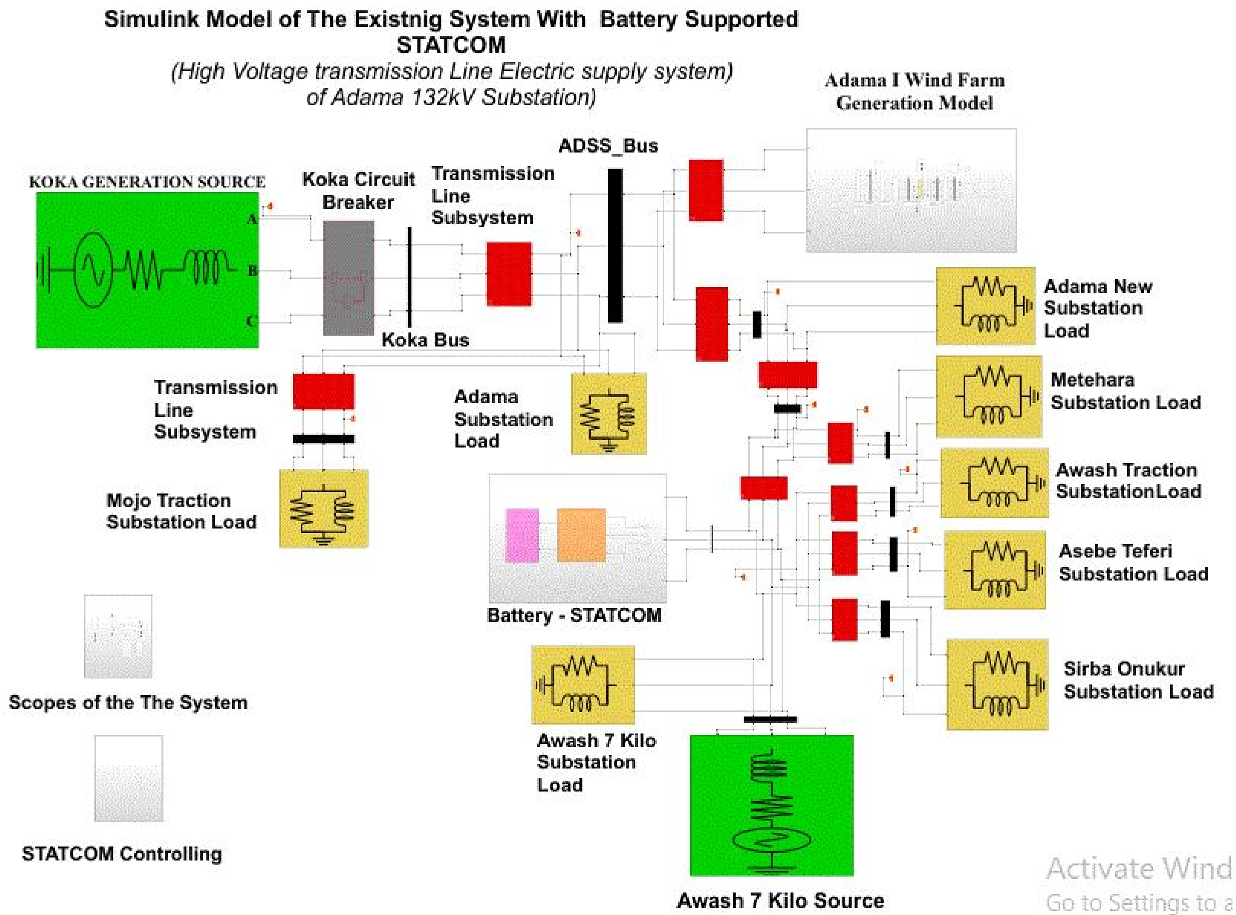

Figure 3.24 simulink Model of the overall High voltage transmission network of Adama substation electric supply system with Battery supported STATCOM

CHAPTER FOUR
RESULTS AND DISCUSSIONS

4.1 Introduction

This chapter contained the simulation findings and assessments of how well a 15 MVAR battery-supported STATCOM improved the voltage profiles on the high-voltage transmission lines of the electric supply system for the Adama substation. Particle Swarm Optimization (PSO) suggested the best location and size for the STATCOM at the Awash 7-Kilo substation bus (A7KSS). As a point of reference, other locations at the Adama wind farm bus were also taken into account.The voltage profile of the system was assessed under various situations using power flow analysis, with a particular focus on the Koka generation contingency case. Load flow analysis using the Newton-Raphson method was conducted to evaluate the existing voltage profile and identify critical buses affected by voltage drops. Based on the integration of the STATCOM, the results showed notable increases in voltage stability. Detailed evaluations indicated that the PSO-proposed STATCOM at the Awash 7-Kilo substation bus yielded the best voltage profile improvement.The present analysis underscored the efficacy of the placement suggested by PSO and highlighted the advantages of alternative placements in enhancing voltage profiles during crucial circumstances.In the MATLAB 2021a environment, every system model, both with and without battery-supported STATCOM, was run. Additionally, the load flow analysis and PSO code algorithm were developed in the MATLAB code window, using the same version for both load flow and PSO placement and sizing analyses.

4.2 Matlab code Results and discussion of the system

Case 1: Voltage Magnitude of the Existing System

The MATLAB code results for the existing system indicate that the voltage magnitudes for all system buses are satisfactory. The minimum voltage magnitude is 0.952 at the ASTSS Bus, while the rest are above this value. This is because all three sources carry the maximum load throughout the system, and the Adama I Wind Farm generates maximum power based on the provided data. Although power generation varies, affecting voltage magnitudes, this analysis assumes a constant speed, which produces constant power.Among the three sources, the Adama I

Wind Farm is significant. Due to the variable nature of wind, the power generated can fluctuate, leading to variations in voltage magnitude. However, in this analysis, I am only considering the contingency for Koka generation, one of the three sources.

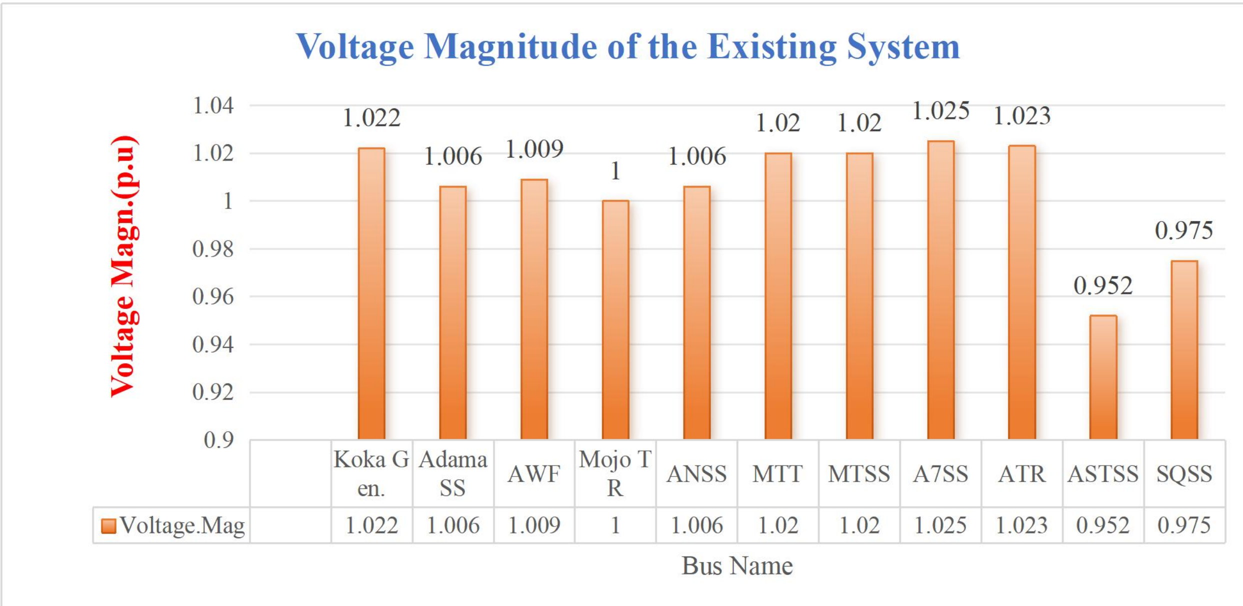

Figure 4.1 Voltage Magnitude of the Existing System

Case 2: Voltage magnitude of the system when Kok generations is interrupted

During the Koka contingency condition, the voltage magnitude for the entire bus system decreases. The load carried by the Koka generation is then transferred to the Awash 7-kilo line, which also results in a voltage drop. Due to this voltage drop, the Adama I Wind Farm cannot continue generating power, even if wind is available, because the wind farm requires a minimum voltage of 0.942 p.u. (124.4 kV) to remain connected. To regulate the voltage, load shedding is implemented as a corrective action.

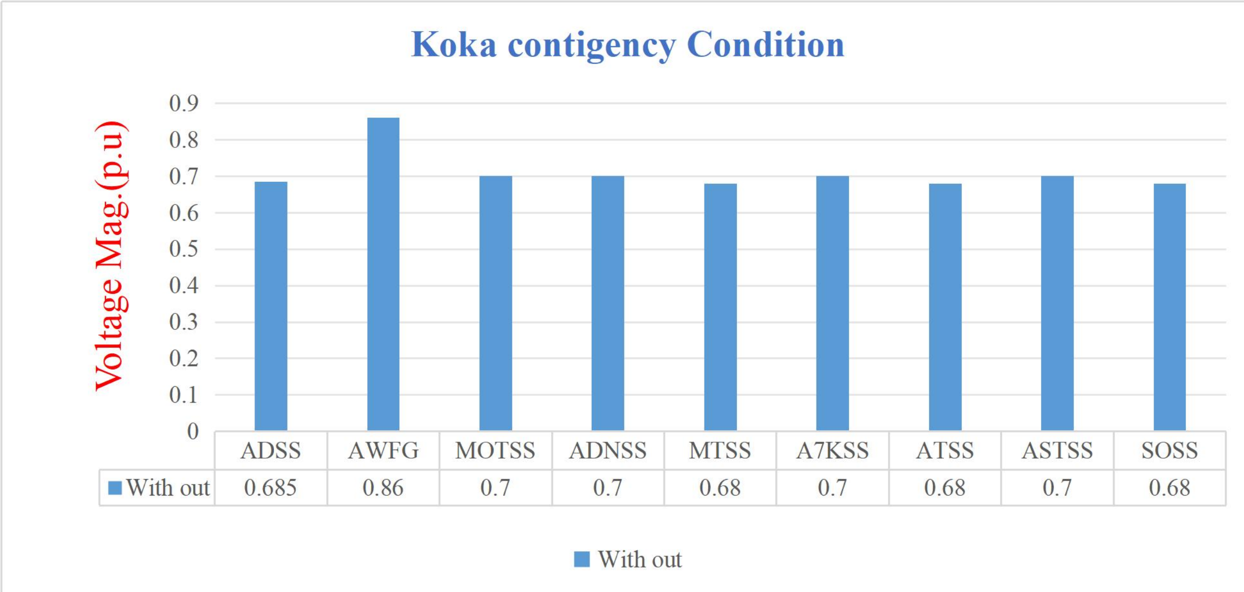

Figure 4.2 Voltage magnitude of the system when Koka generation is interrupted

4.3 Matlab Simulink Results and discussion of the system

The inverter output voltage of 620 volts and the 40 MW of electricity generated by the Adama wind farm are displayed in the figures 4.3.

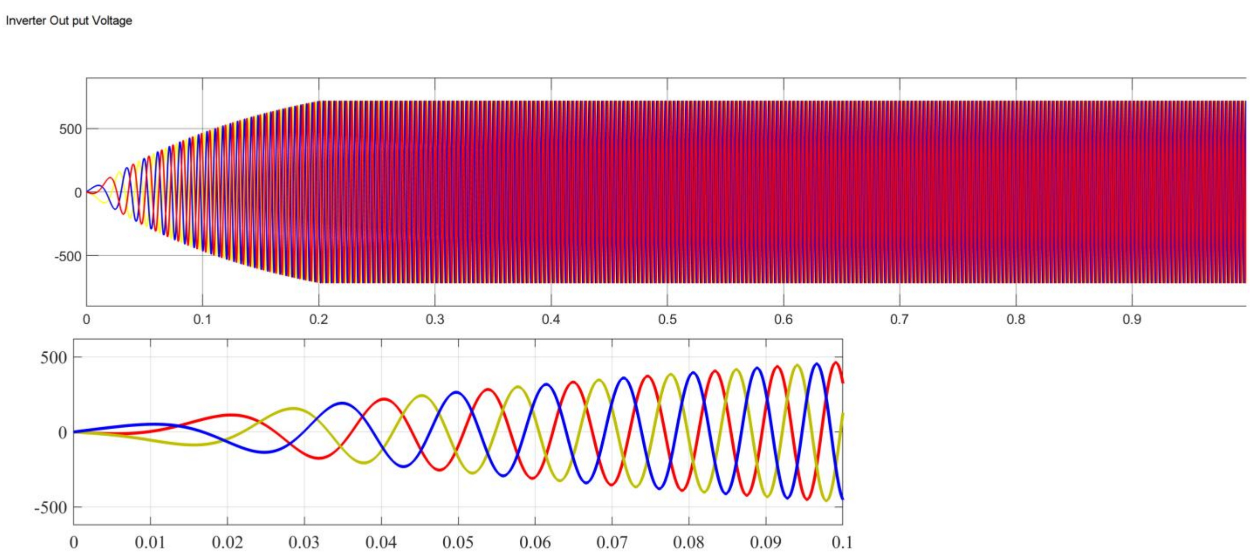

(a)

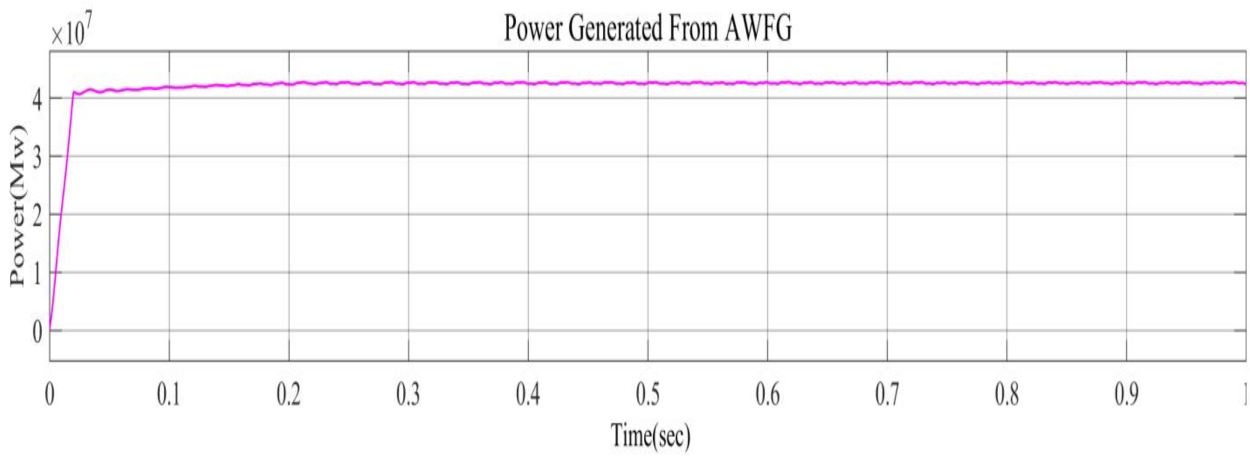

(b)

Figure 4.3 Simulink results for the inverter's output voltage and power generated at AWFG are shown in (a) and (b).

Case 1: Simulink model results for contingencies in the Koka Line

Figure 4.4 shows the disruption at the Koka bus resulting from the contingency interrupt caused by Koka generation during the 0.4 to 0.7 seconds. This interruption impacts all system network buses inside the high-voltage electric supply system of the Adama substation.

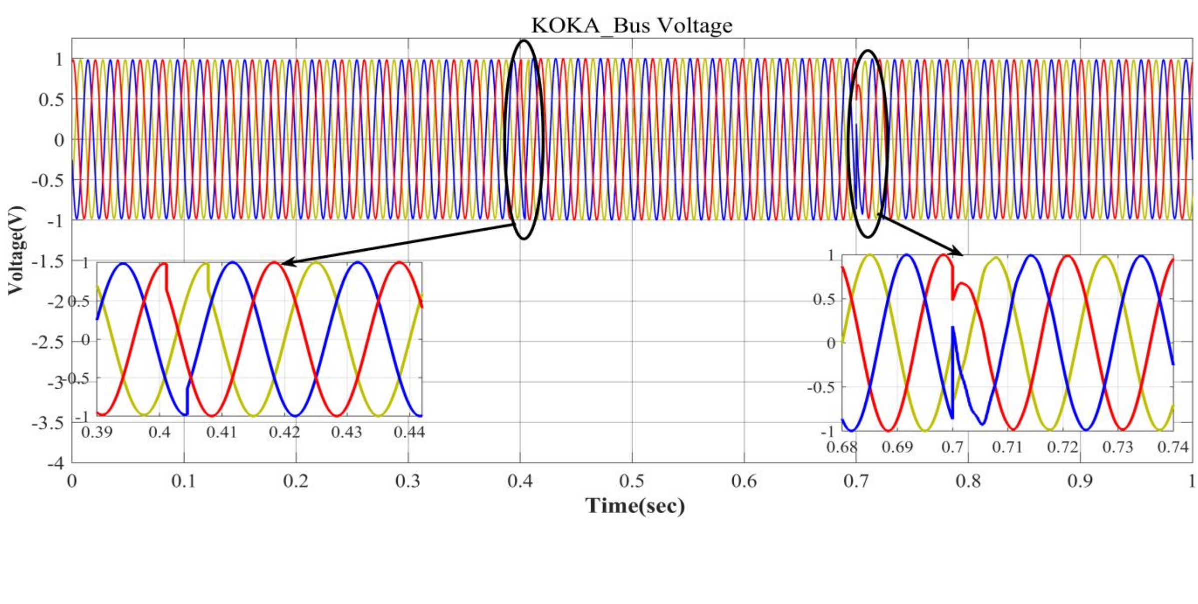

(a)

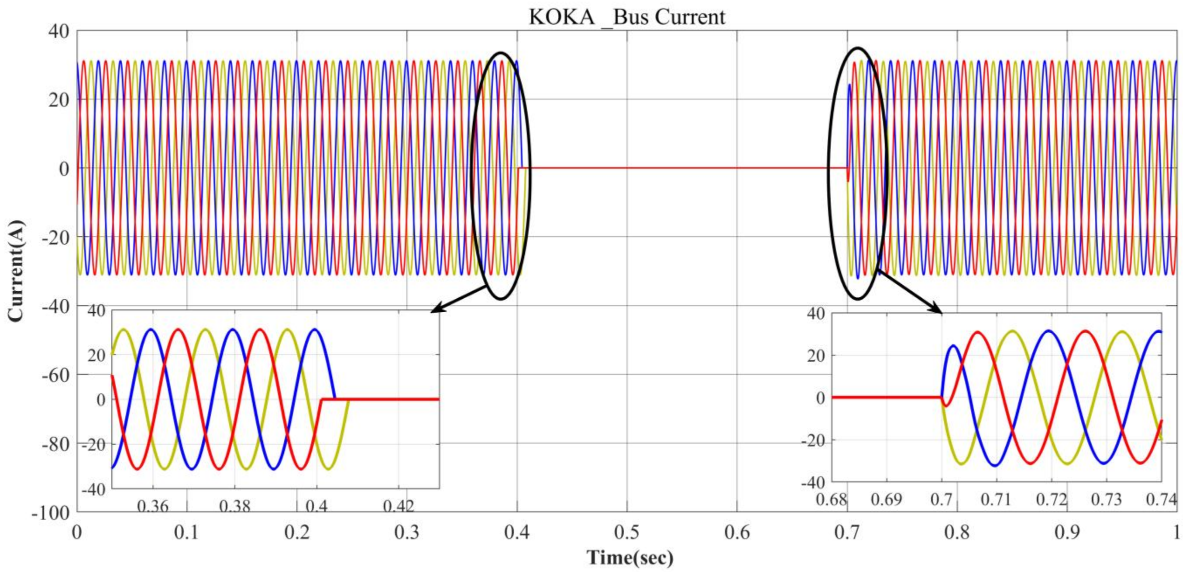

(b)

Figure 4.4 Simulink results for the inverter's output voltage and power generated at AWFG are shown in (a) and (b).

Bus of the Adama Substation Before and after the STATCOM was installed

During the contingency period from 0.4 seconds to 0.7 seconds, the voltage magnitude drops to 0.685 p.u. However, after placing a 15 MVAR STATCOM at the A7KSS Bus, the voltage magnitude improves to 1 p.u. This improved voltage level reduces the need for load shedding and allows the Adama I Wind Farm to continue delivering power to the system network.

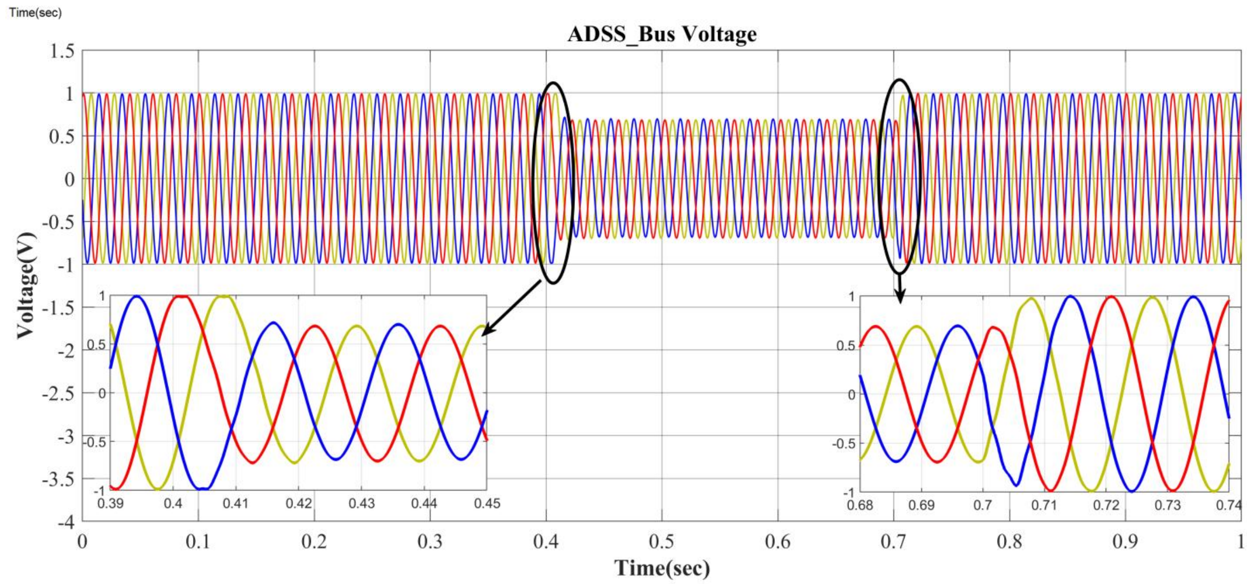

(a)

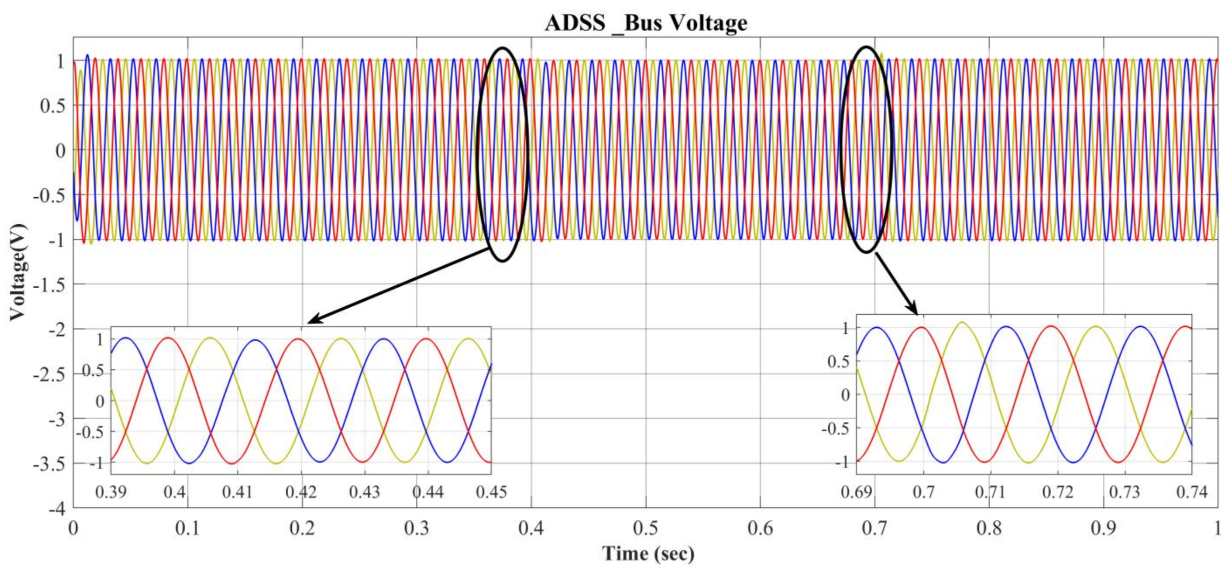

(b)

*Figure 4.5 (a),(b) Simulink model result of ADSS Bus Voltage Before and after STATCOM Placemen*t

The Simulink results below illustrate the root mean square (RMS) voltages of the ADSS bus before and after STATCOM placement in the system. The graph demonstrates that the STATCOM effectively compensates the voltage, as shown in the improved voltage levels.

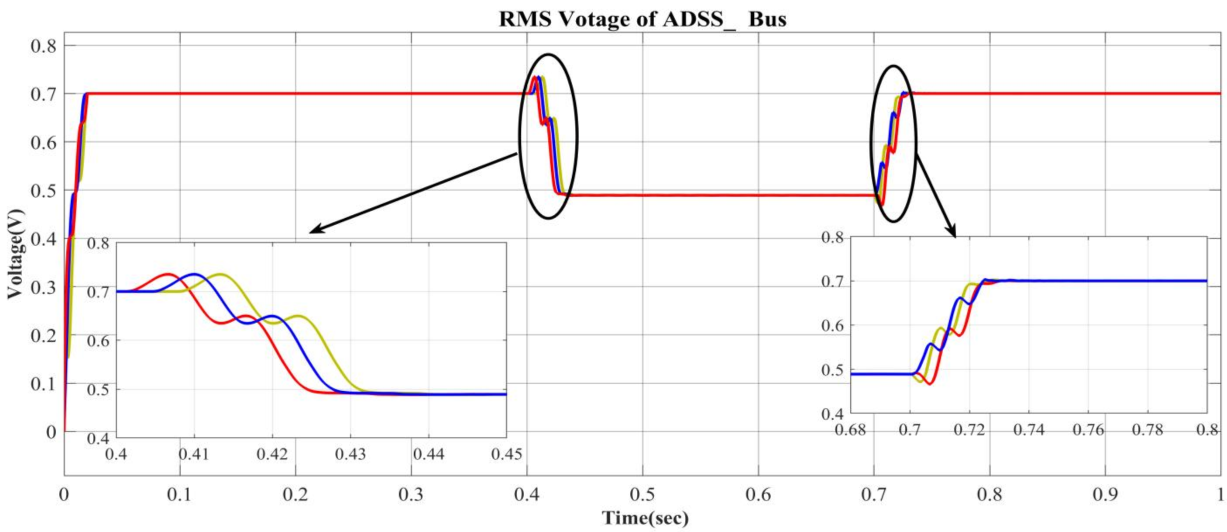

(a)

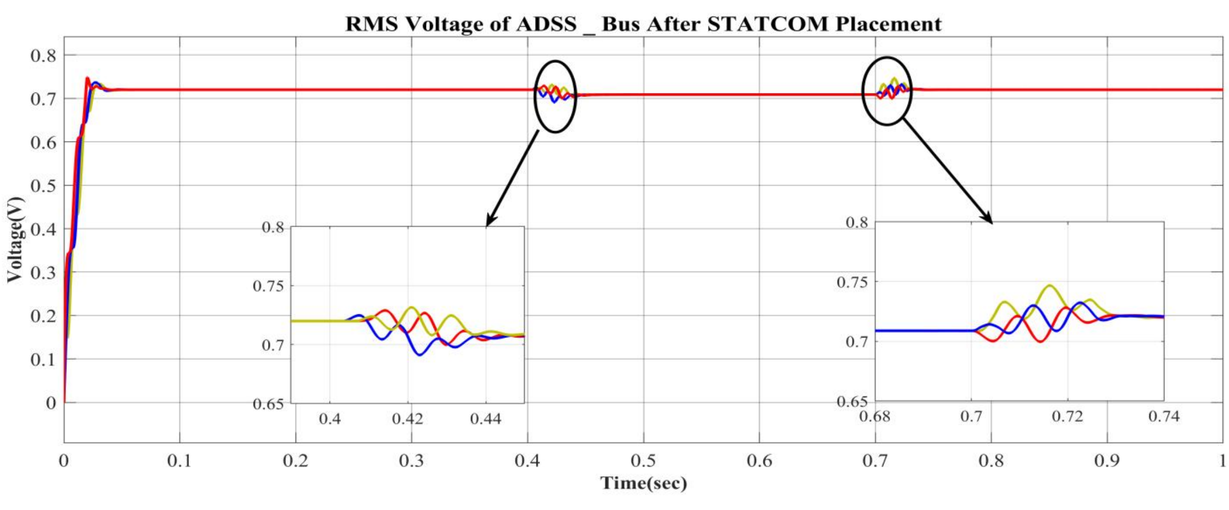

(b)

Figure 4.6 (a), (b) shows the ADSS Bus RMS Voltage Simulink model result before and after STATCOM placement.

Bus of the Awash 7-kilo substation Before and after the STATCOM was installed

Before and after the STATCOM is installed, the voltage profile at the Awash 7-kilo substation (A7KSS) bus is improved during contingency time. During this 0.4–0.7 second simulation time, the system voltage is 0.7 p.u. But once the STATCOM is installed, the voltage profile is improved to 0.97 p.u.

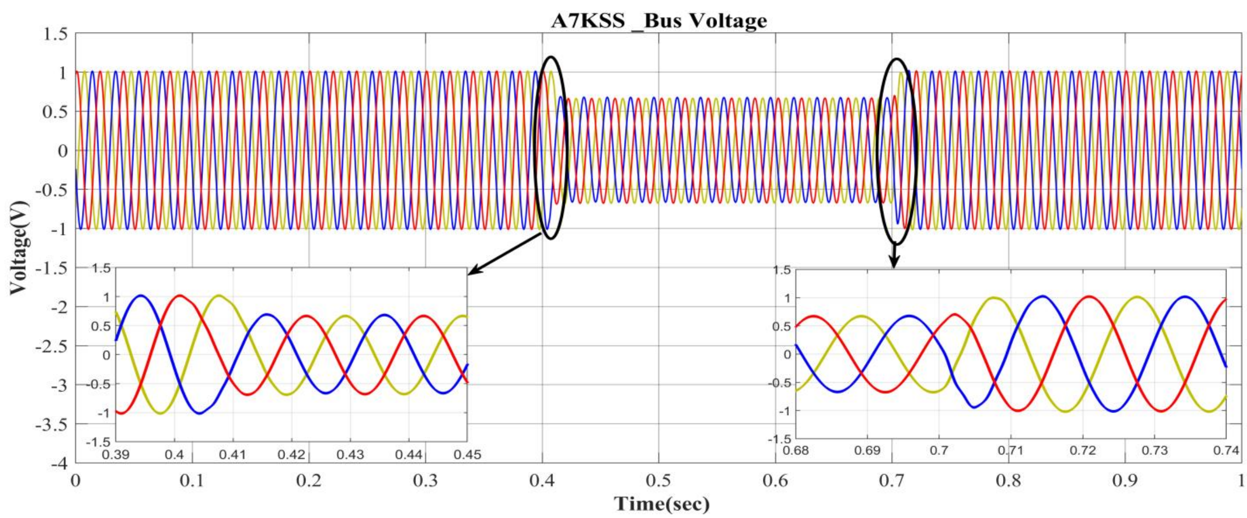

(a)

(b)

Figure 4.7 (a),(b) Simulink model result of A7KSS Bus Voltage Before and after STATCOM Placement

The results of the Simulink model for the A7KSS bus current before and after STATCOM placement are shown simply in the figure below, demonstrating an improvement in bus current when compared during contingency and compensation.

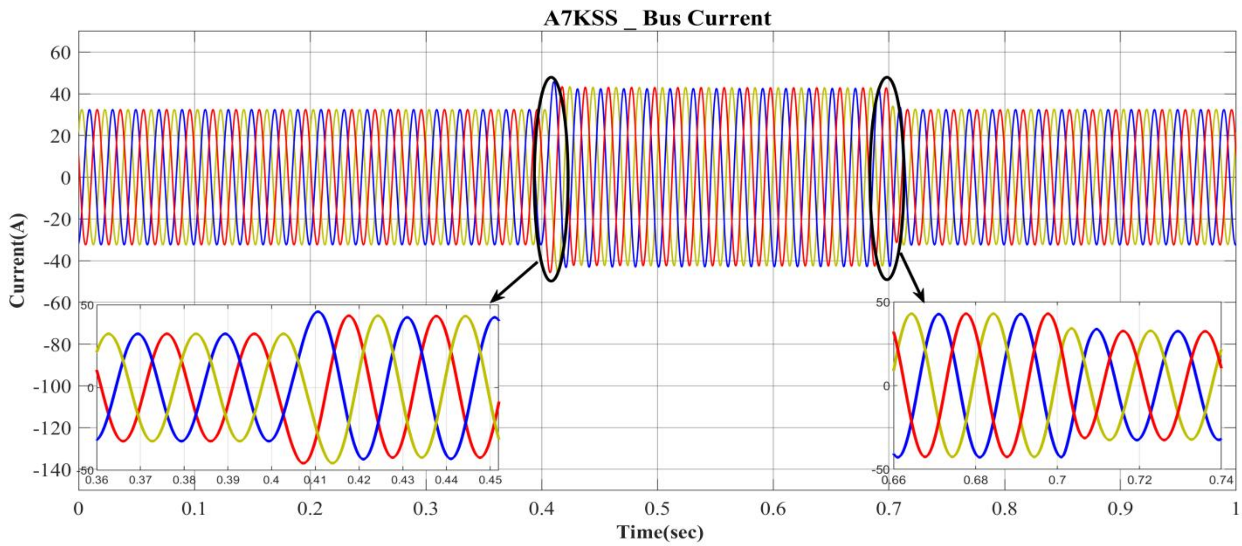

(a)

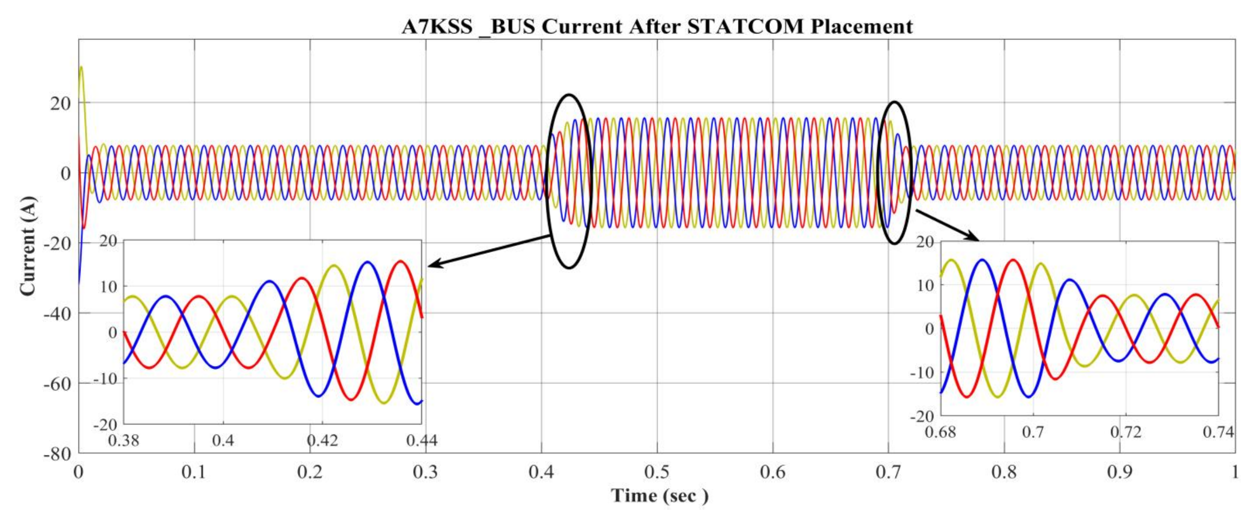

(b)

Figure 4.8 (a),(b) Simulink model result of A7KSS Bus Current Before and after STATCOM Placement

The Simulink results below illustrate the root mean square (RMS) voltages of the A7KSS bus before and after STATCOM placement in the system. The graph demonstrates that the STATCOM effectively compensates the voltage, as shown in the improved voltage levels.

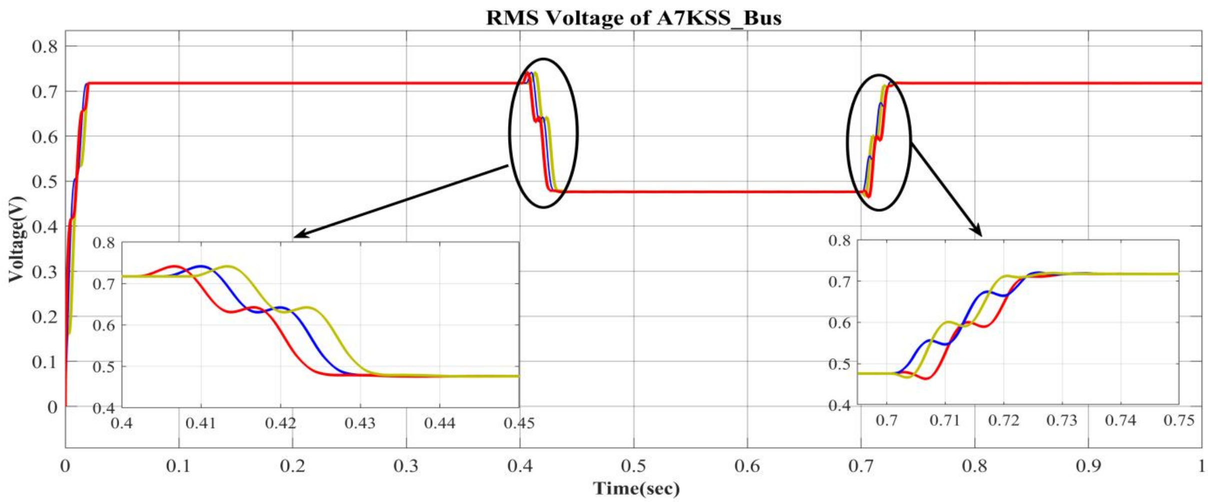

(a)

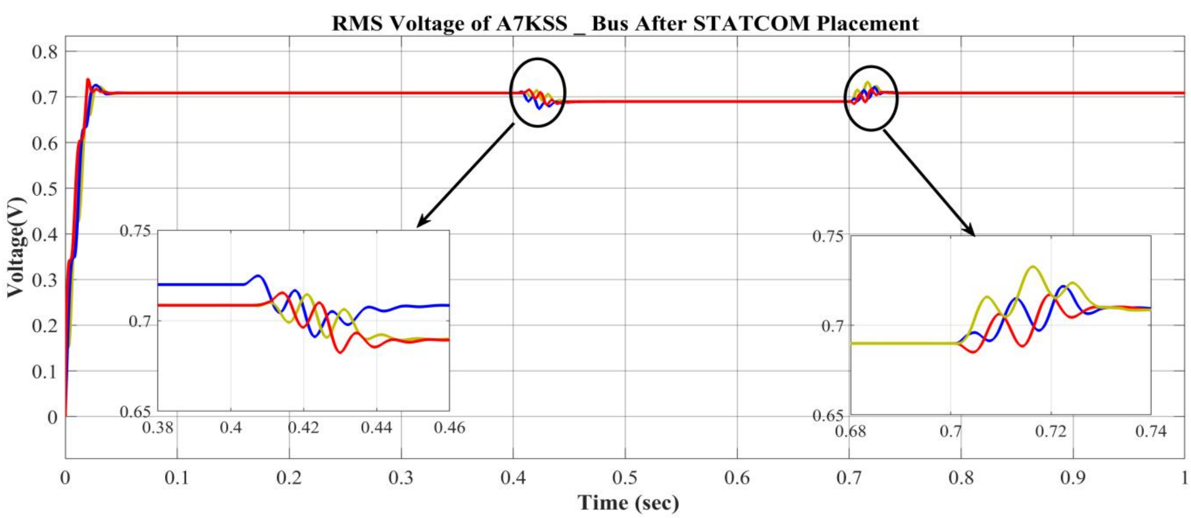

(b)

Figure 4.9 (a), (b) shows the A7KSS Bus RMS Voltage Simulink model result before and after STATCOM placement.

Buses of the AWFG substation Before and after the STATCOM was installed

The results indicate a significant improvement in the voltage profile at the 132 kV bus. Before the STATCOM was placed, during the contingency period from 0.4 seconds to 0.7 seconds, the voltage magnitude was 0.86 p.u. This low voltage level triggered the under-voltage relay, causing the breaker to trip and disconnecting the Adama I Wind Farm (AWFG) because the voltage level dropped below 0.942 p.u. However, after the STATCOM was installed, the voltage magnitude improved to 1.02 p.u., which keeps the breaker closed and allows uninterrupted electricity generation.

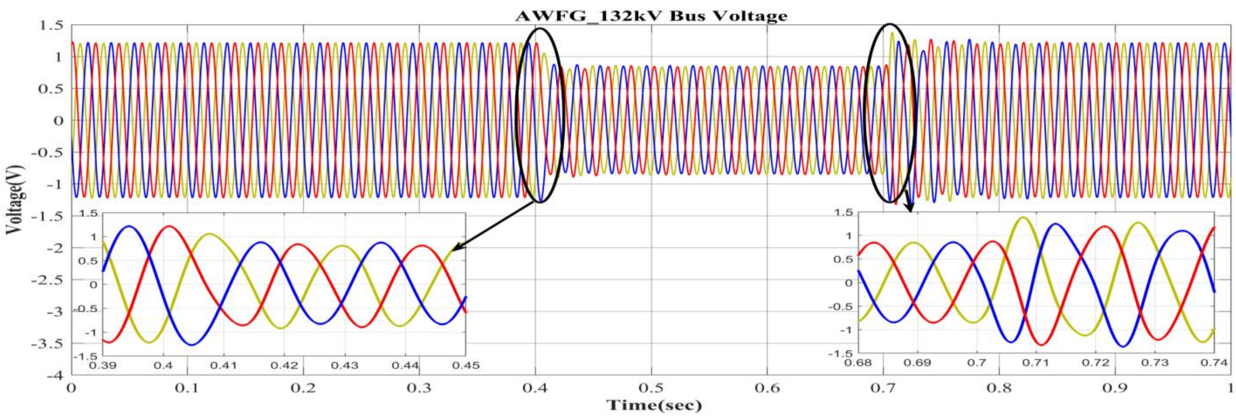

(a)

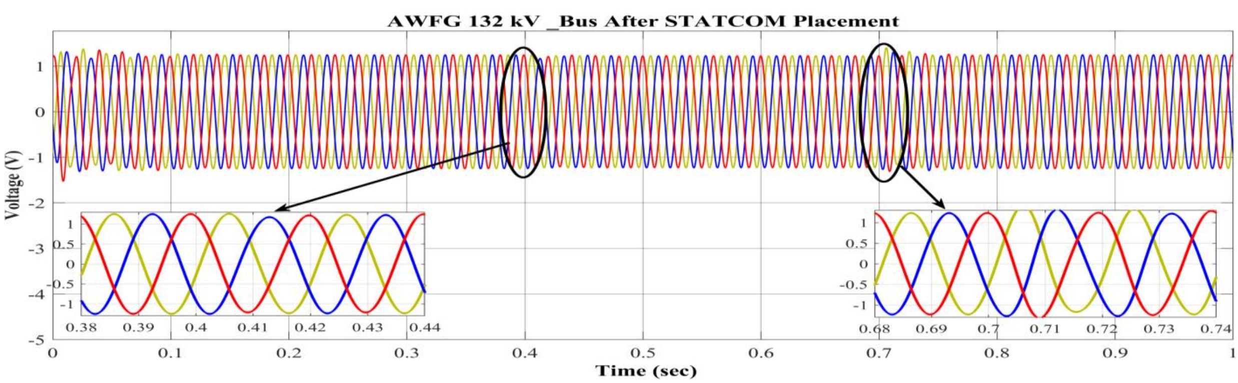

(b)

Figure 4.10 (a),(b) Simulink model result of AWFG 132kv Bus Voltage Before and after STATCOM Placement

The results of the Simulink model for the AWFG 132kV bus current before and after STATCOM placement are shown simply in the figure below, demonstrating an improvement in bus current when compared during contingency and compensation.

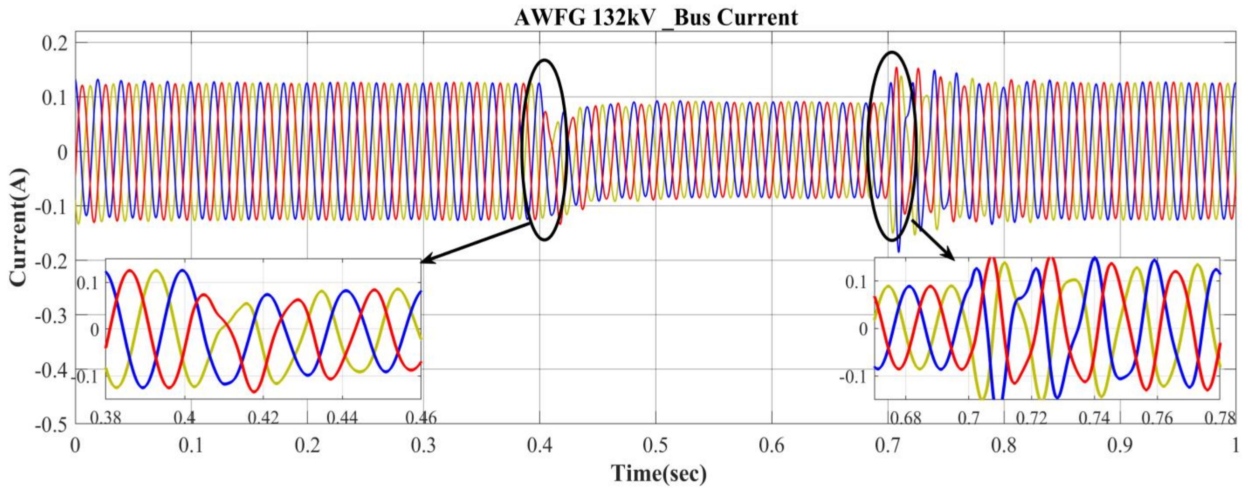

(a)

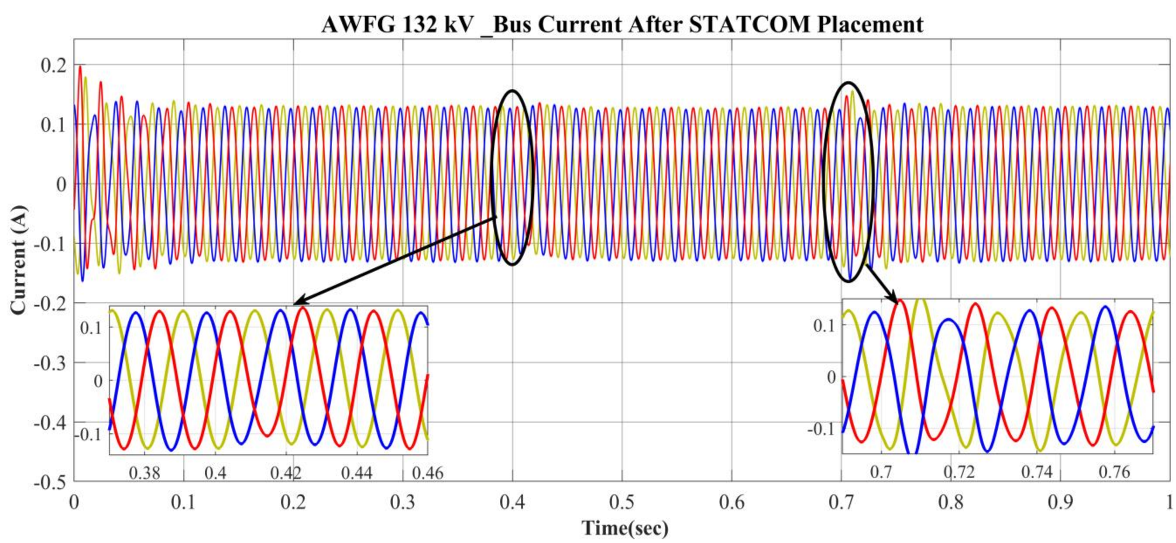

(b)

Figure 4.11 (a),(b) Simulink model result of AWFG 132kV Bus Current Before and after STATCOM Placement

The results of the Simulink model for the generated power from AWFG before and after STATCOM placement are shown simply in the figure below, demonstrating an improvement in generating power due to the contigency duration of 0.4 seconed to 0.7 seconed. The generated power is disturbed, but after placement of the STATCOM, the disturbed power becomes compensated.

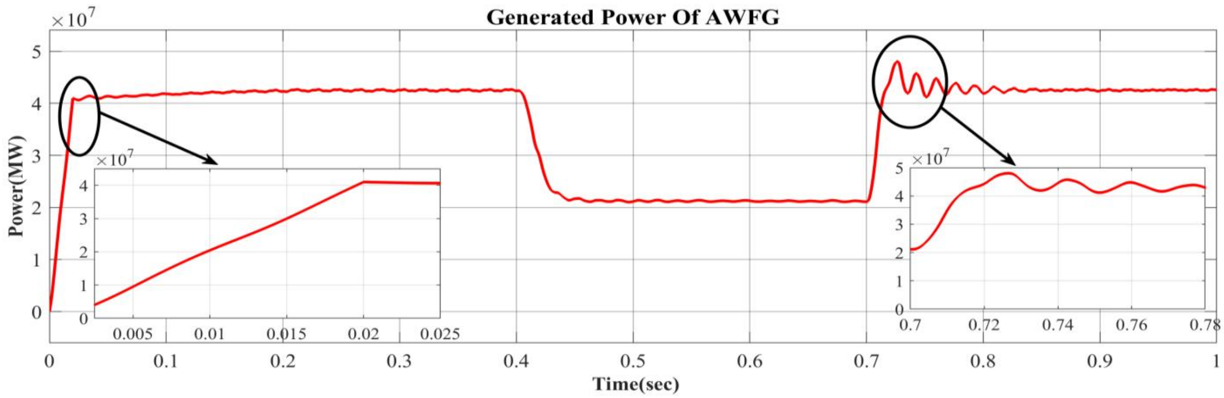

(a)

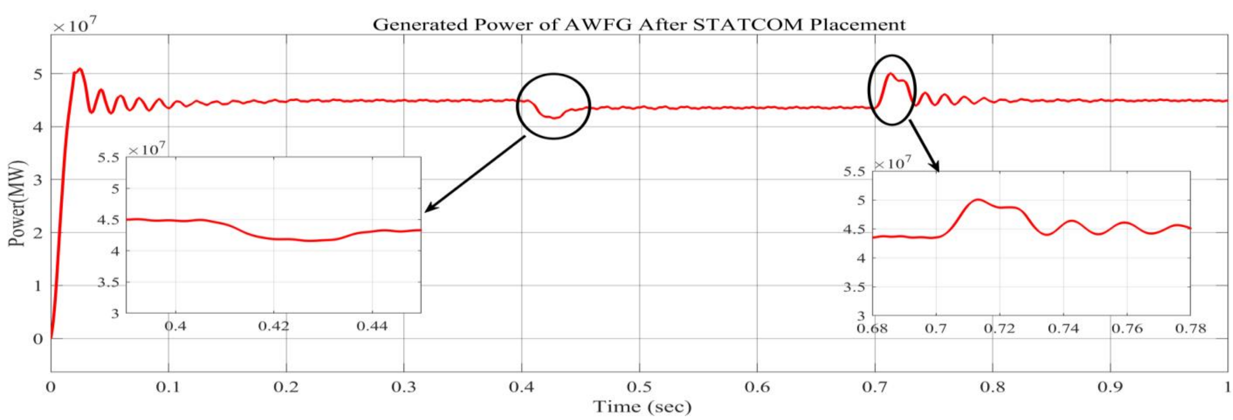

(b)

Figure 4.12 (a),(b) Simulink model result of AWFG 132kV Bus Current Before and after STATCOM Placement

Response of Battery Supported STATCOM

The STATCOM for a 15MVAR rating is Results are shown in the figures below. It includes the input and absorbing status of reactive power, current, and voltage.

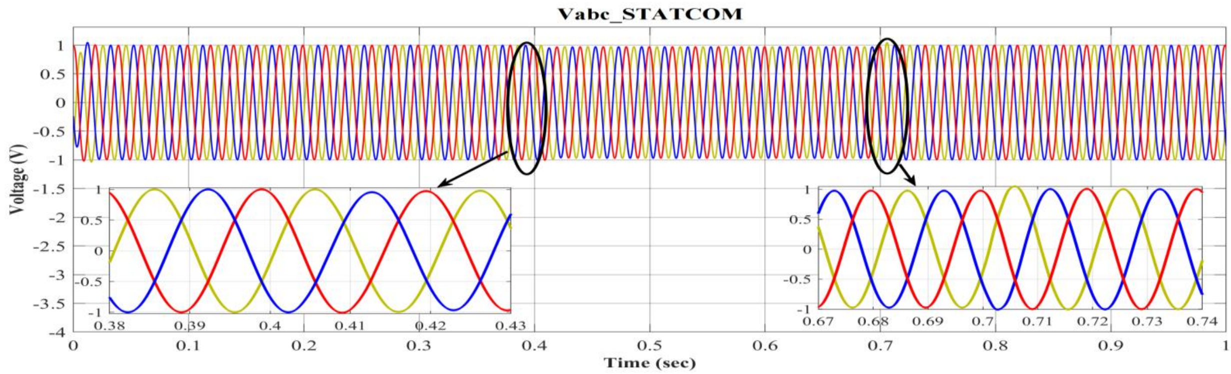

(a)

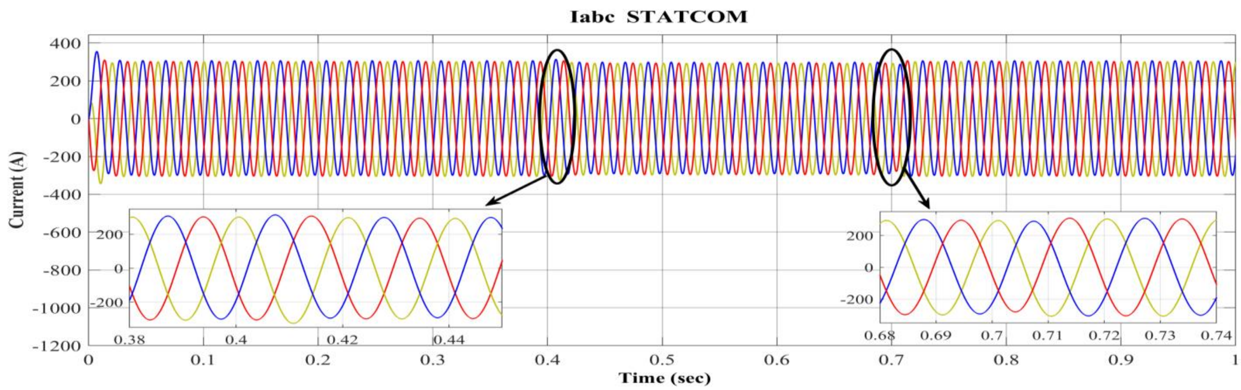

(b)

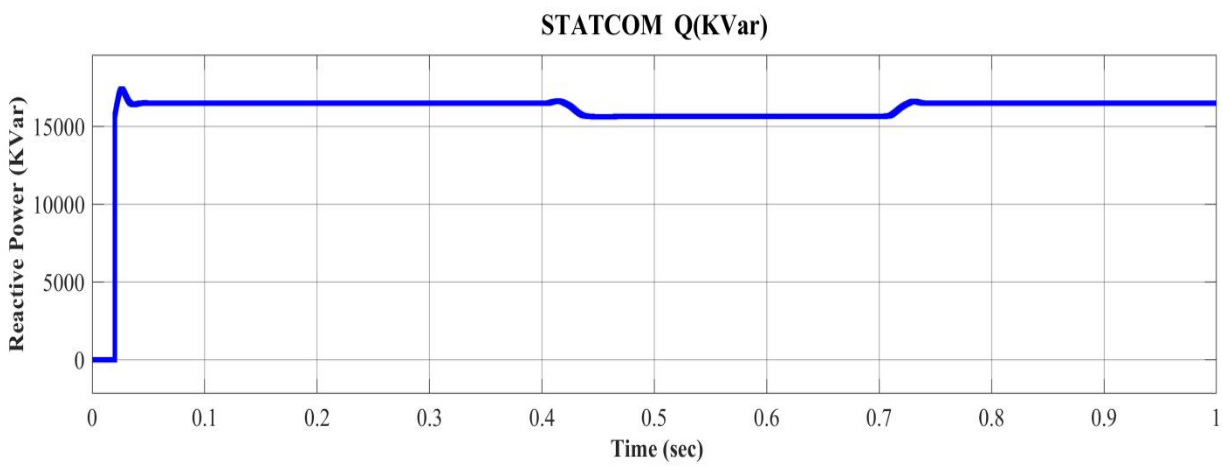

(C)

Figure 4.13 a,b,c Simulink model results of STATCOM Voltage,Current and Reactive Power respectively

Response of Battery Energy Storage

From the figures shown below, the state of charge, battery voltage, battery current, and voltage at the DC link are shown. Each graph shows the whole normal condition and the contigency condition for a time of 0.4 to 0.7 seconds.

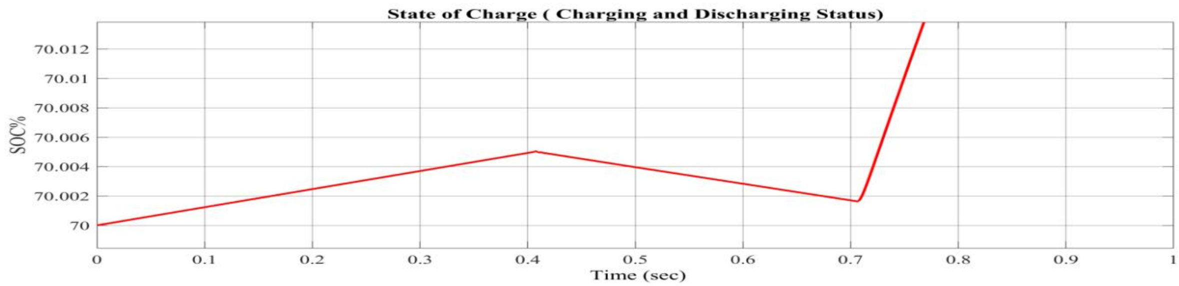

Figure 4.14 State-of-charge characteristics of the battery

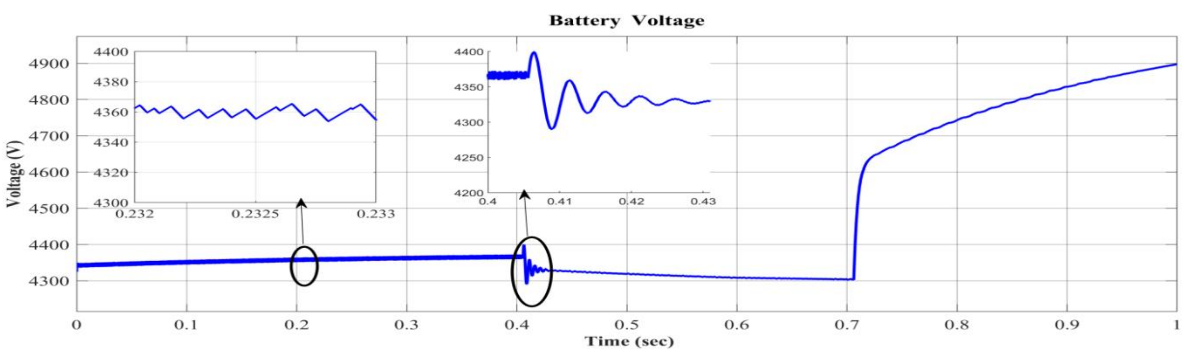

Figure 4.15 Battery Voltage status

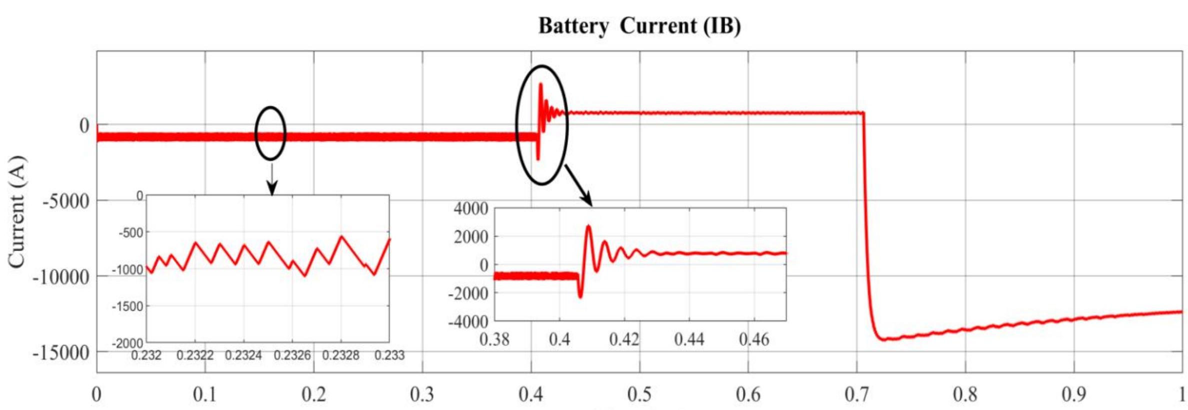

Figure 4.16 Battery Current status

The state of charge (SOC) of the battery is gradually increasing, and that current is also negative. We can observe that at 70% SOC, battery voltage is around 4368V, which exceeds the nominal voltage since, as the state of charge of the battery is increased, battery voltage exceeds its nominal voltage. When an interruption occurs at the 0.4 to 0.7 second mark, the battery state of charge begins to decrease and the current begins to rise and as shown in the figure below

4.4 Comparing the voltage magnitude with different bus locations

The STATCOM placement and sizing are decided by the particle swarm optimization technique, which is that the bus used by PSO is the A7KSS Bus, and the sizing is 15 MVAR. Furthermore, when we install the STATCOM at a different place, like ADSS or AWFG,. The voltage magnitude will be enhanced as below and show that the place that was decided by PSO is acceptable due to the voltage enhanced value on the A7KSS being better than the others.

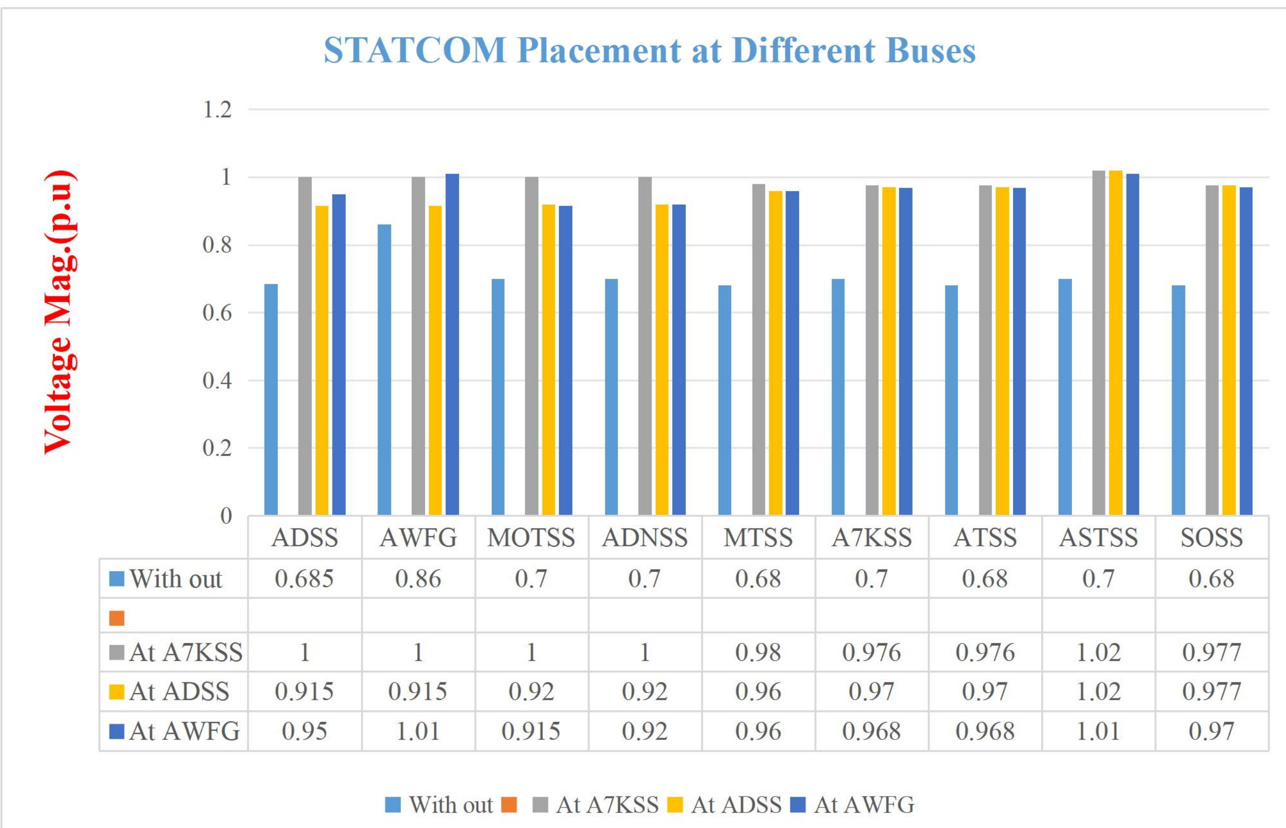

	ADSS	AWFG	MOTSS	ADNSS	MTSS	A7KSS	ATSS	ASTSS	SOSS
With out	0.685	0.86	0.7	0.7	0.68	0.7	0.68	0.7	0.68
At A7KSS	1	1	1	1	0.98	0.976	0.976	1.02	0.977
At ADSS	0.915	0.915	0.92	0.92	0.96	0.97	0.97	1.02	0.977
At AWFG	0.95	1.01	0.915	0.92	0.96	0.968	0.968	1.01	0.97

Figure 4.17 Comparison of Bus Voltage with different location of STATCOM Placement

5.CONCLUSIONS AND RECOMMENDATIONS

The high-voltage transmission lines of the Adama substation electric supply system were intended to have their voltage profile enhanced. Based on the findings obtained with and without the battery-backed STATCOM, the following conclusions, suggestions, and potential future work have been made.

5.1 Conclusions

The high-voltage transmission line of the Adama substation electric supply system recurrently faced voltage profile issues, primarily due to contingencies on the Koka incoming line, which was the main line. During an outage of this line, the system voltage throughout the network dropped significantly, recorded as low as 113 kV (0.856 p.u.), whereas the system's nominal voltage was 132 kV. This under-voltage condition caused interruptions in the Adama I wind farm generation and necessitated load-shedding measures to stabilize the system. To address these issues, several techniques were employed to enhance the voltage profile throughout the system network. Load flow analysis carried out by the Newton-Raphson method using MATLAB code was conducted to evaluate the existing voltage profile and identify critical buses affected by voltage drops. Particle Swarm Optimization (PSO) was utilized for the optimal sizing and placement of the STATCOM within the network, ensuring maximum performance benefits such as improved voltage profiles. Additionally, a detailed analysis of the existing system was performed using a Simulink model based on real data gathered from the Ethiopian Electric Power Organization, with simulations conducted using MATLAB version 2021a.

The implementation of a 15 MVAR battery-supported STATCOM at the Awash 7 kilo substation Bus significantly enhanced the voltage profile of the high-voltage transmission lines. The STATCOM effectively mitigated voltage fluctuations, ensuring a more stable and reliable power supply. During a 0.4 to 0.7 second simulation, the system voltage at various buses, including ADSS, AWFG, A7KSS, MTSS, ADNSS, MTSS, ATSS, ASTSS, and SOSS, dropped to 0.68 p.u., 0.86 p.u., 0.7 p.u., 0.7 p.u., 0.7 p.u., 0.68 p.u., 0.68 p.u., 0.7 p.u., and 0.68 p.u., respectively. After installing the 15 MVAR STATCOM, the voltage profiles improved to 1 p.u., 1.02 p.u., 0.978 p.u., 1 p.u., 1 p.u., 0.98 p.u., 0.976 p.u., 1.02 p.u., and 0.977 p.u., respectively. These enhancements prevent voltage-related interruptions at the Adama wind farm and reduce load shedding across the network.Furthermore, during a Koka contingency, if the Adama wind farm continued feeding power to the system due to the compensated voltage, load shedding would have been reduced, and the unsold energy would have been corrected. The use of particle swarm optimization (PSO) for optimizing the STATCOM parameters resulted in an optimal configuration that maximized the performance benefits of improved voltage profiles.

5.2 Recommendations

I recommend that EEP implement battery-supported STATCOMs within the system network, specifically at the Awash 7-Kilo substation bus. This implementation will provide practical validation of the simulation results and demonstrate the effectiveness of STATCOM technology in enhancing voltage stability. Additionally, integrating battery-supported STATCOMs with renewable energy sources like solar and wind can further stabilize the voltage profile and enhance the sustainability of the power supply. Finally, conducting a comprehensive economic analysis to assess the cost-benefit ratio of implementing battery-supported STATCOMs at the Awash 7-Kilo substation will justify further investments in advanced voltage regulation technologies, considering both initial and long-term operational savings.

5.3 Future Work

Future research should focus on optimizing STATCOM performance using advanced techniques such as genetic algorithms (GA) or artificial neural networks (ANN) and comparing these methods with particle swarm optimization (PSO). Conducting simulations and analysis with varying wind speeds to understand the dynamic response of the Adama I wind farm under different operating conditions is recommended. This research will provide insights into how fluctuating wind speeds affect power generation and the interaction with STATCOM, helping to optimize control strategies and enhance grid stability.

REFERENCES

Anjali Atul Bhandakkar and Lini Mathew Dr. (2018). Real-Time-Simulation of IEEE-5-Bus Network on OPAL-RT-OP4510 Simulator. *Materials Science and Engineering* (pp. 1-13). Chandigarh, India: IOP Publishing.

Boldea, I. (2017). *Synchronous Generators* (2nd ed.). Boca Raton: Engineering & Technology. doi:https://doi.org/10.1201/b19310

Bukola Babatunde Adetokun,Christopher Maina Muriithi . (2021). Application and control of flexible alternating current transmission system devices for voltage stability enhancement of renewable-integrated power grid: A comprehensive review. *Heliyon*, 1-7.

Chanan Singh; Panida Jirutitijaroen; Joydeep Mitra. (2019). Introduction to Power System Reliability. *Wiley-IEEE Press*, 185 - 191.

DESSALEGN BITEW AEGGEGN, AYODEJI OLALEKAN SALAU , YALEW GEBRU. (2020). Load flow and contingency analysis for transmission line outage. *ARCHIVES OF ELECTRICAL ENGINEERING*, 581-594.

Dung VO TIEN, Radomir GONO, Zbigniew LEONOWICZ, Petr KREJCI. (2019). Load Flow Analysis in Power System Network Incorporating STATCOM: A Comparison of the Direct and Indirect Algorithm of the Newton-Raphson Method. *POWER ENGINEERING AND ELECTRICAL ENGINEERING*, 13-23.

Ebenezer K. Ojo, Ojerinde I. Akinremi, Adesupo H. Adeleke. (2023). An Optimal Placement of STATCOM Controller on 14-Bus IEEE Standard Test Transmission Network using Particle Swarm Optimization. *FUOYE Journal of Engineering and Technology*, 45-52.

EEP. (2019, 0 0). *Ethiopian Electric Power (EEP).* Retrieved from Power Transmission: https://www.eep.com.et/en/power-transmission/

Fabliha Ahmed, Silvia Tasnim, and Shourin Rahman Aura. (2021). *EJECE, European Journal of Electrical Engineering and Computer Science*, 35-43.

H Ali, A Rahardjo, A Setiawan, F H Jufri and F Husnayain. (2019). Voltage profile improvement analysis during the loss of transmission lines on 150kv subsystem using static synchronous compensator. *IOP Conf. Series* (pp. 1-7). Depok: IOP Publisher.

Hagos Gebrekidan Berhe, Milkias Berhanu Tuka. (2018). Reactive Power Compensation and Voltage Support in Wind Farms Using PV-STATCOM (Case study at Adama-I Wind farm, Ethiopia). *International Journal of Power Systems*, 75-86.

Hau, E. (2013). *Wind Turbines Fundamentals, Technologies, Application, Economics.* (H. Renouard, Trans.) Springer Berlin Heidelberg., Germany . Retrieved from https://www.google.com.et/books/edition/Wind_Turbines/KeNEAAAAQBAJ?hl=en&sa=X&ved=2ahUKEwjLktHVtKiGAxW6SvEDHZVuHwkQiqUDegQIAxAC

Hussein, S. (2021). *Intelligent STATCOM Voltage Regulation using Fuzzy Logic Control.* Dubai: RIT Scholar Works.

Lovati, S. (2023, 05 31). *Energy Needs a Smarter Approach*. Retrieved from EEtimes: https://www.eetimes.com/increase-efficiency-reduce-loss-in-the-power-grid/

M O Okelola, S O Ayanlade and E I Ogunwole. (2021). Particle Swarm Optimization for Optimal Allocation of. *Journal of Physics: Conference Series* (pp. 1-7). Ibadan: IOP.

Marcin Szott, Szymon Wermi´nski , Marcin Jarnut, Jacek Kaniewski and Grzegorz Benysek. (2021). Battery Energy Storage System for Emergency Supply and Improved Reliability of Power Networks. *energies* (pp. 1-20). Zielona Góra, Poland: MDPI.

Muluneh Lemma Woldesemayat,Ashenaf Tesfaye Tantu. (2022). Security Enhancement of Power Systems through Interline Power Flow Controller (IPFC) under Contingency Condition: A Case Study and Analysis-EEP 400 kV System. *Hindawi*, 1-12.

Myat Phone Myint1, and Soe Soe Ei Aung2. (2022). OPTIMAL SIZING AND ALLOCATION OF STATCOM FOR HIGH VOLTAGE TRANSMISSION SYSTEM VOLTAGE STABILITY IMPROVEMENT USING PSO ALGORITHM. *Global Scientific* , 1738-1747.

Myat Phone Myint1, and Soe Soe Ei Aung2. (2022). Optimal Sizing And Allocation Of Statcom For High Voltage Transmission System Voltage Stability Improvement Using Pso Algorithm . *Global scientific journal*, 1738-1747.

O. M. Komolafe , and K. M. Udofia . (2020). REVIEW OF ELECTRICAL ENERGY LOSSES IN NIGERIA. *Nigerian Journal of Technology (NIJOTECH)*, 246-254.

Rasool, A. A., Abbas, N. M., Sheikhyounis, K. (2022). Determination of optimal size and location of static synchronous compensator for power system bus voltage improvement and loss reduction using whale optimization algorithm. *Journal of Enterprise Technologies*, 26-34.

S. M. Mehedi Hasan and Abu Hena MD Shatil. (2021, May 15). Design and Comparison of Grid Connected Permanent Magnet Synchronous Generator. *AIUB JOURNAL OF SCIENCE AND ENGINEERING, 20*(2), 40-46. doi:10.53799/ajse.v20i2.136

Sibdas Mondal1,Sk. Rabiul Hossain2,Bijay Kumar Mudi3,Prof. Gautam Kumar Panda4,Prof. Pradip Kumar Saha5. (2014, April). Modelling and Simulation Result of a Permanent Magnet Synchronous Generator of Wind Turbine System. *International Journal of Advanced Research in Electrical, Electronics and Instrumentation Engineering, 3*(4), 9506-9511. doi:10.1109/ROPEC.2015.7395143

Suliman, M. Y. (2023). Voltage Profile Improvement Using Static Synchronous Compensator STATCOM. *Journal of Information, Communication, and Intelligence Systems (JICIS)*, 36-42.

T Sucita, Y Mulyadi and W S Saputra. (2018). Load Shedding Analysis Because of Contingency Damage (N- 2) at Transmission Lines 150 kV Subsystem Cirata. *IOP Conference Series: Materials Science and Engineering* (pp. 1-8). Bandung: IOP.

Tariq, H.; Czapp, S.; Tariq,. (2022). Comparative Analysis of Reactive Power Compensation Devices in a Real Electric Substation. *Energies*, 1-17.

Tebeje Tesfaw Wondie ,Teshome Goa Tella. (2022). Voltage Stability Assessments and Their Improvement Using Optimal Placed Static Synchronous Compensator (STATCOM). *Hindawi*, 1-12.

Ummidi Sirisha,M Sobha,Arun Kumar Ch. (2020). Power System Contingency Analysis by using Voltage and Active Power Performance Index. *International Journal for Modern Trends in Science and Technology*, 52-60.

V.Harika,G. Madhavi. (2018). Optimal Power flow with STATCOM using Particle Swarm Optimization. *nternational Journal for Research in Engineering Application & Management*, 571-576.

Zaid Hamodat 1,Ismail Khudhur Hussein 2,Bilal Abdullah Nasir 3. (2023). An Accurate Efficiency Calculation for PMSG Utilized in Renewable Energy Systems. *Journal of Robotics and Control (JRC), 4*(4), 458-465. doi:10.18196/jrc.v4i4.18441

APPENDIX A

1) PMSG and Wind Turbine Parameters

Parameters	Symbol	Value and Units
Rated Speed	ωe	1460.7rpm
Electromagnetic torque	Te	0.24Nm
Stator Resistance	Rs	5Ω
Stator d-axis Inductance	Ld	0.1H
Stator d-axis Inductance	Lq	0.1H
Permanent Magnet Flux	Ψf	0.314Wb
Number of Pole Pair	Zp	2

Air density	ρ	1.225kg/m^3
Power Coefficients	C_p	0.48
Wind Speed	V_w	11m/s
Radius	r	38.42m
Tip speed Ratio	λ	8.1
Rotor Speed	ω_r	152.89 rad/s
Coefficients	C_1, C_2, C_3, C_4, C_5, and C_6	0.5176, 116, 0.4,5,21, and 0.0068 respectively
Mechanical Power	P_m	1.5MW
Damping Coefficients	B	0.0197
Equivalent Inertia	J_{eq}	0.003kg/m^2

2) DC-to-DC Boost Converter Parameters

Parameters	Symbol	Value and Units
Capacitor	C	48.579e-6 F
Inductor	L	742.88e-6 H
Load Resistance	R	32.204 Ω
Duty Cycle	D	0.5
Switching frequency	f_s	25KHz

3) 48-pulse GTO's voltage source converter Parameters

S.No	Elements	**Parameters**
1.	GTO based VSC	8
2.	Zig -zag Transformer	4 each of 15MVA,33 KV
3.	Pulse Number	48
4.	Nominal AC source Voltage	132KV
5.	Nominal DC link Voltage	4KV
6.	GTO switching frequency	50Hz
7.	DC Capacitor	125mf
8.	DC voltage controller	Kpdc = 4, KIdc = 250
9.	Decoupled current controller	Kpd = 30 ,Kpq = 60
10.	AC Voltage Controller	Kpt = 0.12 , Kit = 5
11.	DC link Capacitor Voltage Balancer	Kb = 0.001,Ki = 0.0001
12.	Short circuit level	132kV,50Hz,3%Zn,100MVA

APPENDIX B

1) Koka 132kV Incoming Line Interruption

SNo.	132kV Koka Line Interruption Date	Cause of Interruption	Time Interr-uption	Recon-nection time	Differe-nce (hr)	Moment Load MW	Moment Load A	Unsold Energy (KWh)
1.	30/1/2023	Due To Over Current	12:27	12:50	0:23	65	294	24916.66
2.	29/3/2023	No signal	6:24	6:30	0:06	45.5	206	4550.00
3.	10/4/2023	CT Failure at Koka	15:17	17:42	2:25	47	212	113583.3
4.	18/4/2023	For Maintenance	23:12	00:58	01:46	34	155	60066.66
5.	23/6/2023	Due To Over Current	11:07	11:22	0:15	44	194	11000
6.	6/7/2023	Due To Over current	9:05	9:21	0:16	44	194	11733.33
7.	21/7/2023	For Maintenance	22:08	0:38	2:30	44	194	110000
8.	24/7/2023	Due To SC	4:37	7:03	02:26	30	135	73000
9.	31/8/2023	Due To Conductor Burst @B-Phase	06:43	12:27	05:44	39.8	185	218186.6
10.	18/9/2023	Defective relay to read the fault	16:02	18:30	02:28	34	158	83866.66
11.	24/9/2023	Due to over current	12:44	13:49	01:05	67	303	72583.33
12.	2/12/2023	For Maintenance	06:39	08:29	01:50	27	129	49500.00
13.	26/12/2023	Due to Earh Fault	09:58	10:08	00:10	56	280	9333.33
14.	29/12/2023	For Maintenance	6:48	8:37	1:49	47	212	85,383.3

NB: You can contact to Adama substation In charge :-Mr. Birhanu Bonger(+251911745228)

2) Adama I Wind Power Plant Outage Report

No.	Interruption Date	Cause of Interruption	Interruption time	Re-connection time	Differe-nce (hr)	Energy Loss(MU)
1.	30/01/2023	System Voltage drop 128kv-113kv	12:23	12:57	00:34	0 MU
2.	29/03/2023	External voltage block	06:25	06:57	00:32	0 MU
3.	10/4/2023	System Voltage drop _119kv	15:18	18:02	02:44	0.058MU
4.	10/5/2023	System Voltage drop_119kv	8:15	9:13	0:58	0.00197MU
5.	23/6/2023	System Voltage drop_ 114kv	11:08	11:39	0:31	0.0033MU
6.	6/7/2023	External Voltage Drop	9:05	9:52	0:47	0.0083MU
7.	24/7/2023	External Voltage Drop	04:35	06:25	01:50	0.041MU
8.	29/8/2023	External Voltage Drop	12:45	13:52	01:07	0.01716MU
9.	31/8/2023	External Voltage Drop	06:44	13:44	07:00	0.0557MU
10.	18/9/2023	External Voltage Drop	16:03	16:24	0:21	0.005022909 MU
11.	24/09/2023	External Voltage Drop	12:55	13:56	1:01	0.0003104 MU
12.	3/12/2023	External Voltage Drop	20:31	20:36	0:05	0.001156MU
13.	18/12/2023	External Voltage Drop	17:03	17:31	0:28	0.001107MU
14	26/12/2023	External Voltage Drop	9:53	10:17	0:24	0.01324 MU

APPENDIX C

1) Data for Awash 7 kilo Power plant (Substation)

ETHIOPIAN ELECTRIC POWER

East Region Substation Operation and Maintenance Office

AWASH 7 KILO POWER PLANT (SUBSTATION) : - Monthly Peak, Minimum & Average Load Report

Month : - APRIL Year :- 2023

No_	Sabstation Name	Region	Transformer Name	Voltage Level	Peak Load						Minimum Load						Average/Day Load	
					Power (MW)	Current (Amp)			Date	Time	Power (MW)	Current (Amp)			Date	Time	MW	Amp
7	Awash 7 Kilo	>>	KVKOKA-230 kv	230 KV	132	1.1	318	320	10/4/2023	20:00	70	0.4	172	176	6/4/2023	8:00	74.63	120.32
			DIRE DAWA||| 230 kv	230 KV	98	254	252	260	8/4/2023	12:00	62	10	182	183	20/04/2023	14:00	79.39	206.43
			ADAMA 132 KV Incoming	132 Kv	11.6	89	94	88	6/4/2023	11:00	1	6	3	3	24/04/2023	4:00	6.80	47.27
			ASEBE TEFERE 132 KV	132 Kv	13.5	59	59	60	26/04/2023	19:00	1	28	29	28	5/4/2023	6:00	7.36	36.79
			AWASH TRACTION 132 KV	132 Kv	36	80	85	92	5/4/2023	14:00	3.4	19	10	17	14/04/2023	2:00	4.26	21.24
			SIREBA KUNKURU 132 KV	132 Kv	17	85	90	94	17/04/2023	21:00	3.1	17	8	16	14/04/2023	3:00	4.11	19.96
			NURAERA 66 KV OUT.	66 kV	6.4	62	62	61	6/4/2023	11:00	1.6	17	17	17	26/04/2023	3:00	24.75	2.830
			AMIBAEA 66KV OUT	66 kV	2.1	21	21	23	24/04/2023	20:00	0.6	6	7	7	5/4/2023	15:00	13.63	1.31

Federal Dem. Republic of Ethiopia Ethiopian Electric Power Awash 7 kilo S.P.P

Petros Ashamo Awash 7 kilo Substation Power Plant (S.P.P) Manager

ETHIOPIAN ELECTRIC POWER

East Region Substation Operation and Maintenance Office

AWASH 7 KILO POWER PLANT (SUBSTATION) : - Monthly Peak, Minimum & Average Load Report

Month : - APRIL Year :- 2023

No_	Sabstation Name	Region	Transformer Name	Voltage Level	Peak Load						Minimum Load						Average/Day Load	
					Power (MW)	Current (Amp)			Date	Time	Power (MW)	Current (Amp)			Date	Time	MW	Amp
7	Awash 7 Kilo	EAST	230/132 kv Autotransformer 1.230kv side		36	96	96	94	10/4/2023	17:00	0.6	1.7	1.7	1.4	17/04/2023	17:00	5.80	18.83
			230/132 kv Autotransformer 2. 230kv side		38	90	97	95	10/4/2023	16:00	0.1	5	5	0.1	1/4/2023	22:00	4.76	17.34
			230/132 kv Autotransformer 1.132kv side		16	85	91	63	6/4/2023	11:00	1	8	9	11	20/04/2023	14:00	6.65	35.57
			230/132 kv Autotransformer 2.132kv side		16	84	95	95	6/4/2023	11:00	5	5	4	0.3	16/04/2023	17:00	7.05	33.65
			132/66/15kv Power tra 1.132kv side															
			132/66/15kv Power tra 2.132kv side		10.2	55	56	56	6/4/2023		1.3	6	7	7	10/9/2023	2:00	29.68	5.53
			132/66/15kv Power tra 1. 66kv side															
			132/66/15kv Power tra 2. 66kv side		6.9	75	75	76	6/4/2023		2.2	21	24	23	9/4/2023	7:00	37.12	3.40
			15 KV INCOOMING(1)															
			15 KV INCOOMING(2)		3.8	180	176	178	12/4/2023	11:00	1.7	84	83	84	22/04/2023	0:00	110.4	2.31
			AWASH 7KILO 15KV LIN(1)OUT															
			AWASH 7KILO 15KV LIN(2)OUT		1.9	88	87	86	12/4/2023	17:00	0.1	25	26	27	4/4/2023	4:00	54.22	1.35
			AWASH 40 (15KV)OUT		1.6	78	73	77	04/04/203	19:00	0.4	23	23	23	21/04/2023	3:00	47.63	0.97
			FACTOREY 15KV OUT		0.8	40	36	36	12/4/2023	11:00	0.1	1	1	1	1/4/2023	6:00	10.82	0.22

Federal Dem. Republic of Ethiopia Ethiopian Electric Power Awash 7 kilo S.P.P

Petros Ashamo Awash 7 kilo Substation Power Plant (S.P.P) Manager

ETHIOPIAN ELECTRIC POWER

East Region Substation Operation and Maintenance Office

AWASH 7 KILO POWER PLANT (SUBSTATION) : - Monthly Peak, Minimum & Average Load Report

Month : - MAY Year :- 2023

No_	Sabstation Name	Region	Transformer Name	Voltage Level	Peak Load						Minimum Load						Average/Day Load	
					Power (MW)	Current (Amp)			Date	Time	Power (MW)	Current (Amp)			Date	Time	MW	Amp
7	Awash 7 Kilo	EAST	230/132 kv Autotransformer 1.230kv side		40	111	107	103	10/5/2023	12:00	0.9	1	1	0.1	17/05/2023	16:00	5.63	17.11
			230/132 kv Autotransformer 2. 230kv side		43	105	119	105	21/05/2023	12:00	0.1	0.5	6	6	30/05/2023	23:00	7.27	15.88
			230/132 kv Autotransformer 1.132kv side		39	182	172	171	10/5/2023	12:00	1.2	3	6	7	6/5/2023	0:00	6.40	32.28
			230/132 kv Autotransformer 2.132kv side		40	176	175	146	10/5/2023	12:00	1	18	20	18	11/5/2023	3:00	6.69	30.63
			132/66/15kv Power tra 1.132kv side		7.5	40	41	41	8/05/202	11:00	0.7	3	3	3	19/05/2023	17:00	0.5	10.57
			132/66/15kv Power tra 2.132kv side		11.8	64	65	65	17/05/2023	19:00	0.7	3	3	2	2/5/2023	4:00	4.60	21.99
			132/66/15kv Power tra 1. 66kv side		7.7	88	85	84	18/05/2023	11:00	0.6	8	8	6	30/05/2023	23:00	4.3	20.74
			132/66/15kv Power tra 2. 66kv side		7	65	68	69	10/5/2023	13:00	0.4	3	5	5	20/05/2023	10:00	3.10	16.78
			15 KV INCOOMING(1)															
			15 KV INCOOMING(2)		4.1	192	193	192	3/5/2023	17:00	0.02	1	0	0	19/05/2023	17:00	1.5	15.35
			AWASH 7KILO 15KV LIN(1)OUT															
			AWASH 7KILO 15KV LIN(2)OUT		1.7	84	84	76	26/05/2023	19:00	0.5	39	33	39	6/5/2023	6:00	1.20	56.67
			AWASH 40 (15KV)OUT		1.4	69	64	66	23/05/2023	9:00	0.3	13	13	12	14/05/2023	22:00	2.50	51.08
			FACTOREY 15KV OUT		0.9	40	36	39	17/05/2023	10:00	0.02	1	1	1	1/5/2023	5:00	0.5	10.57

ETHIOPIAN ELECTRIC POWER

East Region Substation Operation and Maintenance Office

AWASH 7 KILO POWER PLANT (SUBSTATION) : - Monthly Peak, Minimum & Average Load Report

Month : - MAY Year :- 2023

No_	Sabstation Name	Region	Transformer Name	Voltage Level	Peak Load						Minimum Load						Average/Day Load	
					Power (MW)	Current (Amp)			Date	Time	Power (MW)	Current (Amp)			Date	Time	MW	Amp
7	Awash 7 Kilo	EAST	230/132 kv Autotransformer 1.230kv side		40	111	107	103	10/5/2023	12:00	0.9	1	1	0.1	17/05/2023	16:00	5.63	17.11
			230/132 kv Autotransformer 2. 230kv side		43	105	119	105	21/05/2023	12:00	0.1	0.5	6	6	30/05/2023	23:00	7.27	15.88
			230/132 kv Autotransformer 1.132kv side		39	182	172	171	10/5/2023	12:00	1.2	3	6	7	6/5/2023	0:00	6.40	32.28
			230/132 kv Autotransformer 2.132kv side		40	176	175	146	10/5/2023	12:00	1	18	20	18	11/5/2023	3:00	6.69	30.63
			132/66/15kv Power tra 1.132kv side		7.5	40	41	41	8/05/202	11:00	0.7	3	3	3	19/05/2023	17:00	0.5	10.57
			132/66/15kv Power tra 2.132kv side		11.8	64	65	65	17/05/2023	19:00	0.7	3	3	2	2/5/2023	4:00	4.60	21.99
			132/66/15kv Power tra 1. 66kv side		7.7	88	85	84	18/05/2023	11:00	0.6	8	8	6	30/05/2023	23:00	4.3	20.74
			132/66/15kv Power tra 2. 66kv side		7	65	68	69	10/5/2023	13:00	0.4	3	5	5	20/05/2023	10:00	3.10	16.78
			15 KV INCOOMING(1)															
			15 KV INCOOMING(2)		4.1	192	193	192	3/5/2023	17:00	0.02	1	0	0	19/05/2023	17:00	1.5	15.35
			AWASH 7KILO 15KV LIN(1)OUT															
			AWASH 7KILO 15KV LIN(2)OUT		1.7	84	84	76	26/05/2023	19:00	0.5	39	33	39	6/5/2023	6:00	1.20	56.67
			AWASH 40 (15KV)OUT		1.4	69	64	66	23/05/2023	9:00	0.3	13	13	12	14/05/2023	22:00	2.50	51.08
			FACTOREY 15KV OUT		0.9	40	36	39	17/05/2023	10:00	0.02	1	1	1	1/5/2023	5:00	0.5	10.57

3) Adama 132kV Substation Loa Data

MEGABIT-2016 LOAD REPORT

Substation :- Nazareth NAZRETH - II Date: 1/4/2204 (23/07/2016)

Existing Capacity> 2 X 25 MVA AND 1X 50MVA MONTH Mar-24

No	Bay/Feeder	Peak Load		Date	Time	Minimum		Date	Time	Average Load	Current Transformer		Cabel
		Power MW	Current (A)			Power MW	Current(A)				Ration	Present Connection	C.S.A (mm2)
	132 Kv Line / Feeder												
1	Koka Incoming Feeder	82	392	25-Mar-2024	8:00	34	157	3/2/2024	4:00	56	800/400/1	800/1	
2	Awash 7 Kilo Out Going	47.7	110	7-Mar-2024	7:00	7	38	3/12/2024	8:00:00	32	800/400/1	800/1	
3	132KV WIND INCOMING										600/1	600/1	
4	Mojo Tra 132 KV Outgoing	0.11	11	19-Mar-2024	11:00	0.1	10	3/28/2024	3:00	0.1	600/300/1	600/1	
5	Transformer 1	19.2	94	5-Mar-2024	7:00	8	42	3/14/2024	2:00	13	300/150/1	150/1	
6	Transformer 2	19.2	94	5-Mar-2024	7:00	8	42	3/14/2024	2::00	13	300/150/1	150/1	
	15KV												
1	Transformer 1 Feeder	19.2	780	5-Mar-2024	7:00	8	320	3/14/2024	2,00	13	1200/600/1	1200/1	2X240
2	Transformer 2 Feeder	19.2	780	5-Mar-2024	7:00	8	320	3/14/2024	2:00	13	1200/600/1	1200/1	2X240
3	Line 1 Wonji	8	321	16-Mar-2024	7:00	5.2	210	3/15/2024	3:00	4.9	300/150/1	300/1	1X185
4	Line 2 (Nazreth)										300/150/1	300/1	1*185
5	Line 3 (Wolenchitie)	8	321	7-Mar-2023	1:00	3.8	124	3/5/2024	1:00	4.8	300/150/1	300/1	1X185
6	Line 4 Berta	6.9	246	1-Mar-2023	5:00	4.4	165	3/11/2024	1:00	4.9	300/150/1	300/1	1X185
7	Line 5 Turk Textail	6.9	248	14-Mar-2023	8:00	3.8	132	3/18/2024	2:00	5.2	300/150/1	300/1	1X185
8	Line 6 Mojo Cement	6.2	243	16-Mar-2023	7:00	4.6	164	3/2/2024	2:00	4.4	300/150/1	300/1	1X185
9	Line 7 Koka Metal	8.2	322	8-Mar-2023	7:00	2.2	82	3/21/2024	1:00	3.8	300/150/1	300/1	1X185
	Trafo 3 (132/15KV)	37	189	8-Mar-2024	7:00	14	72	3/13/2024	1,00	22	600/1	600/1	
1	15 KV Line/Feeder	37	1520	8-Mar-2024	7:00	14	1230	3/26/2024	3:00	22	2500/1	2500/1	2X630
2	M1	9.4	395	30-Mar-2023	8:00	4.8	167	3/22/2024	2:00	6.6	800/1	800/1	2X240
3	M2	5.2	232	12-Mar-2023	3:00	1.4	67	3/29/2024	1:00	3.2	800/1	800/1	2X240
4	M3	7.4	216	10-Mar-2023	1:00	2.2	81	3/11/2024	1:00	3.8	800/1	800/1	2X240
5	M4	9.2	372	7-Mar-2023	1:00	2.6	86	3/26/2024	4:00	5.2	800/1	800/1	2X240
6	M5	9.6	391	19-Mar-2023	10:00	3	123	3/5/2024	2:00	5.1	800/1	800/1	2X240
7	M6	6.2	243	22-Mar-2023	3:00	0.5	20	3/7/2024	18,00	2.3	800/1	800/1	2X240

PREPARED BY : BIRHANU BONGER

DATE : 1/4/2024 (22/06/23/07/2016)

Nazareth S/S II Incharge

MONTHLY SUBSTATION LOAD REPORT

Substation :- Nazerth

Existing Capacity:- 2 X 25 MVA AND 1 X 50MVA

DATE ;01/03/2023 {22/6/2015}

Month: FEB-23

No	Bay/Feeder	Peak Load		Date	Time	Minimum		Date	Time	Average Load	Current Transformer		Cabel
		Power MW	Current (A)			Power MW	Current (A)				Ration	Present Connection	C.S.A (mm2)
	132 Kv Line / Feeder												
1	Koka Incoming Feeder	74	344	23/2/23	11:00	28	140	5/2/2023	23:45	51	800/400/1	800/1	
2	Awash 7 Kilo Out Going	24	105	17/2/23	10:00	8	40	12/2/2023	23:00:00	16	800/400/1	800/1	
3	132KV WIND INCOMING	40	190	17/2/23	8:00	1	5	5/2/2023	23:00	20.5	600/1	600/1	
4	Mojo Tra 132 KV Outgoing	17	96	11/2/2023	17:30	3.4	12	19/2/23	7:00	10.2	600/300/1	600/1	
5	Transsformer 1	19	95	10/2/2023	12:00	11	55	5/2/2023	23:00	15	300/150/1	150/1	
6	Transsformer 2	19	95	10/2/2023	12:00	11	55	5/2/2023	23:00	15	300/150/1	150/1	
	15 KV Line /Feeder												
1	Transsformer 1 Feeder	19	775	10/2/2023	12:00	11	450	5/2/2023	23:00	15	1200/600/1	1200/1	2X240
2	Transsformer 2 Feeder	19	775	10/2/2023	12:00	11	450	5/2/2023	23:00	15	1200/600/1	1200/1	2X240
3	Line 1 Wonji	7.6	310	16/2/23	7:30	2.6	105	19/2/23	23:00	5.1	300/150/1	300/1	1X185
4	Line 2 (Nazreth)												
5	Line 3 (Wolenchitie)	8.2	336	16/2/23	7:30	3.2	130	5/2/2023	22:00	5.7	300/150/1	300/1	1X185
6	Line 4 Berta	6	240	2/2/2023	12:30	2	84	26/2/23	23:00	4	300/150/1	300/1	1X185
7	Line 5 Turk Textail	6.1	245	15/2/23	11:00	1.5	62	3/2/2023	1:00	3.8	300/150/1	300/1	1X185
8	Line 6 Mojo Cement	4.6	185	25/2/23	14:30	1.2	60	5/2/2023	22:00	2.9	300/150/1	300/1	1X185
9	Line 7 Koka Metal	7.8	320	10/2/2023	12:00	2.4	100	5/2/2023	23:00	5.1	300/150/1	300/1	1X185
	Trafo 3 (132/15KV)	37	185	15/2/23	7:30	14	70	4/2/2023	22:00	25.5	600/1	600/1	
1	15 KV Line/Feeder	37	1517	15/2/23	7:30	14	574	4/2/2023	22:00	25.5	2500/1	2500/1	2X630
2	M1	9	384	24/2/23	9:00	3.6	145	3/2/2023	23:00	6.3	800/1	800/1	2X240
3	M2	7.7	305	15/2/23	19:00	1.2	60	11/2/2023	22:00	4.5	800/1	800/1	2X240
4	M3	8.8	369	16/2/23	7:30	3	124	21/2/23	2:00	5.9	800/1	800/1	2X240
5	M4	8.6	362	15/2/23	19:00	2.6	104	20/2/23	1:00	5.6	800/1	800/1	2X240
6	M5	8.5	348	27/2/23	10:00	2	84	5/2/2023	23:00	5.2	800/1	800/1	2X240
7	M6	5.3	215	17/2/23	10:00	0.5	20	6/2/2023	23:00	2.9	800/1	800/1	2X240

Reported By:- Berhanu Sodere

phone number

Signature:______________

Date:- ;01/03/2023

APPENDIX D

Matlab code for Newton-Raphson method and pso

```
% Power flow solution by Newton-Raphson method
ns=0; ng=0; Vm=0; delta=0; yload=0; deltad=0;
nbus = length(busdata(:,1));
for k=1:nbus
n=busdata(k,1);
kb(n)=busdata(k,2); Vm(n)=busdata(k,3); delta(n)=busdata(k, 4);
Pd(n)=busdata(k,5); Qd(n)=busdata(k,6); Pg(n)=busdata(k,7); Qg(n) = busdata(k,8);
Qmin(n)=busdata(k, 9); Qmax(n)=busdata(k, 10);
Qsh(n)=busdata(k, 11);
if Vm(n) <= 0  Vm(n) = 1.0; V(n) = 1 + j*0;
else delta(n) = pi/180*delta(n);
V(n) = Vm(n)*(cos(delta(n)) + j*sin(delta(n)));
P(n)=(Pg(n)-Pd(n))/basemva;
Q(n)=(Qg(n)-Qd(n)+ Qsh(n))/basemva;
S(n) = P(n) + j*Q(n);
end
end
for k=1:nbus
if kb(k) == 1, ns = ns+1; else, end
if kb(k) == 2 ng = ng+1; else, end
Qk = -Vm(n)^2*Ym(n,n)*sin(t(n,n))-J11;
if kb(n) == 1 P(n)=Pk; Q(n) = Qk; end   % Swing bus P
if kb(n) == 2  Q(n)=Qk;
if Qmax(n) ~= 0
Qgc = Q(n)*basemva + Qd(n) - Qsh(n);
if iter <= 7                % Between the 2th & 6th iterations
if iter > 2                 % the Mvar of generator buses are
```

```
if Qgc  < Qmin(n),       % tested. If not within limits Vm(n)
Vm(n) = Vm(n) + 0.01;    % is changed in steps of 0.01 pu to
elseif Qgc  > Qmax(n),   % bring the generator Mvar within
Vm(n) = Vm(n) - 0.01;end % the specified limits.
else, end
A(nn,lm) = 2*Vm(n)*Ym(n,n)*cos(t(n,n))+J22;  %diagonal elements of J2
A(lm,nn)= J33;        %diagonal elements of J3
A(lm,lm) =-2*Vm(n)*Ym(n,n)*sin(t(n,n))-J44;  %diagonal of elements of J4
DC(lm) = Q(n)-Qk;
end
end
DX=A\DC';
for n=1:nbus
nn=n-nss(n);
lm=nbus+n-ngs(n)-nss(n)-ns;
if kb(n) ~= 1
delta(n) = delta(n)+DX(nn); end
if kb(n) == 0
Vm(n)=Vm(n)+DX(lm); end
end
maxerror=max(abs(DC));
if iter == maxiter & maxerror > accuracy
fprintf('\nWARNING: Iterative solution did not converged after ')
fprintf('%g', iter), fprintf(' iterations.\n\n')
fprintf('Press Enter to terminate the iterations and print the results \n')
converge = 0; pause, else, end

end
```

```
if converge ~= 1
tech= ('                    ITERATIVE SOLUTION DID NOT CONVERGE'); else,
tech=('                    Power Flow Solution by Newton-Raphson Method');
end
V = Vm.*cos(delta)+j*Vm.*sin(delta);
deltad=180/pi*delta;
i=sqrt(-1);
k=0;
for n = 1:nbus
if kb(n) == 1
k=k+1;
S(n)= P(n)+j*Q(n);
Pg(n) = P(n)*basemva + Pd(n);
Qg(n) = Q(n)*basemva + Qd(n) - Qsh(n);
Pgg(k)=Pg(n);
Qgg(k)=Qg(n);     %june 97
elseif  kb(n) ==2
k=k+1;
S(n)=P(n)+j*Q(n);
Qg(n) = Q(n)*basemva + Qd(n) - Qsh(n);
Pgg(k)=Pg(n);
Qgg(k)=Qg(n);  % June 1997
% PSO Matlab code
% Define Ybus matrix
Ybus = [
];
% PSO parameters
numParticles = 30;
numIterations = 100;
```

```
lowerBound = [1, 10]; % lower bounds for [placementBus, sizing]
upperBound = [11, 100]; % upper bounds for [placementBus, sizing]

% PSO parameters
w = 0.5; % inertia weight
c1 = 2; % cognitive parameter
c2 = 2; % social parameter

% Initialize particles
particles.position = rand(numParticles, 2) .* (upperBound - lowerBound) + lowerBound;
particles.velocity = zeros(numParticles, 2);
particles.bestPosition = particles.position;
particles.bestCost = inf(1, numParticles);

globalBestPosition = [];
globalBestCost = inf;
particles.bestCost(i) = cost;
particles.bestPosition(i, :) = particles.position(i, :);
end

% Update global best if the current particle is better
if cost < globalBestCost
globalBestCost = cost;
globalBestPosition = particles.position(i, :);
end
end

% Update particle velocities and positions
for i = 1:numParticles
```

```
r1 = rand(1, 2);
r2 = rand(1, 2);

% Update velocity
particles.velocity(i, :) = w * particles.velocity(i, :) ...
+ c1 * r1 .* (particles.bestPosition(i, :) - particles.position(i, :)) ...
+ c2 * r2 .* (globalBestPosition - particles.position(i, :));

% Update position
particles.position(i, :) = particles.position(i, :) + particles.velocity(i, :);

% Ensure particles stay within bounds
particles.position(i, :) = max(particles.position(i, :), lowerBound);
particles.position(i, :) = min(particles.position(i, :), upperBound);

end
end
% Retrieve the best position
bestPlacementBus = round(globalBestPosition(1));
bestSizing = round(globalBestPosition(2));
% Display the best position
disp('Best STATCOM placement and sizing:');
disp(['Placement Bus: ', num2str(bestPlacementBus)]);
disp(['Sizing: ', num2str(bestSizing), ' MVAR']);
```